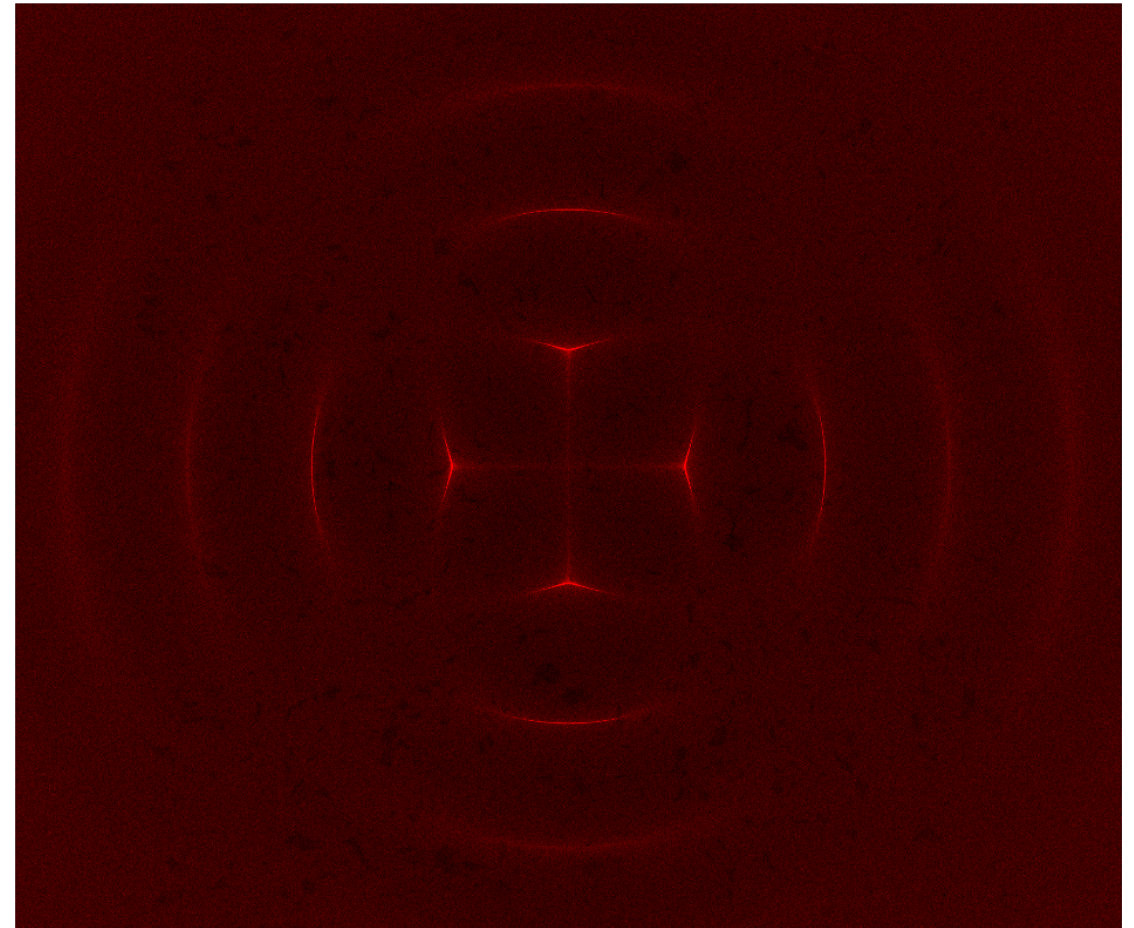
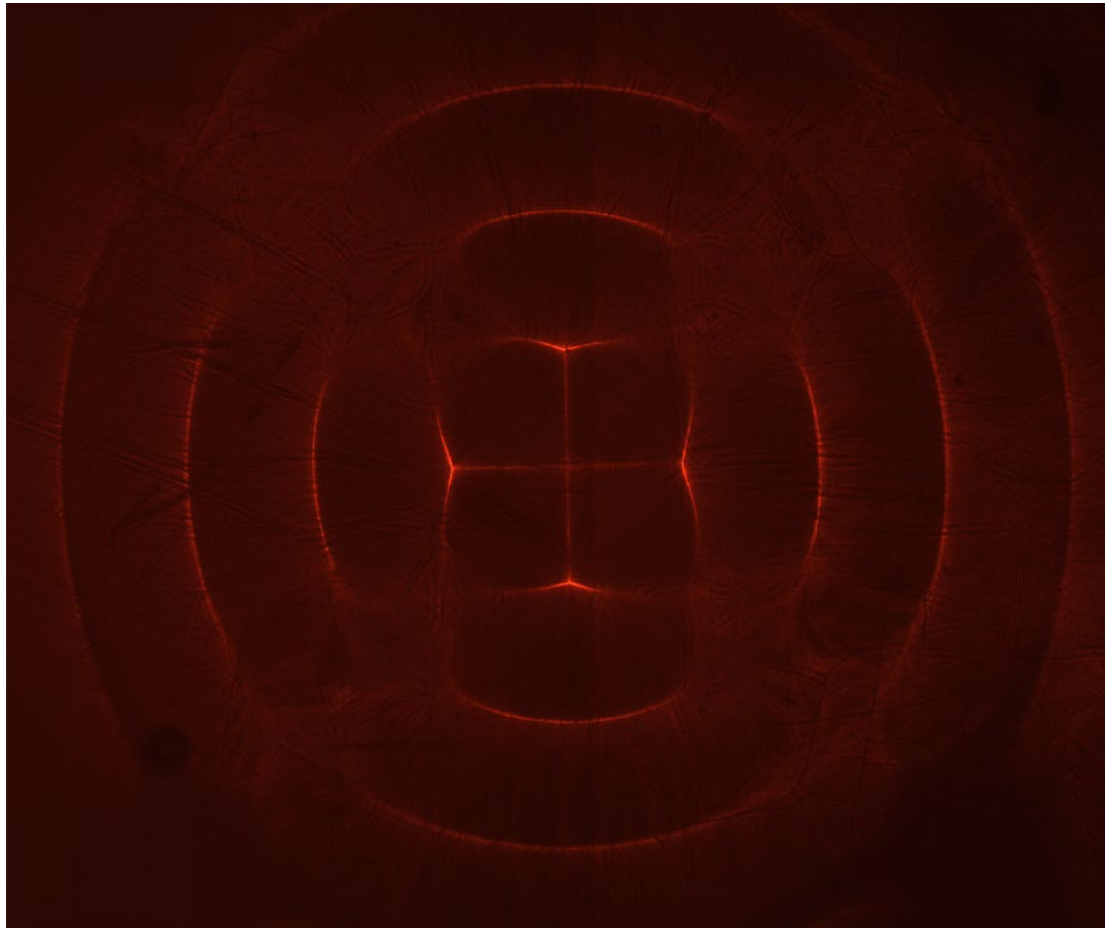


Rendering for scientific imaging applications



15-468, 15-668, 15-868
Physics-based Rendering
Spring 2023, Lecture 17

Course announcements

- We're all done with homework!
- *Please* vote for the topic of tomorrow's reading group.

Overview of today's lecture

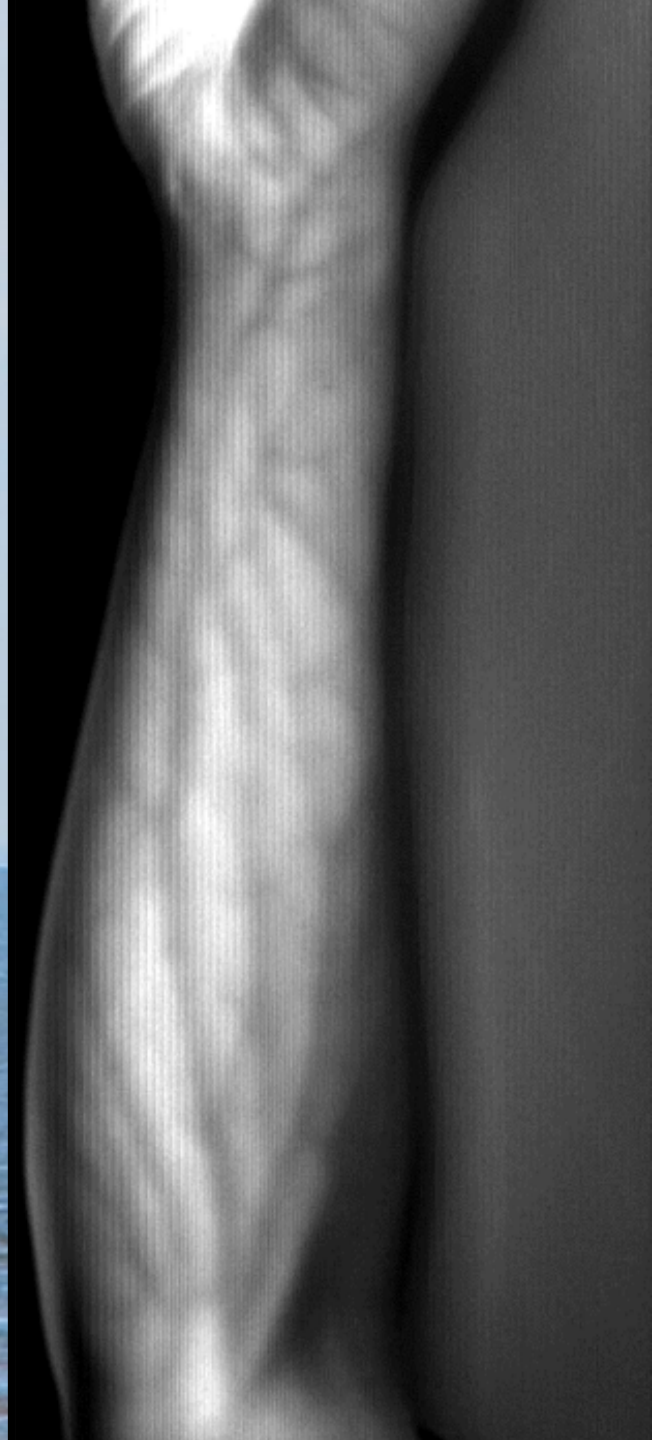
- Rendering continuous refraction.
- GRIN optics.
- Rendering the refractive radiative transfer equation.
- Acousto-optics.
- Rendering speckle.
- Fluorescence microscopy.

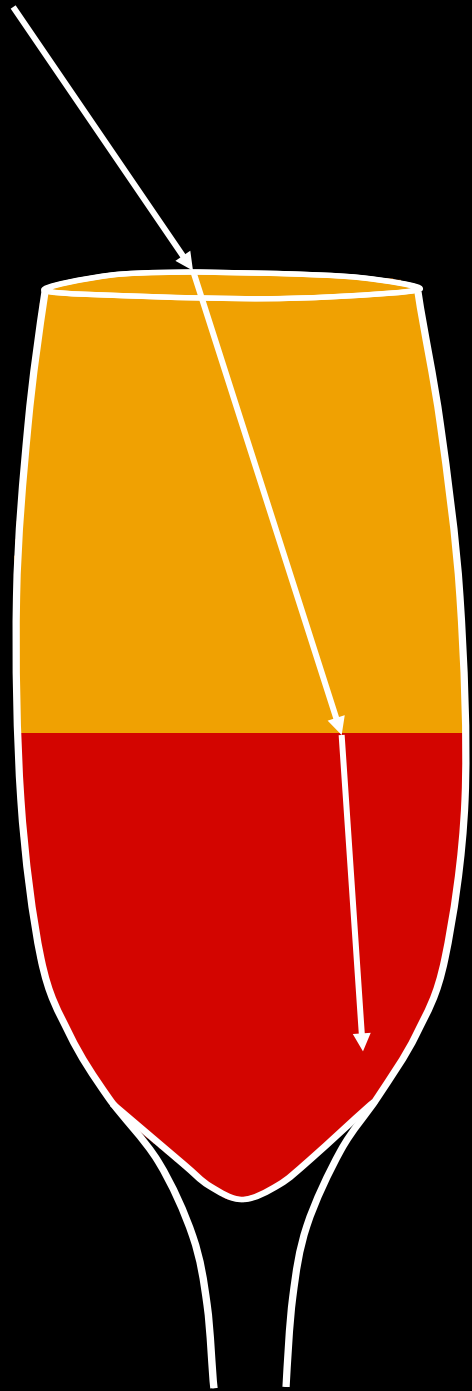
Slide credits

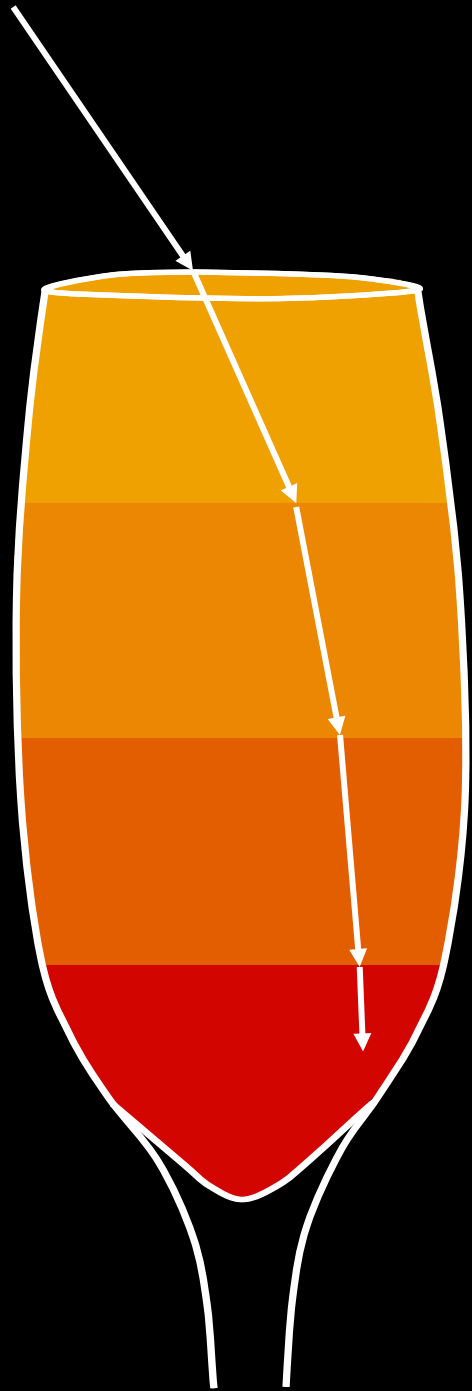
Many of these slides were directly adapted from:

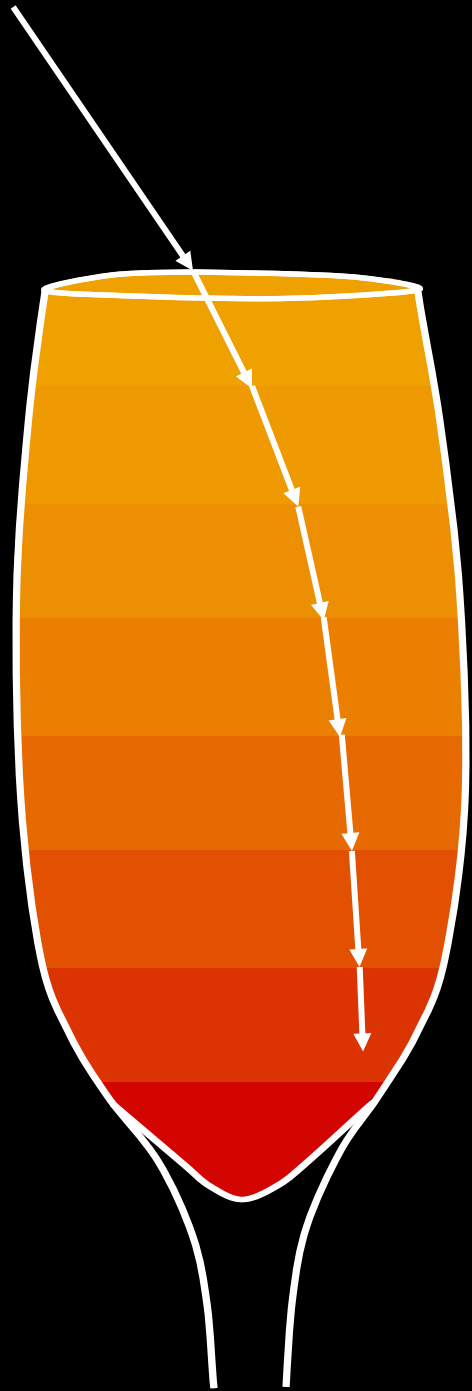
- Adithya Pediredla (CMU).
- Arjun Teh (CMU).
- Chen Bar (Technion).

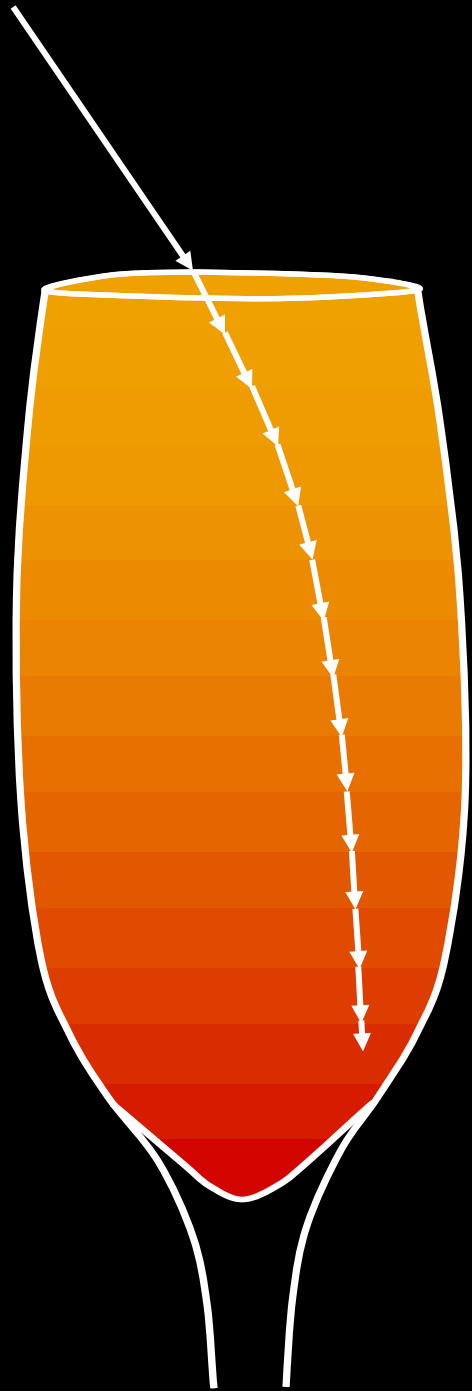
Media with continuously varying refractive index and scattering

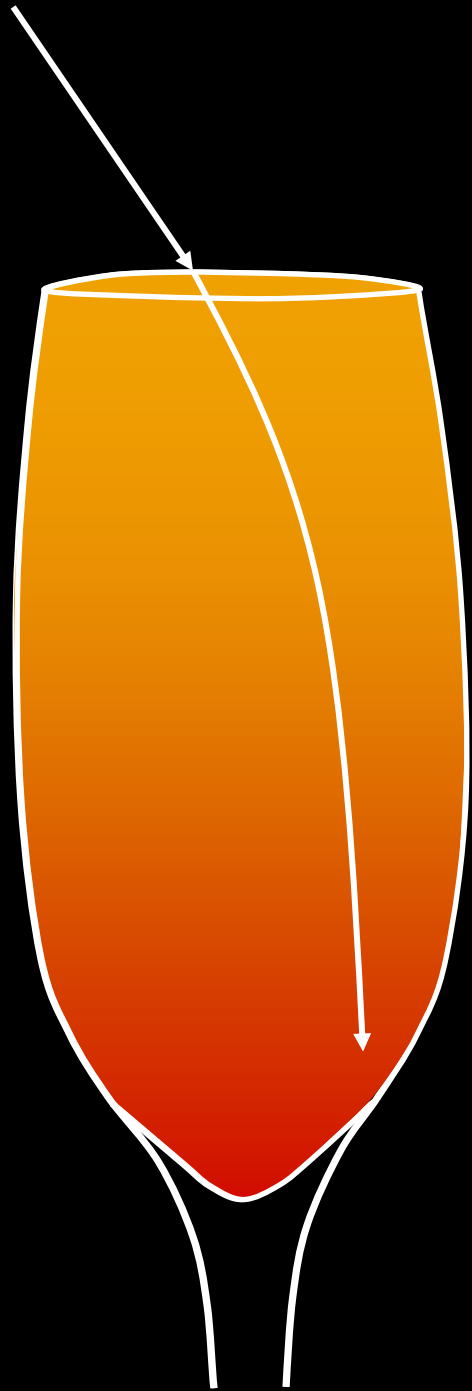




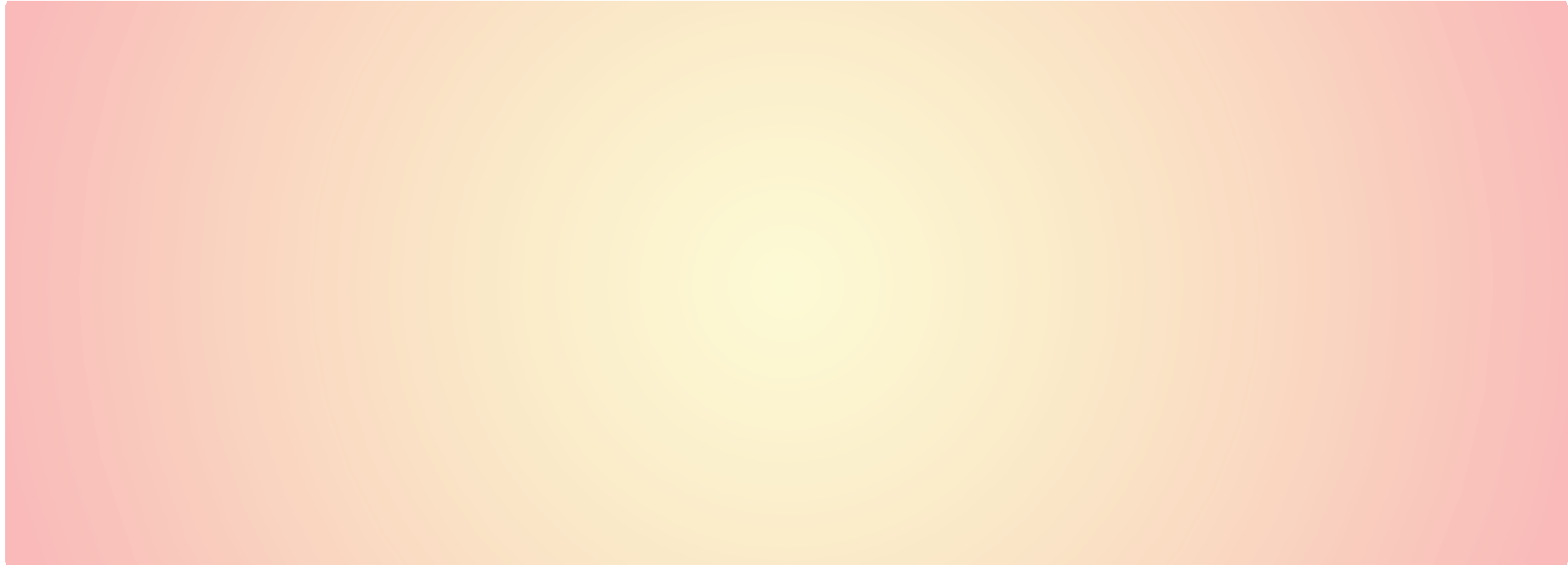






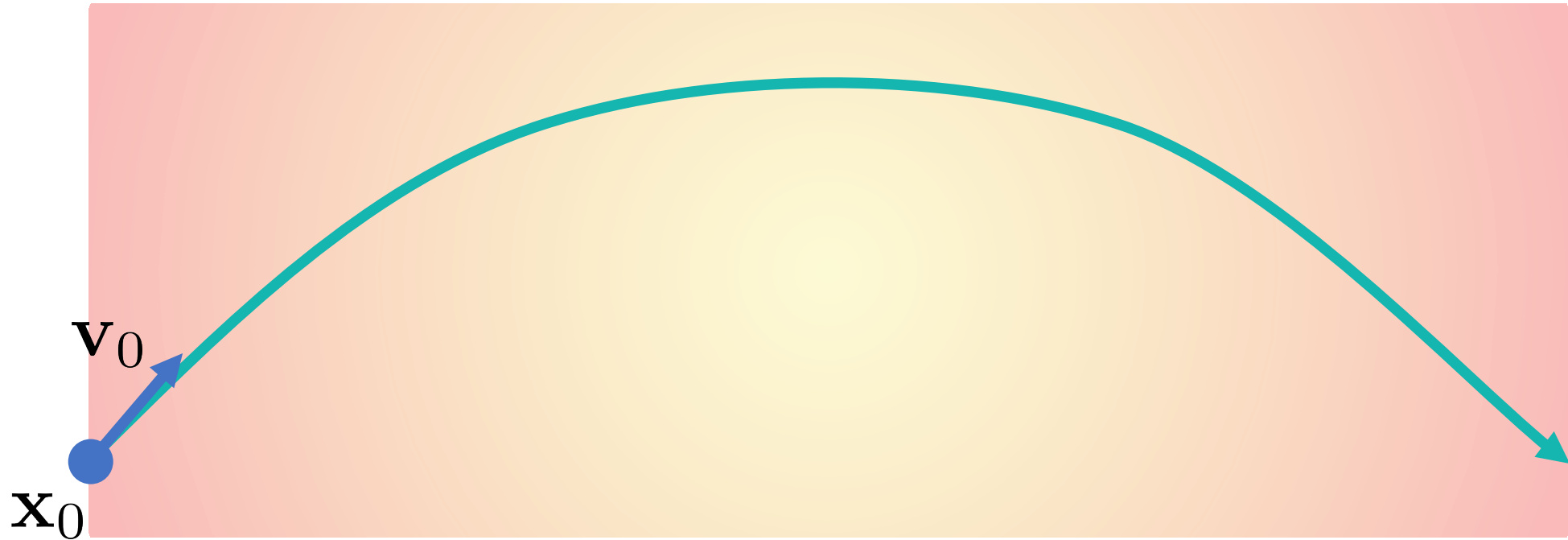


Nonlinear Ray Tracing



$\eta(\mathbf{x})$: refractive index of the volume at location, \mathbf{x}

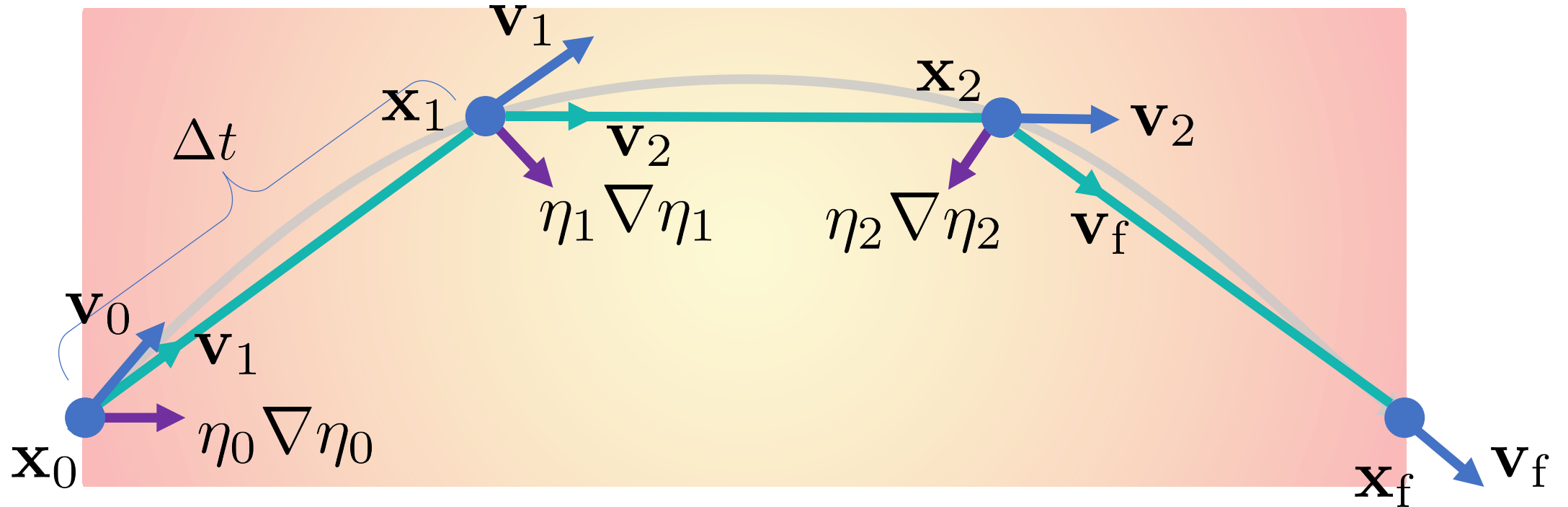
Nonlinear Ray Tracing



$$\frac{d\mathbf{x}}{dt} = \mathbf{v}$$

$$\frac{d\mathbf{v}}{dt} = \eta \nabla \eta$$

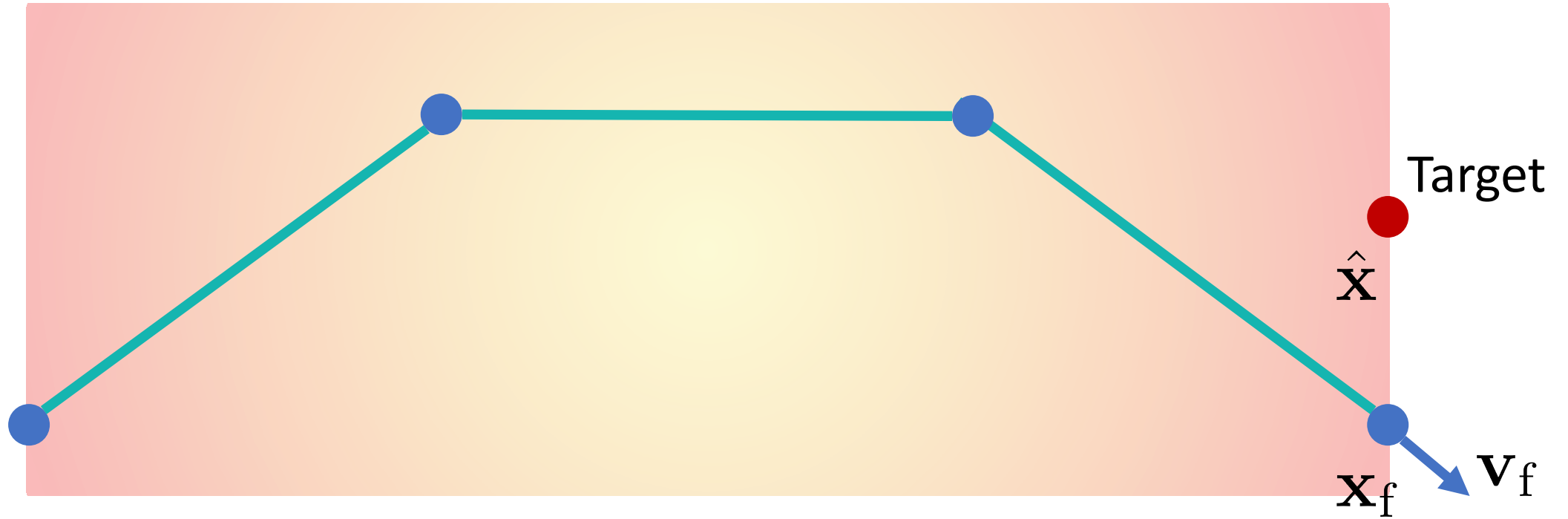
Nonlinear Ray Tracing



$$\mathbf{x}_i = \mathbf{x}_{i-1} + \mathbf{v}_i \Delta t$$

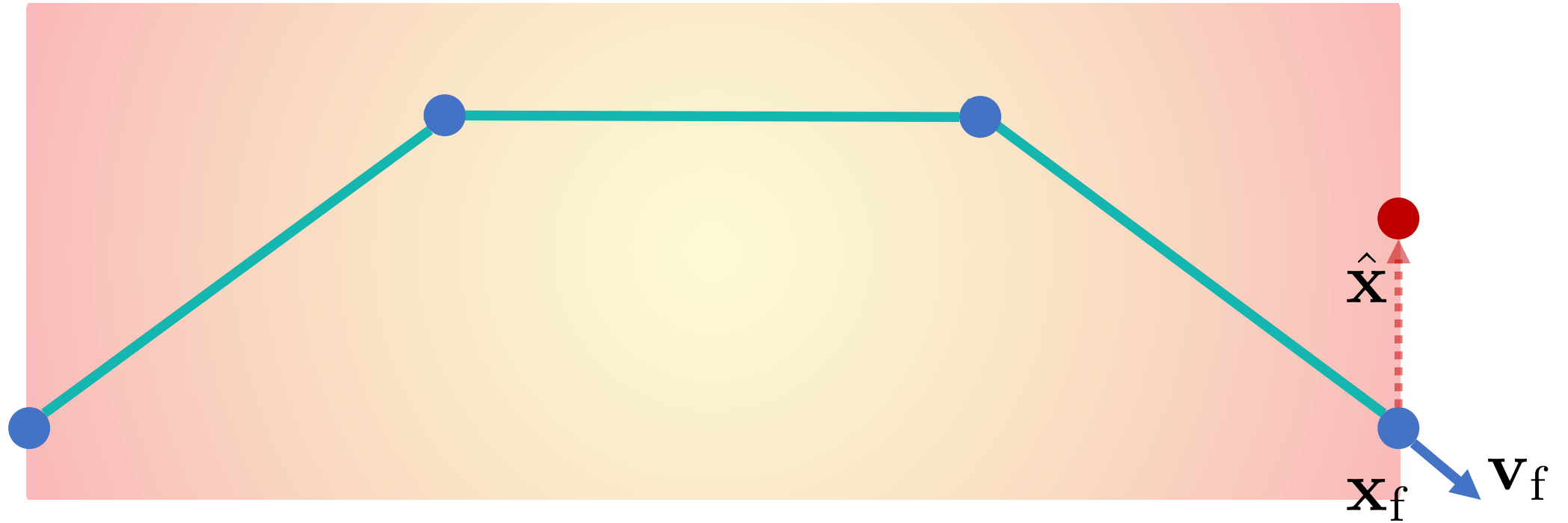
$$\mathbf{v}_i = \mathbf{v}_{i-1} + \eta_{i-1} \nabla \eta_{i-1} \Delta t$$

Nonlinear Ray Tracing



$$\min_{\eta} \|\hat{\mathbf{x}} - \mathbf{x}_f\|^2$$

Nonlinear Ray Tracing



$$\frac{d}{d\eta} \|\hat{\mathbf{x}} - \mathbf{x}_f\|^2$$

Nonlinear Ray Tracing in reverse

$$\min_{\eta} \sum_{i=1}^N \mathcal{F}_i \left[\iint_{(\mathbf{x}_0, \mathbf{v}_0) \in \Omega} C_i \left(\mathbf{x} \left(\sigma_f; \eta, \mathbf{x}_0, \mathbf{v}_0 \right), \mathbf{v} \left(\sigma_f; \eta, \mathbf{x}_0, \mathbf{v}_0 \right) \right) d\mathbf{x}_0 d\mathbf{v}_0 \right]$$

s.t. $\dot{\mathbf{x}}(\sigma; \eta, \mathbf{x}_0, \mathbf{v}_0) = \mathbf{v}, \quad \forall \sigma \in [0, \sigma_f],$
 $\dot{\mathbf{v}}(\sigma; \eta, \mathbf{x}_0, \mathbf{v}_0) = \eta \nabla \eta, \quad \forall \sigma \in [0, \sigma_f],$
 $\mathbf{x}(0; \eta, \mathbf{x}_0, \mathbf{v}_0) = \mathbf{x}_0,$
 $\mathbf{v}(0; \eta, \mathbf{x}_0, \mathbf{v}_0) = \mathbf{v}_0,$

(15)

\mathbf{x}_0

$\hat{\mathbf{x}}$

$$\dot{\lambda} = -(\nabla \eta (\nabla \eta)^\top + \eta \text{Hess}(\eta)) \mu, \quad \forall \sigma \in [0, \sigma_f] \quad (19)$$

$$\dot{\mu} = -\lambda, \quad \forall \sigma \in [0, \sigma_f] \quad (20)$$

$$\lambda(\sigma_f) = \frac{\partial \mathcal{C}}{\partial \mathbf{x}}, \quad (21)$$

$$\mu(\sigma_f) = \frac{\partial \mathcal{C}}{\partial \mathbf{v}}. \quad (22)$$

$\eta \nabla \eta$

$\eta \nabla \eta$

$$\mathbf{x}_{i-1} = \mathbf{x}_i - \mathbf{v}_i \Delta \sigma, \quad (28)$$

$$\mathbf{v}_{i-1} = \mathbf{v}_i - \eta(\mathbf{x}_{i-1}) \nabla \eta(\mathbf{x}_{i-1}) \Delta \sigma, \quad (29)$$

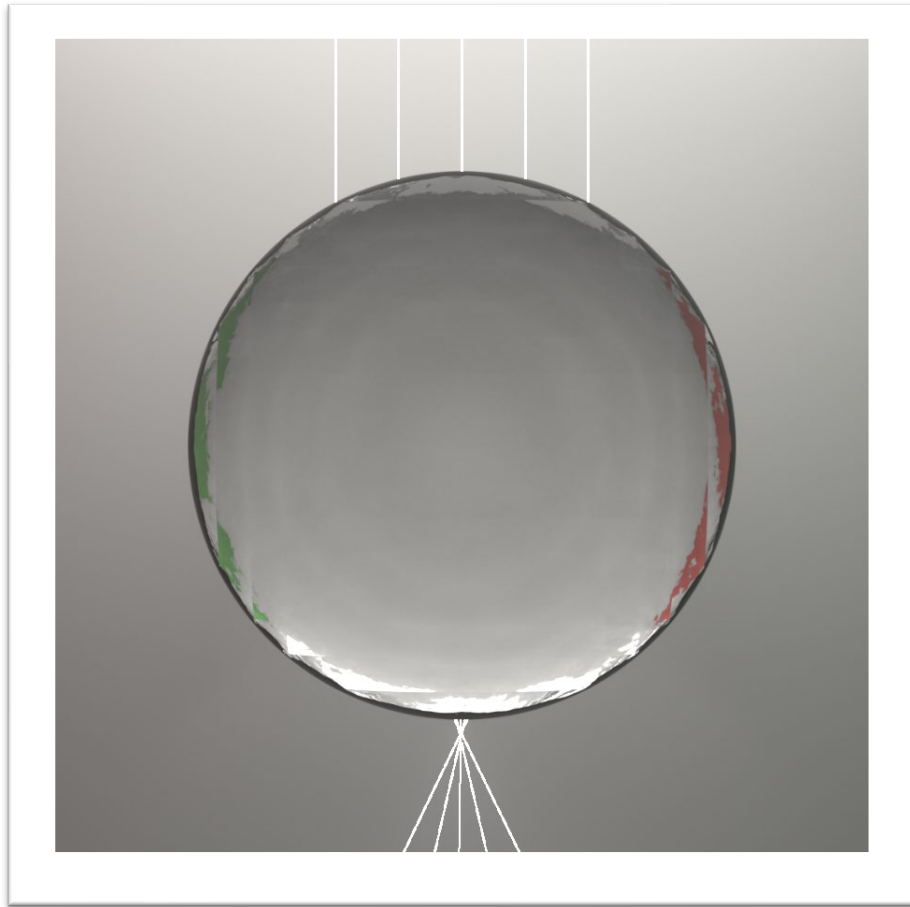
$$\lambda_{i-1} = \lambda_i + (\nabla \eta(\mathbf{x}_{i-1}) (\nabla \eta(\mathbf{x}_{i-1}))^\top + \eta(\mathbf{x}_{i-1}) \text{Hess}(\eta(\mathbf{x}_{i-1}))) \mu_i \Delta \sigma, \quad (30)$$

$$\mu_{i-1} = \mu_i + \lambda_{i-1} \Delta \sigma. \quad (31)$$

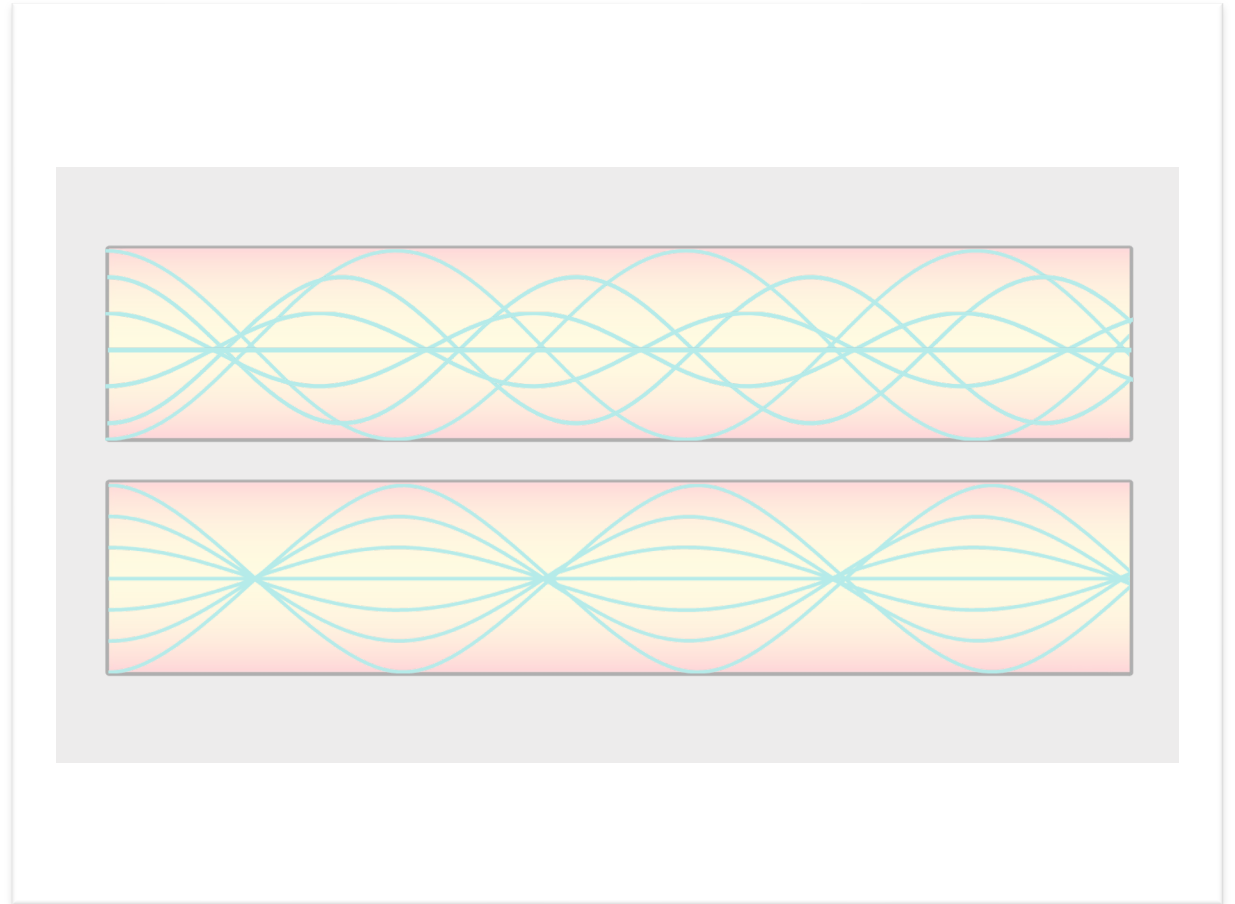
$\eta \nabla \eta$

$\eta \nabla \eta$

Optimizing Gradient-Index (GRIN) Optics

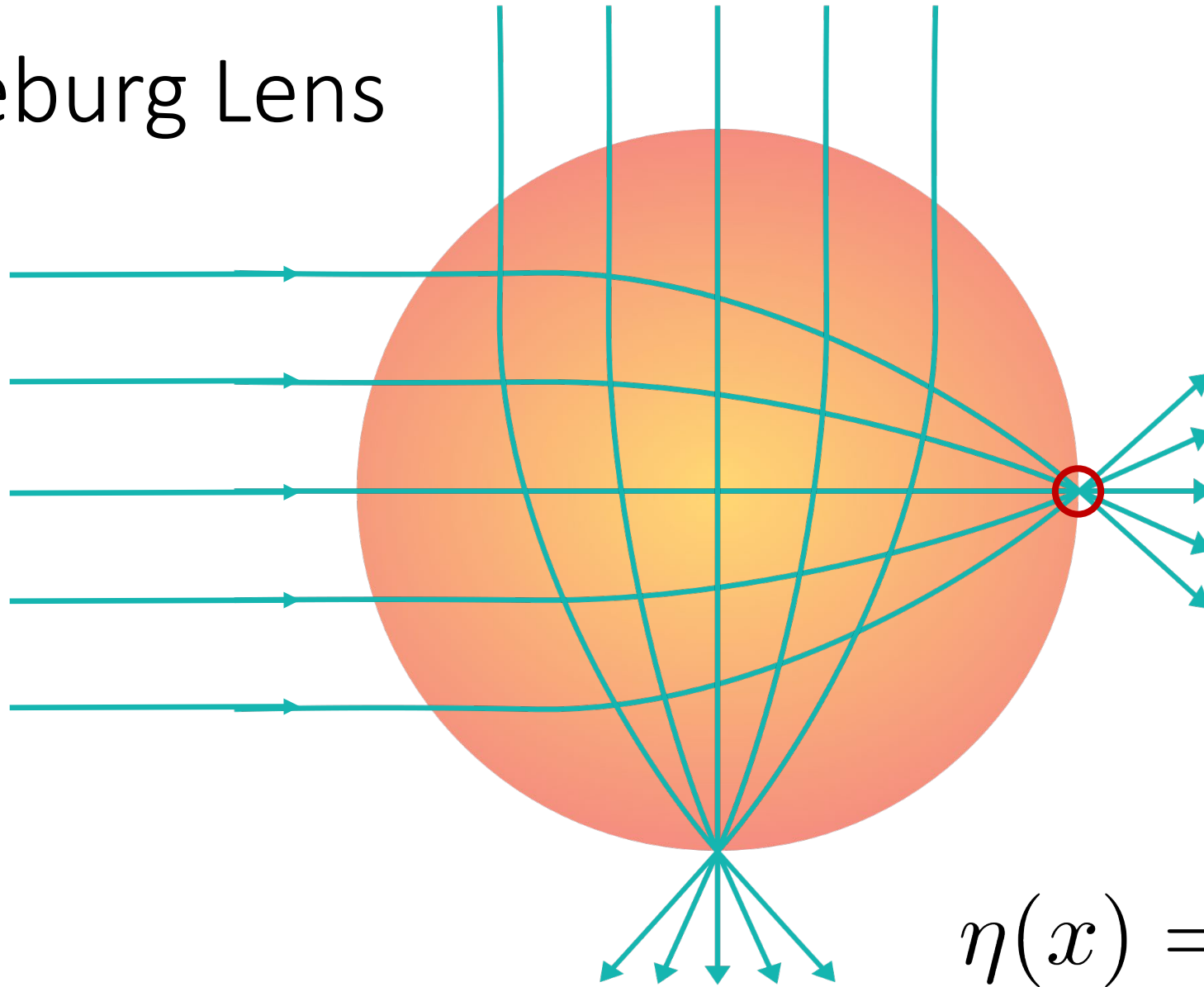


Luneburg Lens



GRIN Fiber

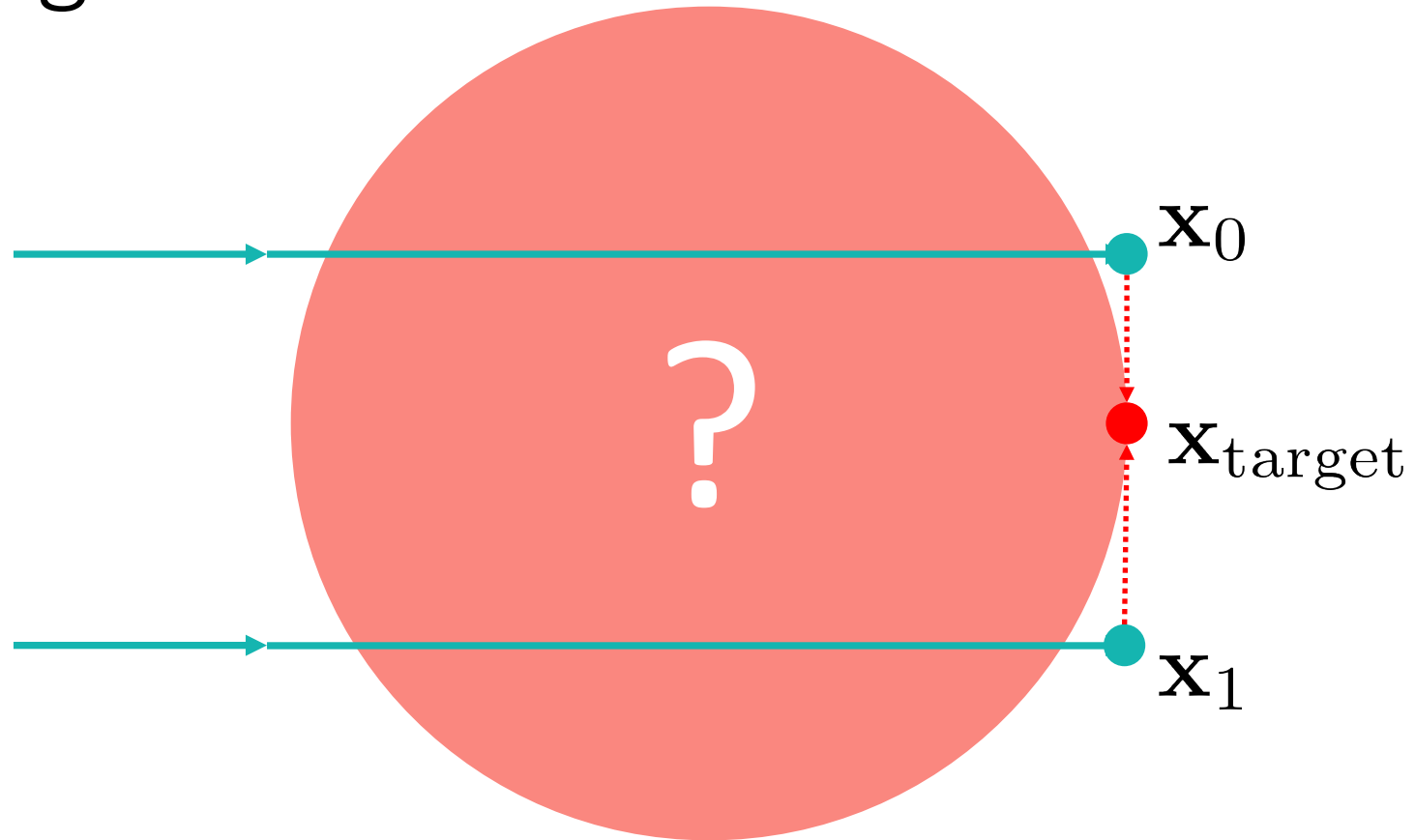
Luneburg Lens



$$\eta(x) = \sqrt{2 - \|x\|^2}$$

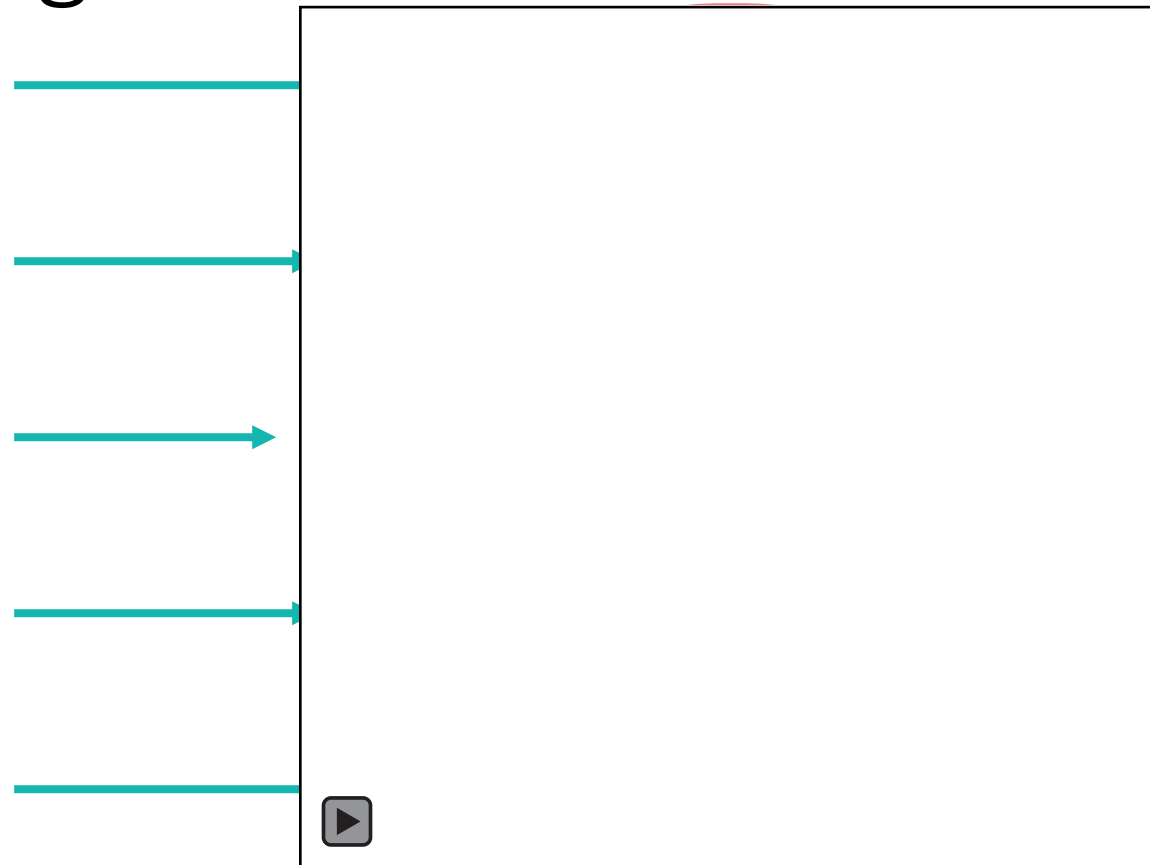
[Luneburg, R. K. 1944]

Luneburg Lens

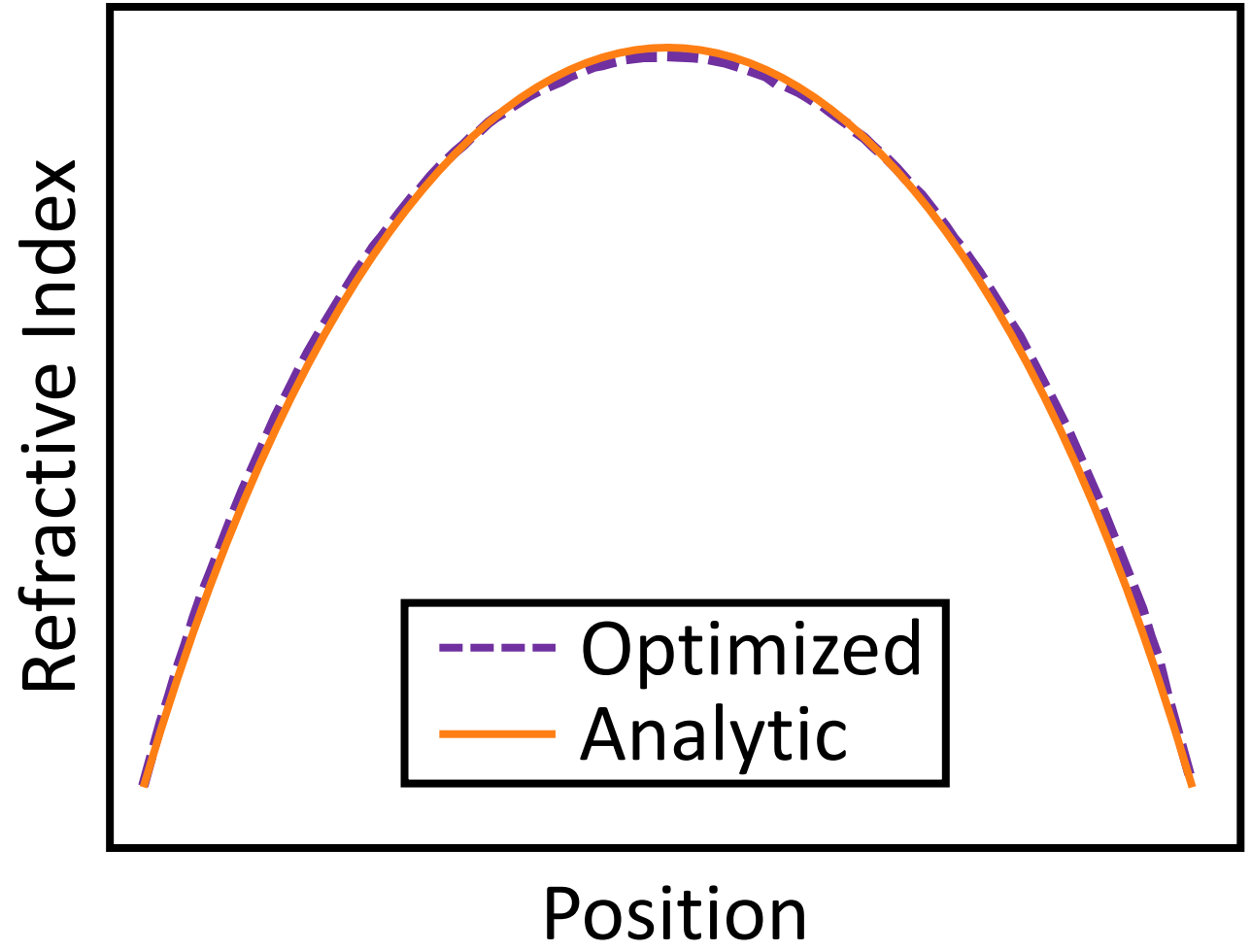
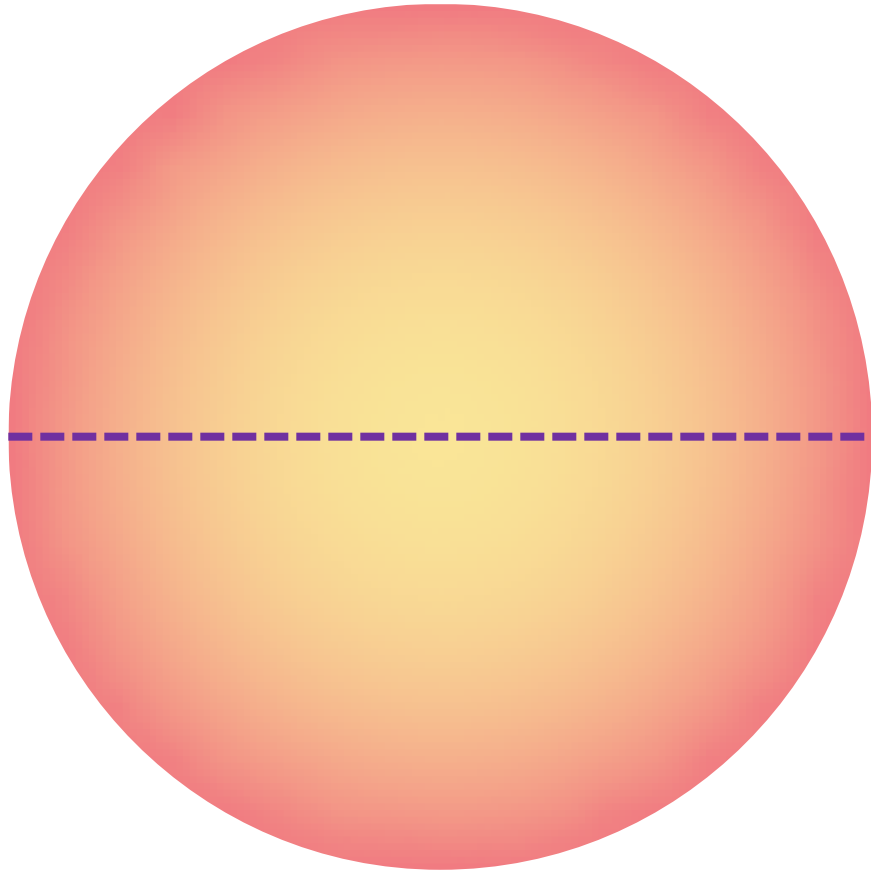


$$\min_{\eta} \sum_{i \in \text{rays}} \|\mathbf{x}_{\text{target}} - \mathbf{x}_i\|^2$$

Luneburg Lens



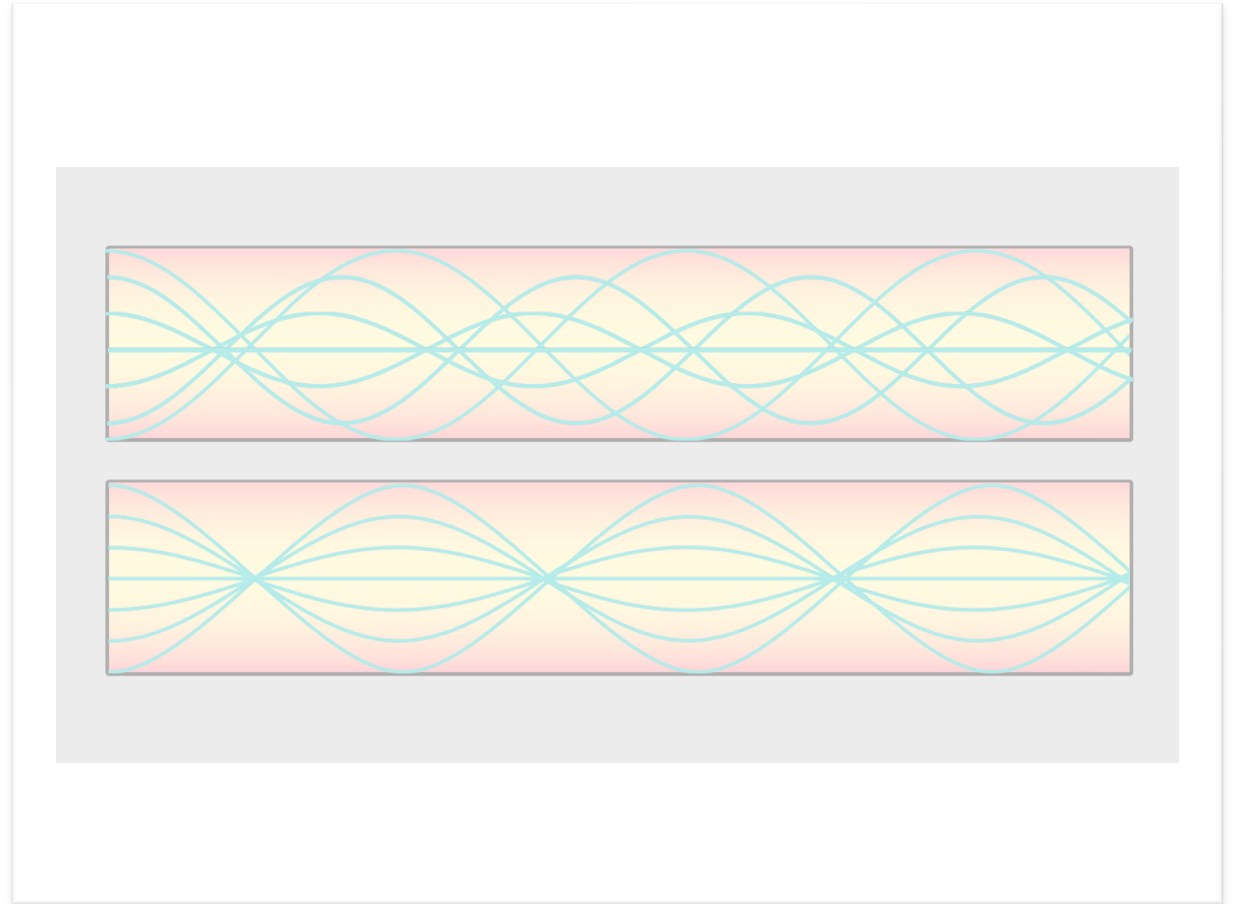
Luneburg Lens



Optimizing Gradient-Index (GRIN) Optics

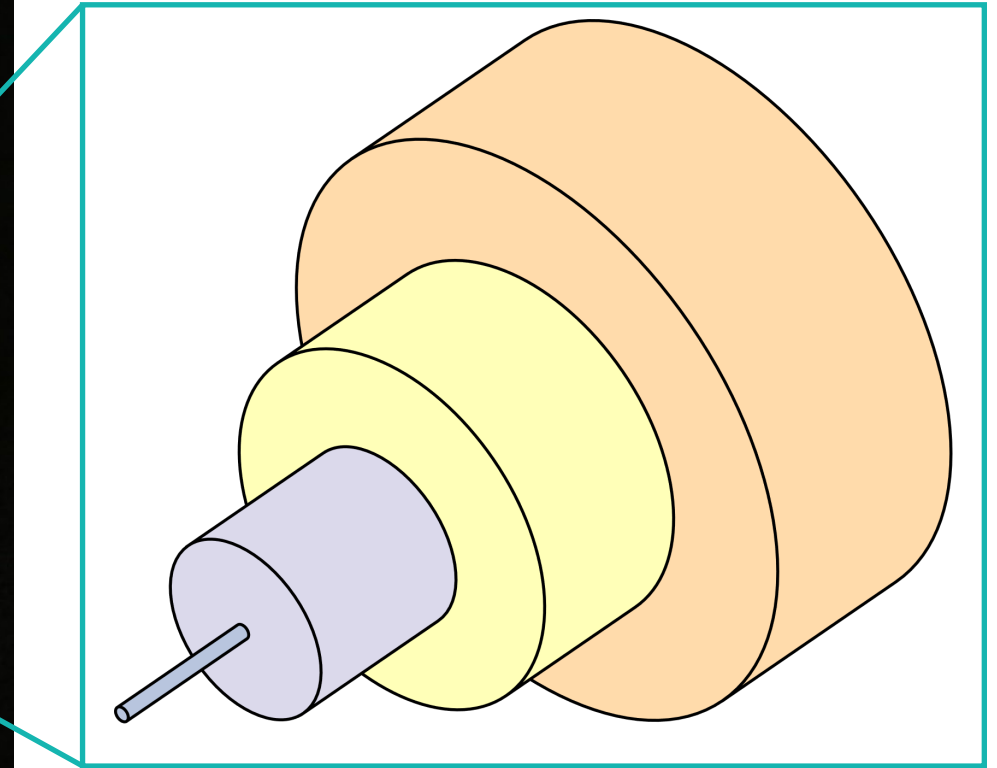
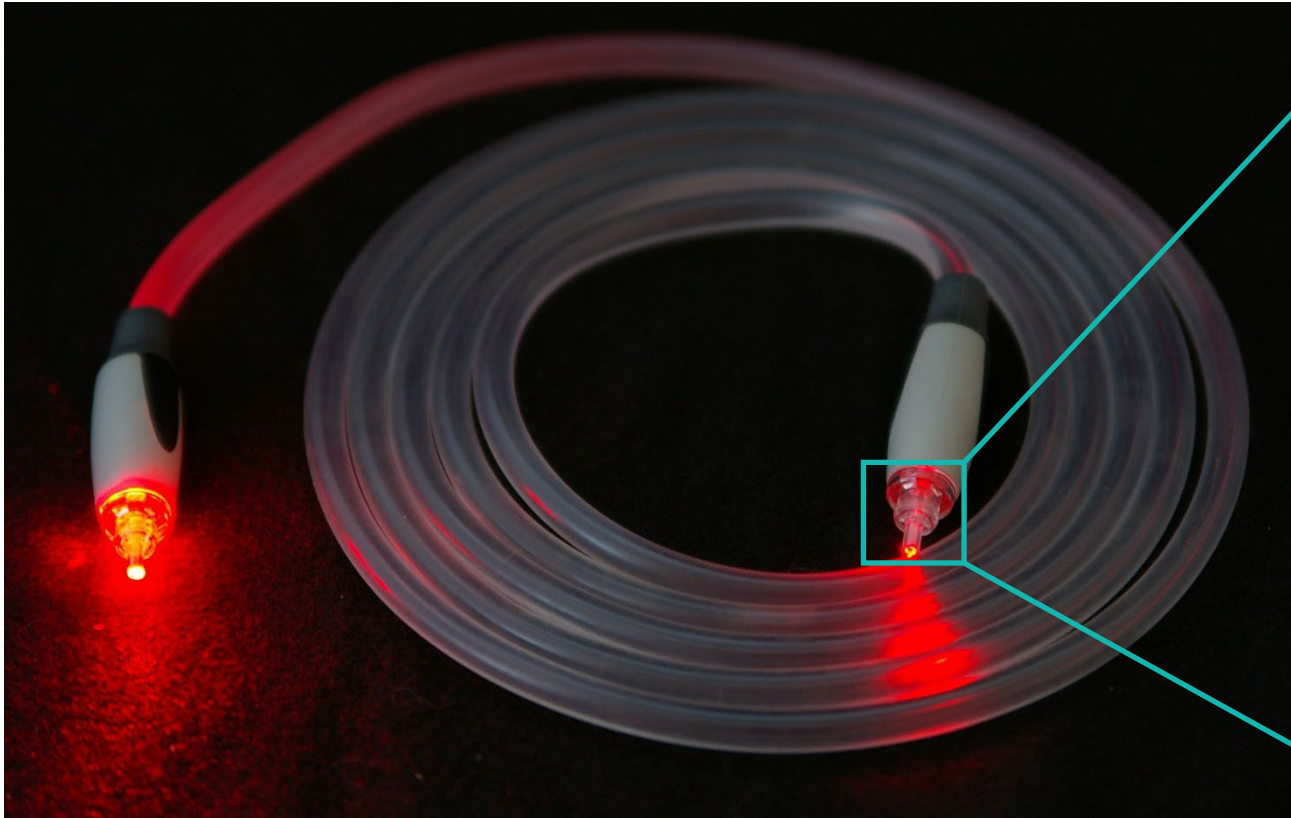


Luneburg Lens



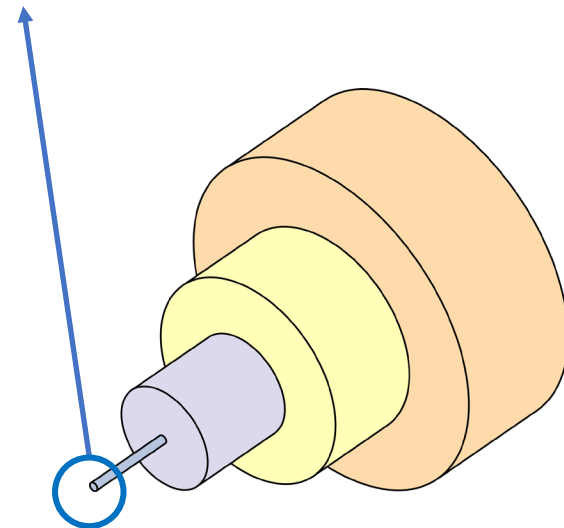
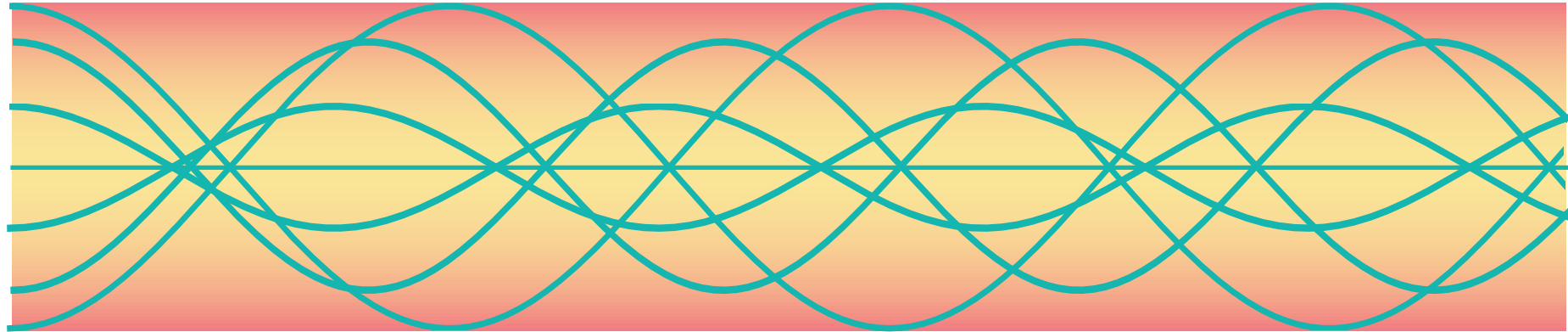
GRIN Fiber

GRIN Fiber



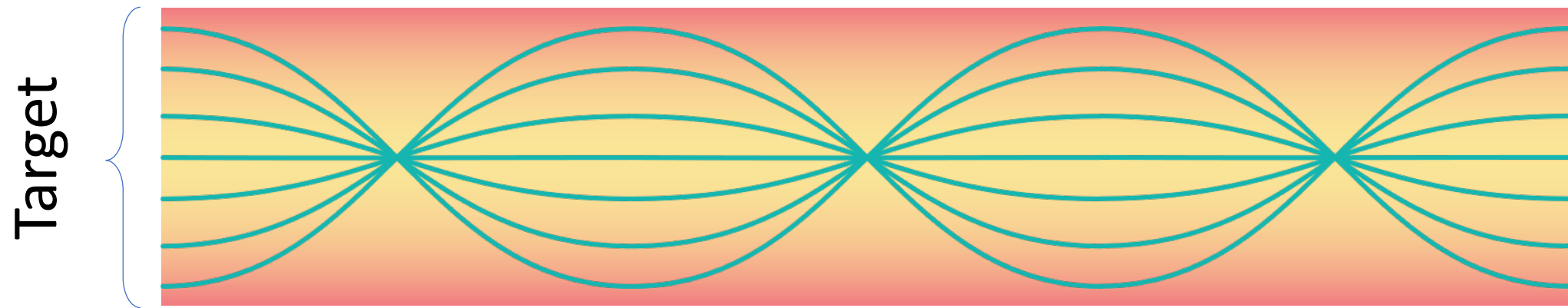
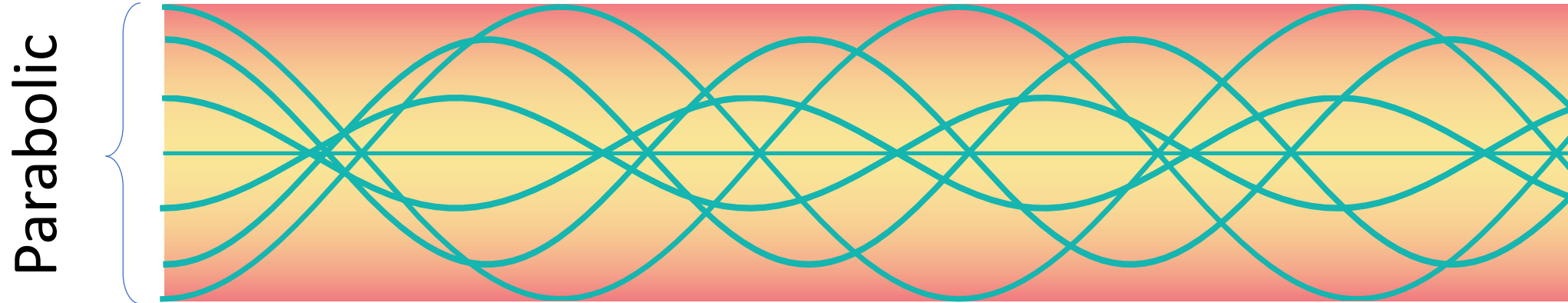
GRIN Fiber

Modal dispersion

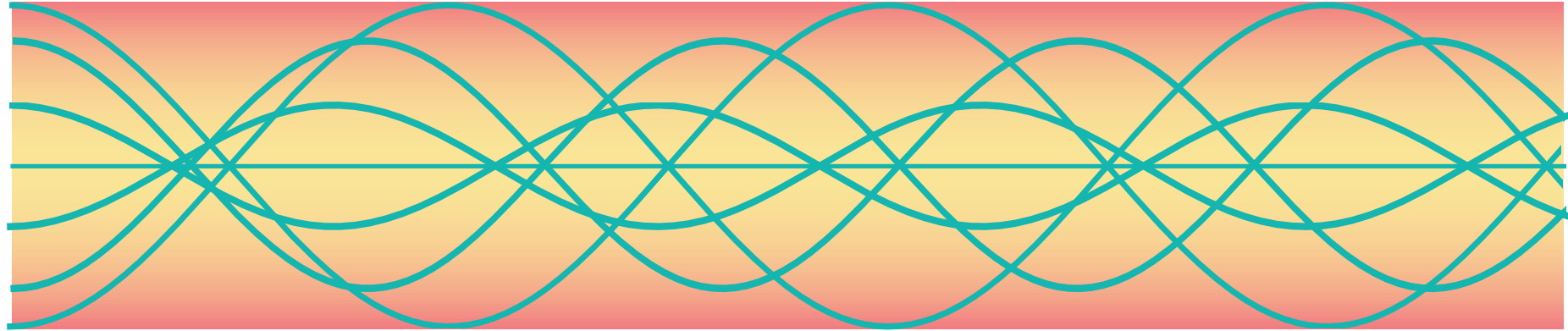


GRIN Fiber

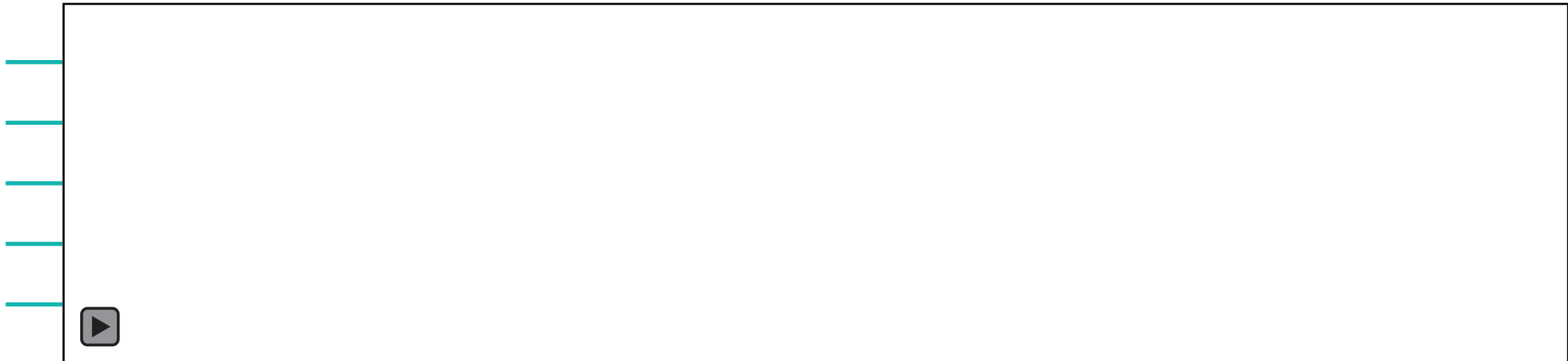
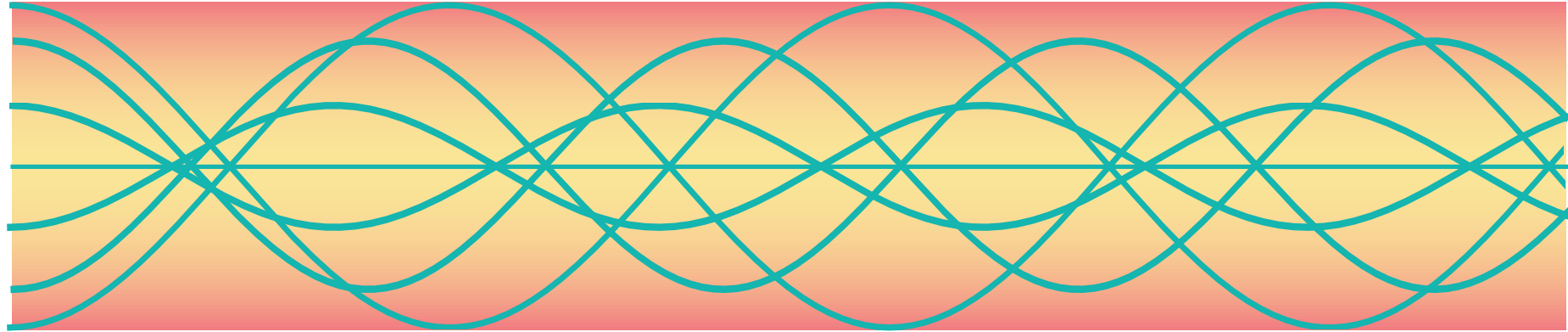
Modal dispersion



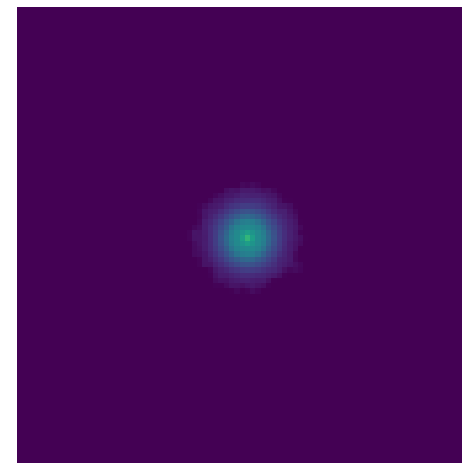
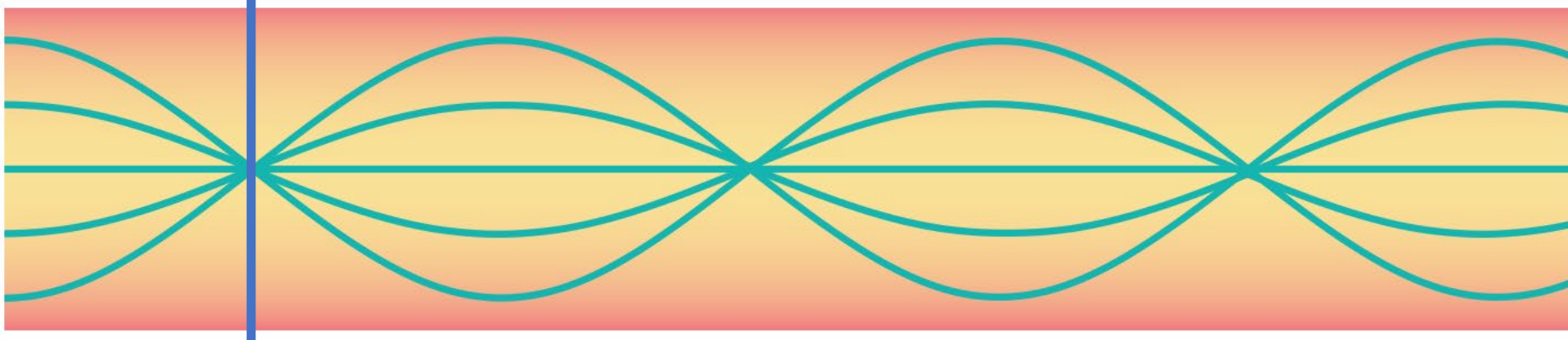
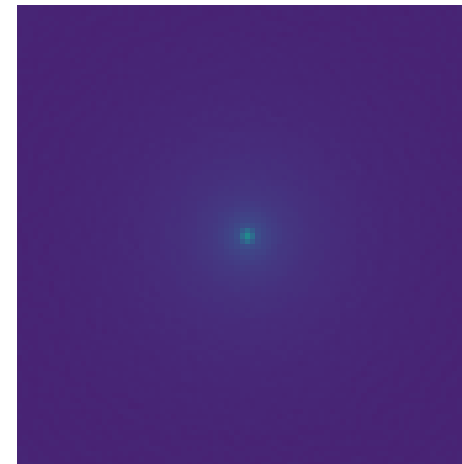
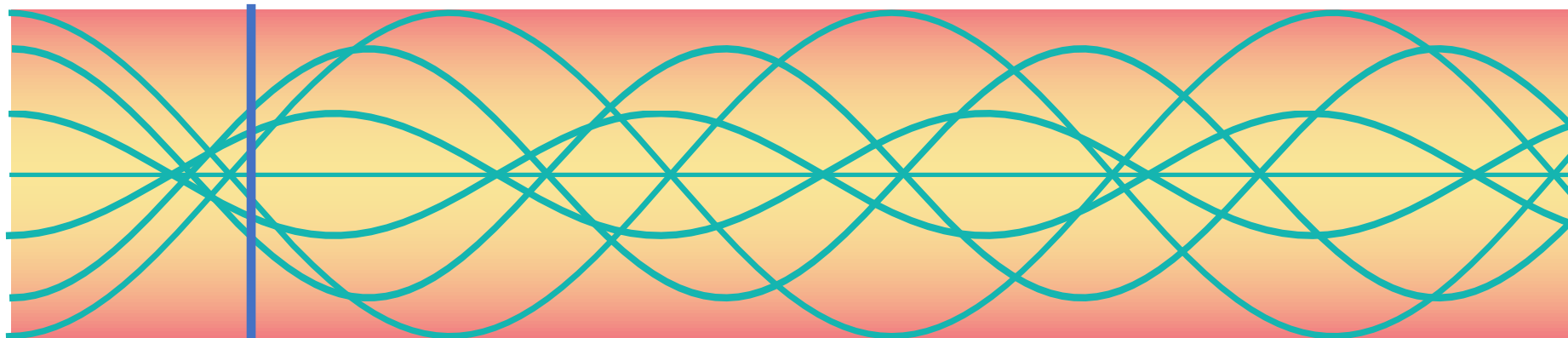
GRIN Fiber



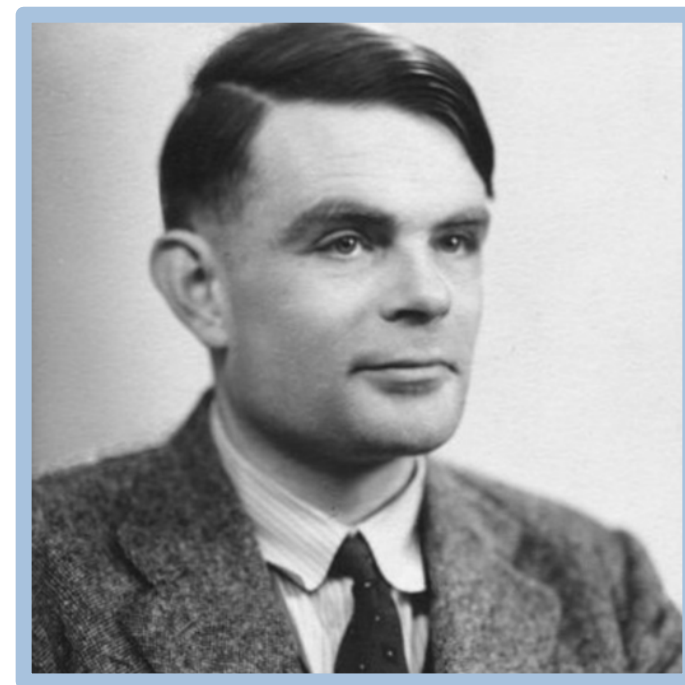
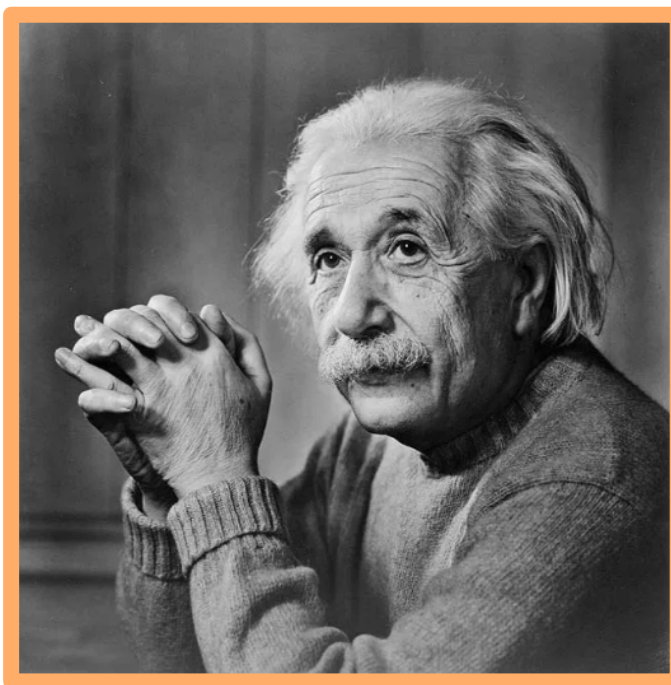
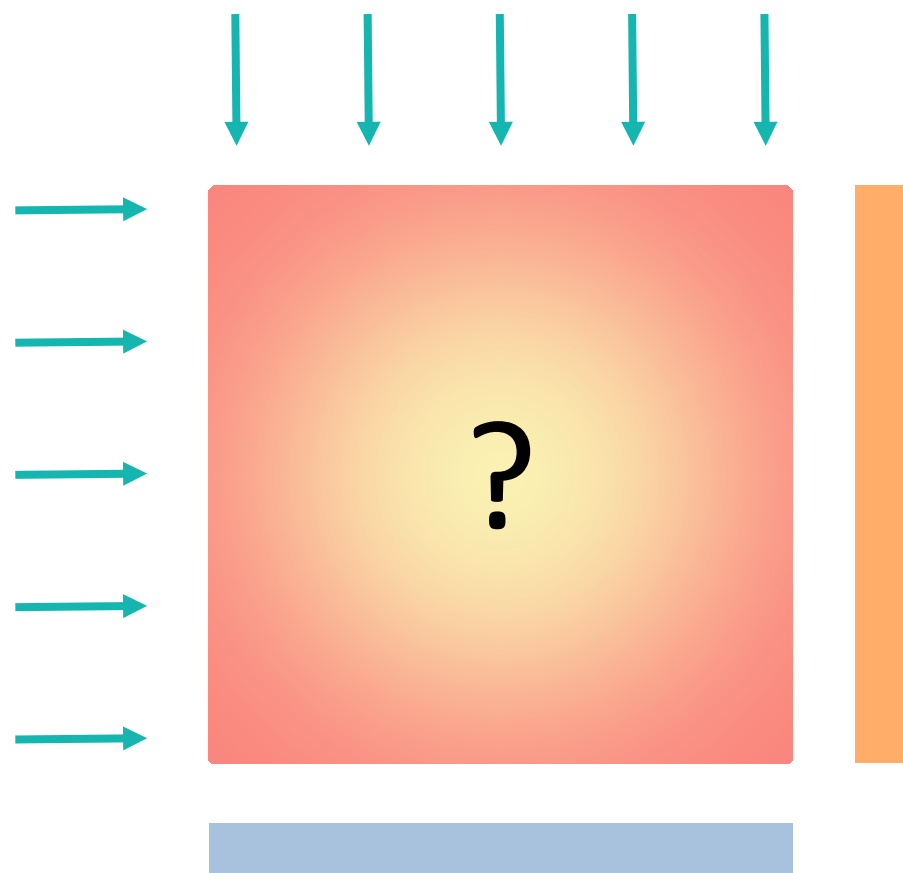
GRIN Fiber



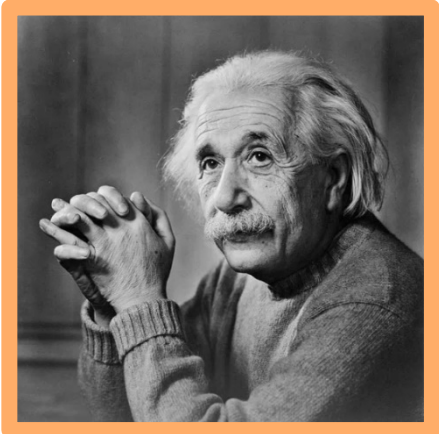
GRIN Fiber



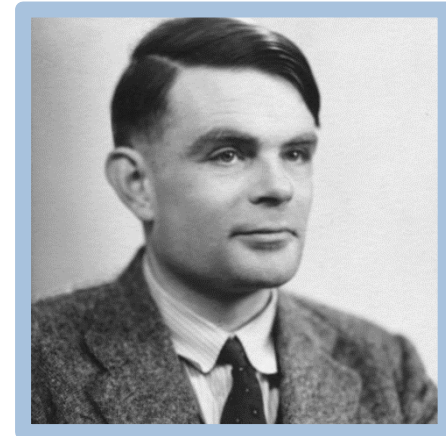
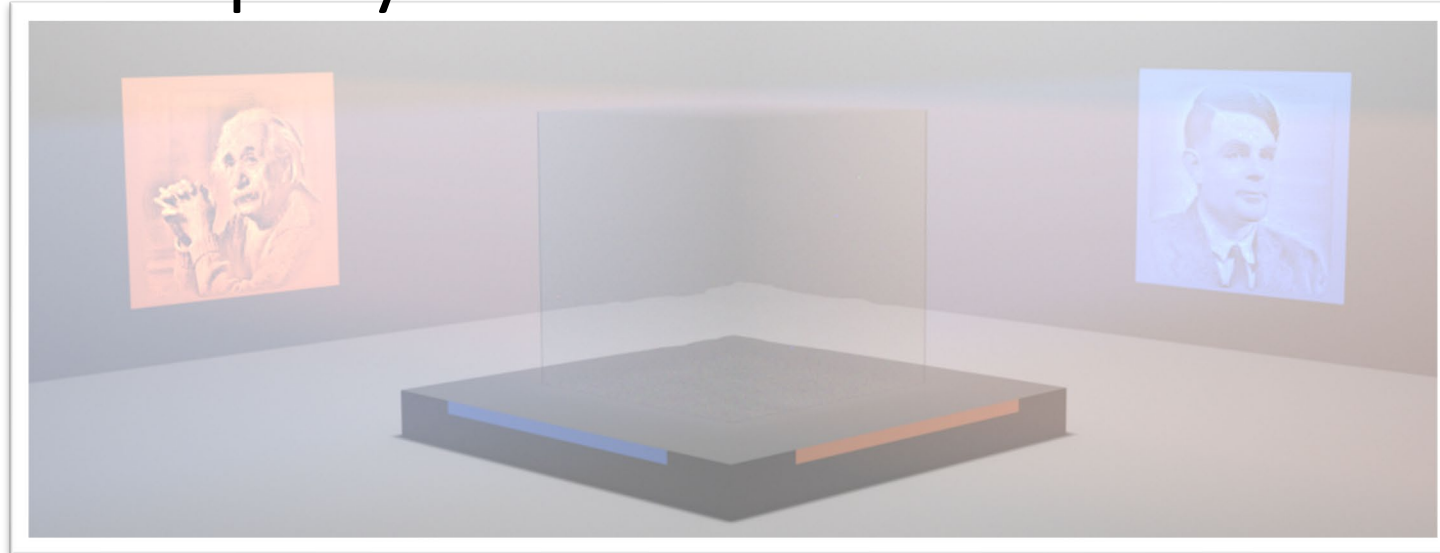
Multiview Display



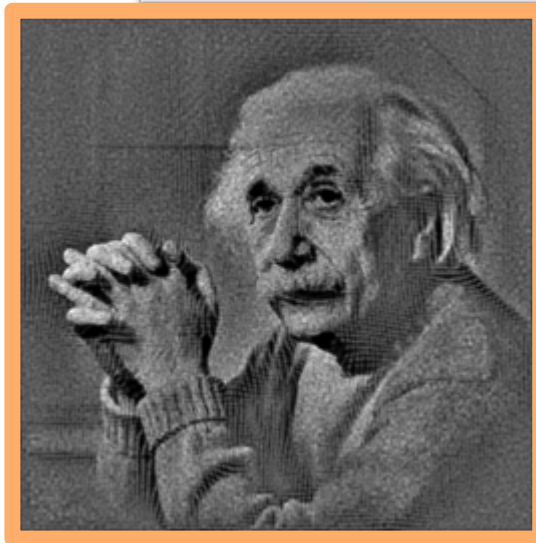
Multiview Display



Target



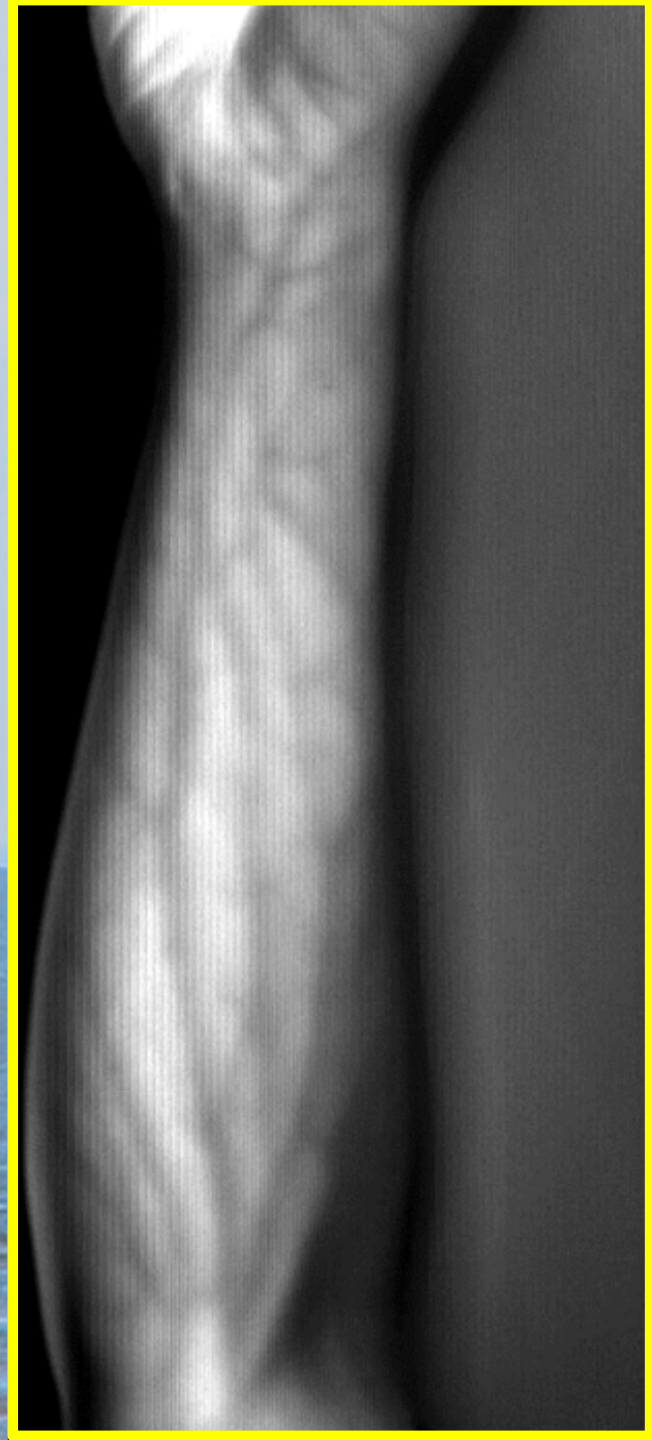
Target



optimization
results



Media with continuously varying refractive index and scattering



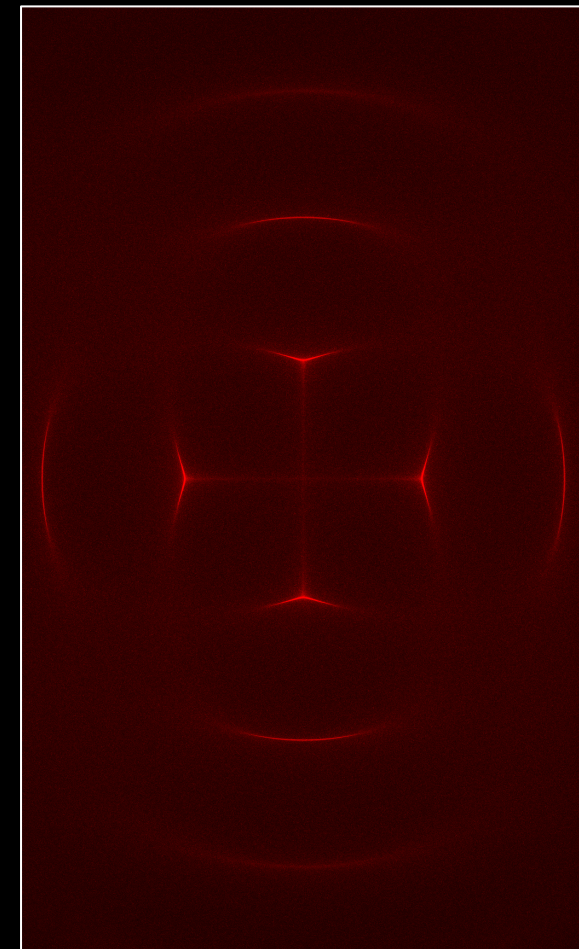
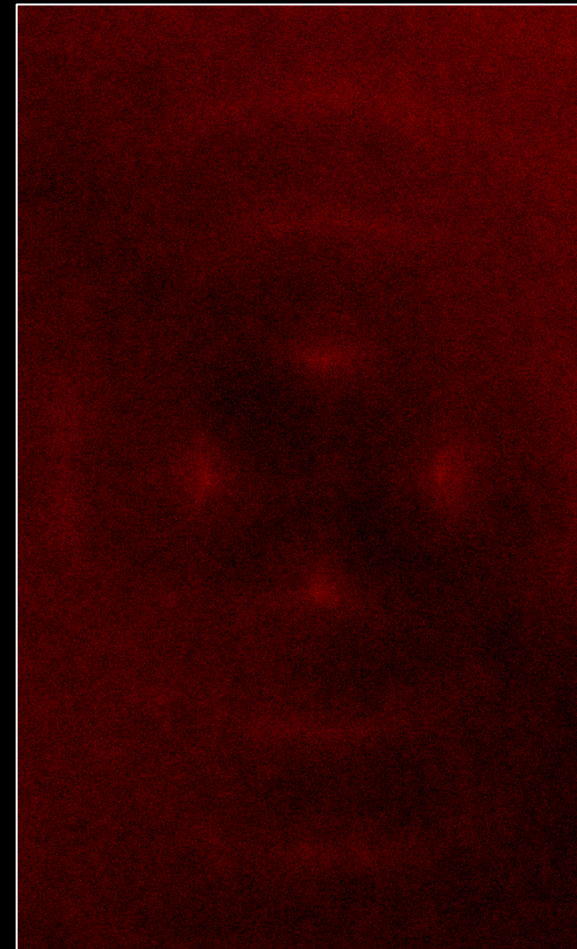
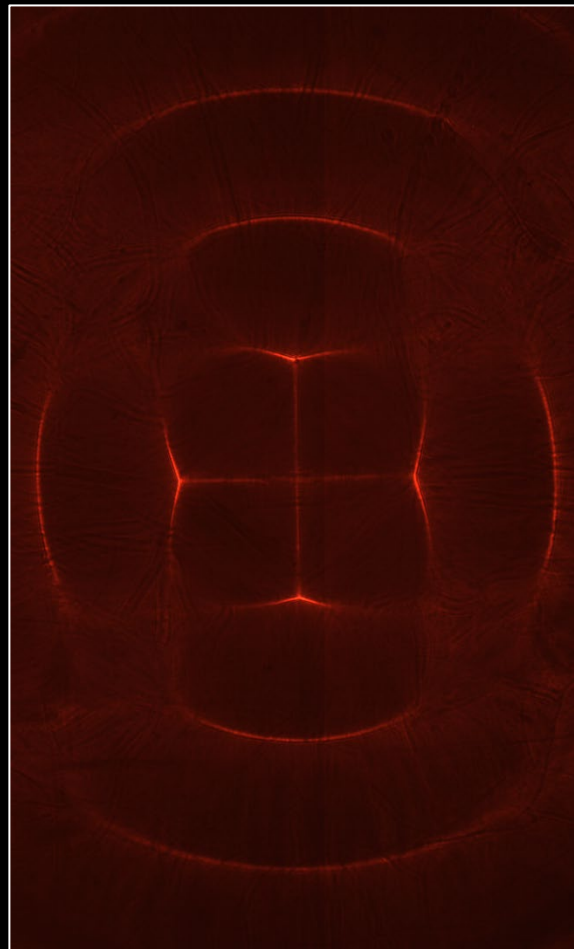
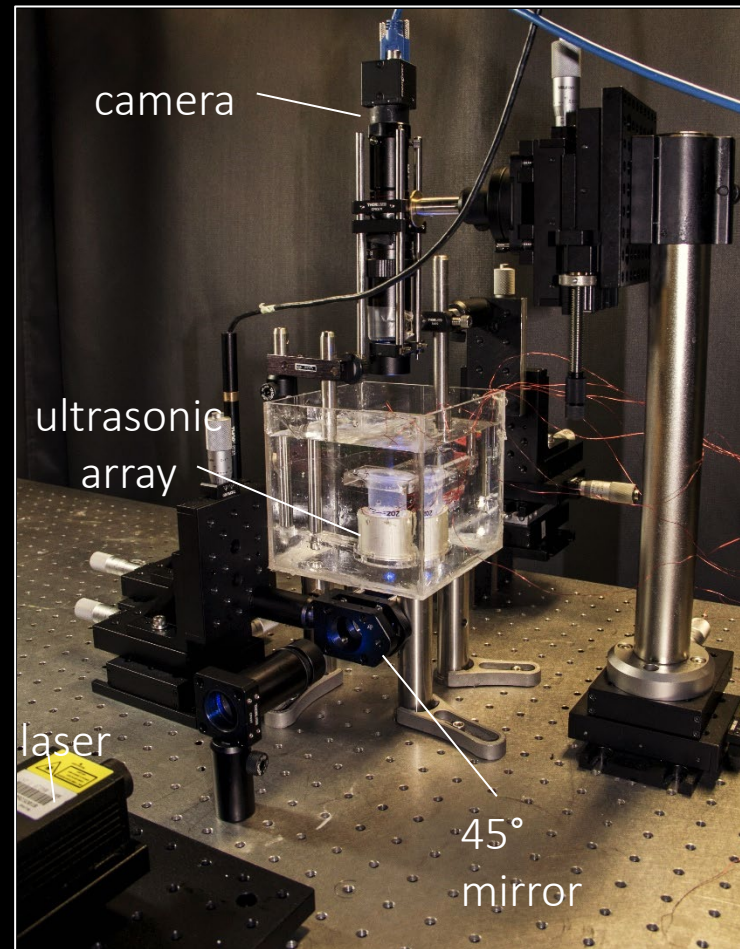
unbiased techniques for scientific imaging

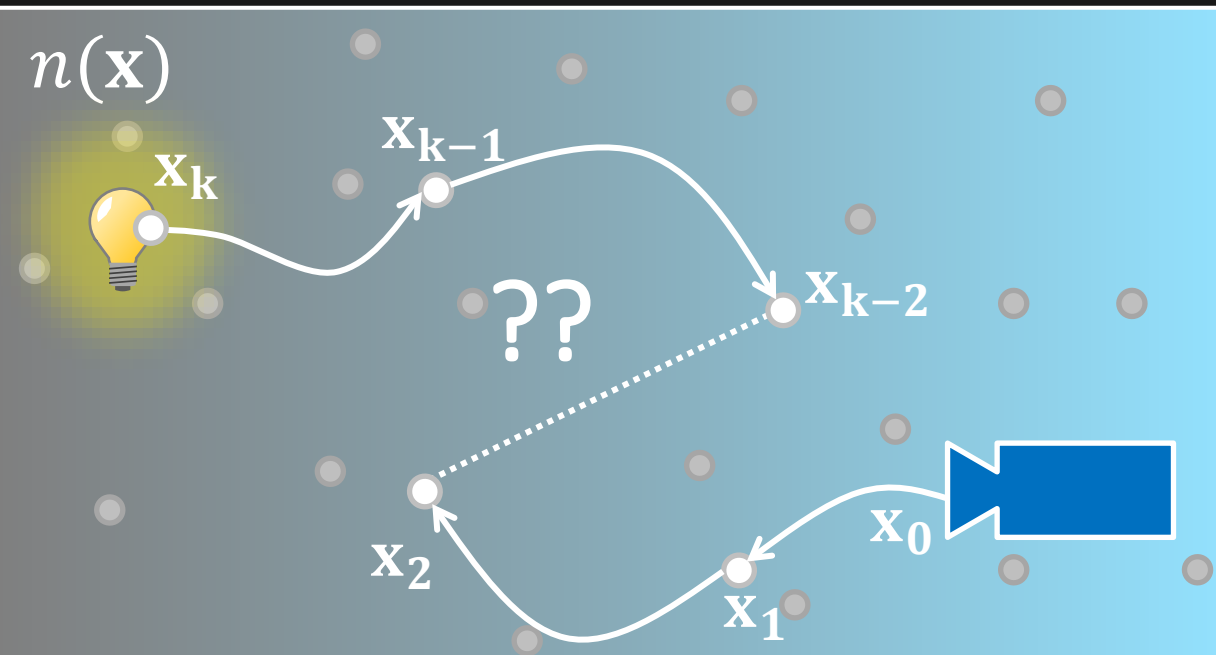
experimental
hardware

experimental
capture

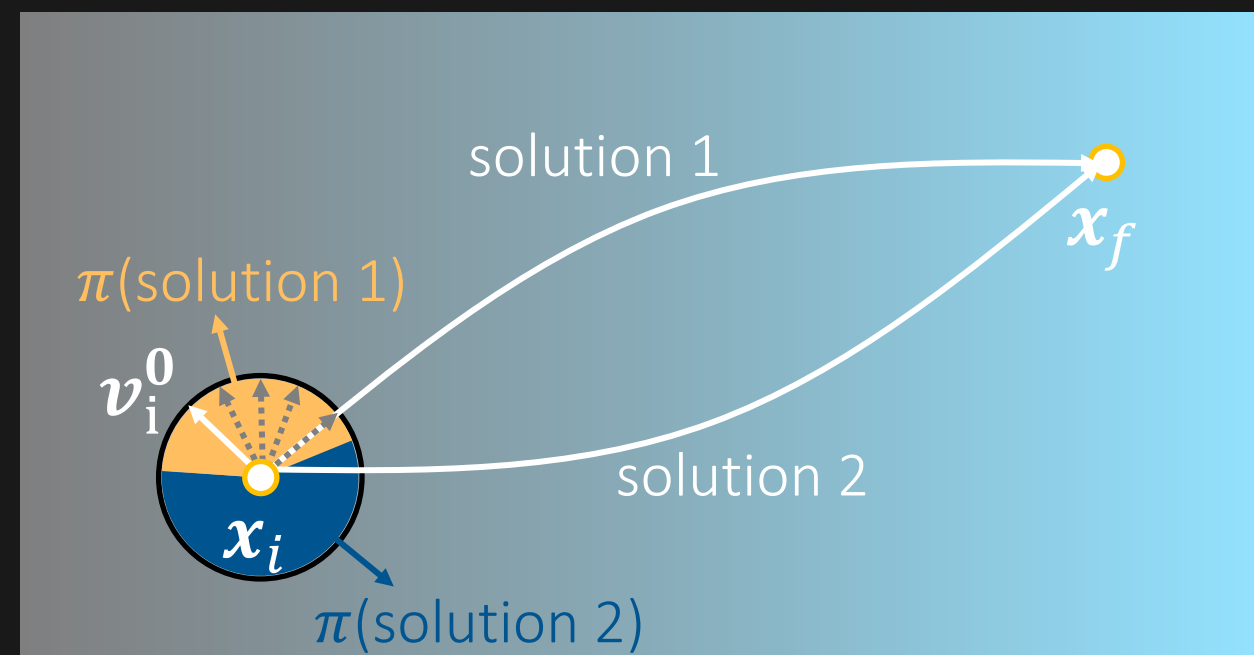
photon mapping

unbiased (ours)

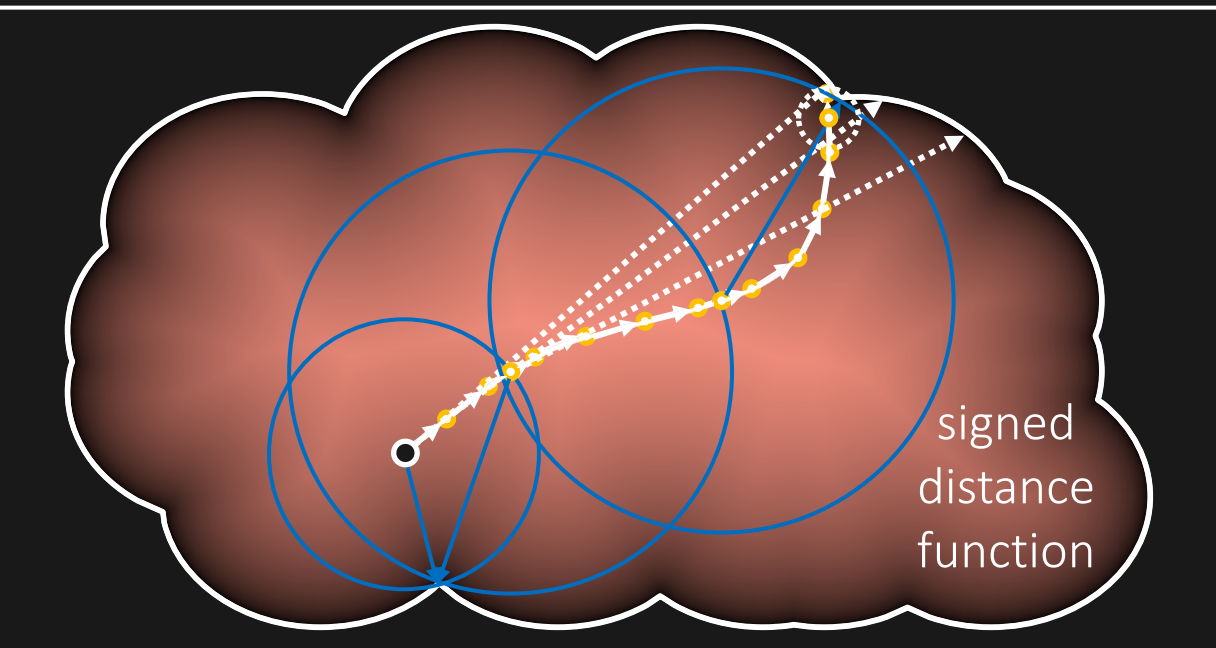




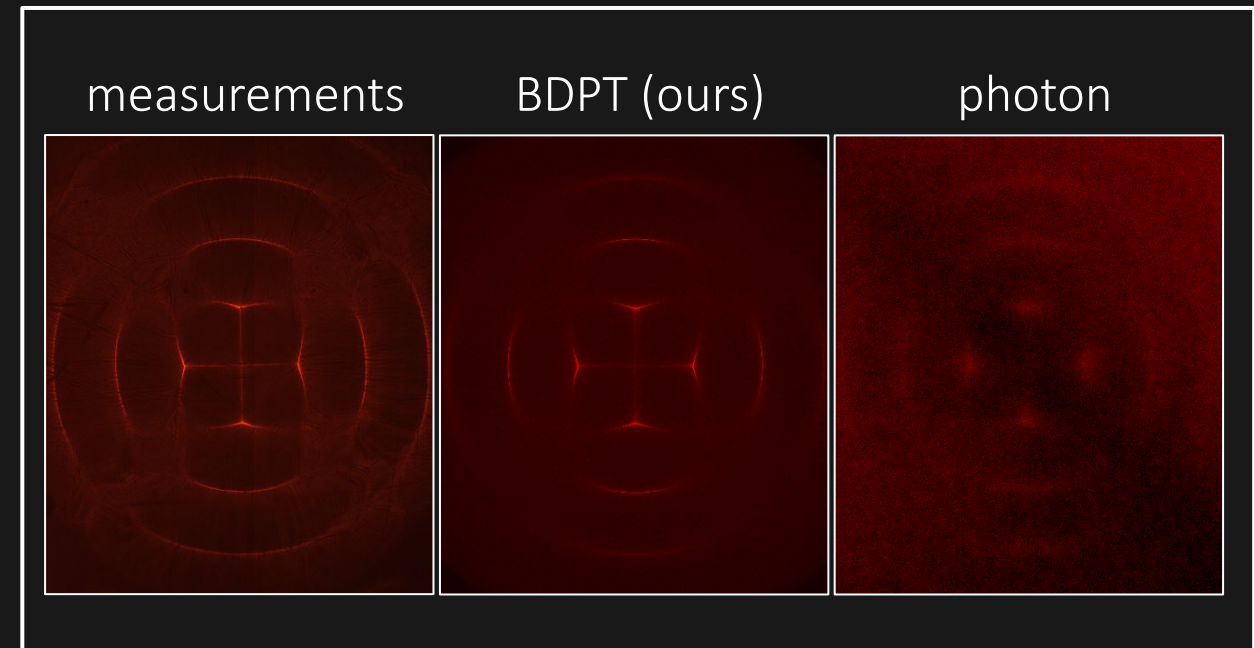
1. background on refractive radiative transfer equation



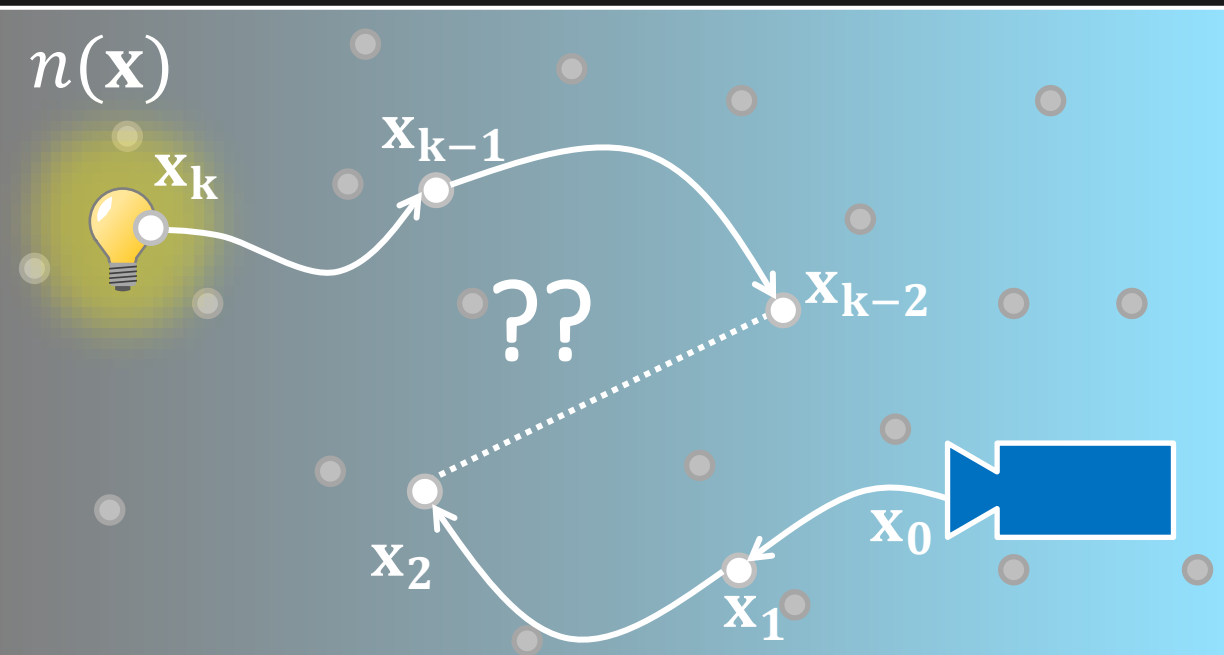
2. direct connections: our solution to unbiased rendering



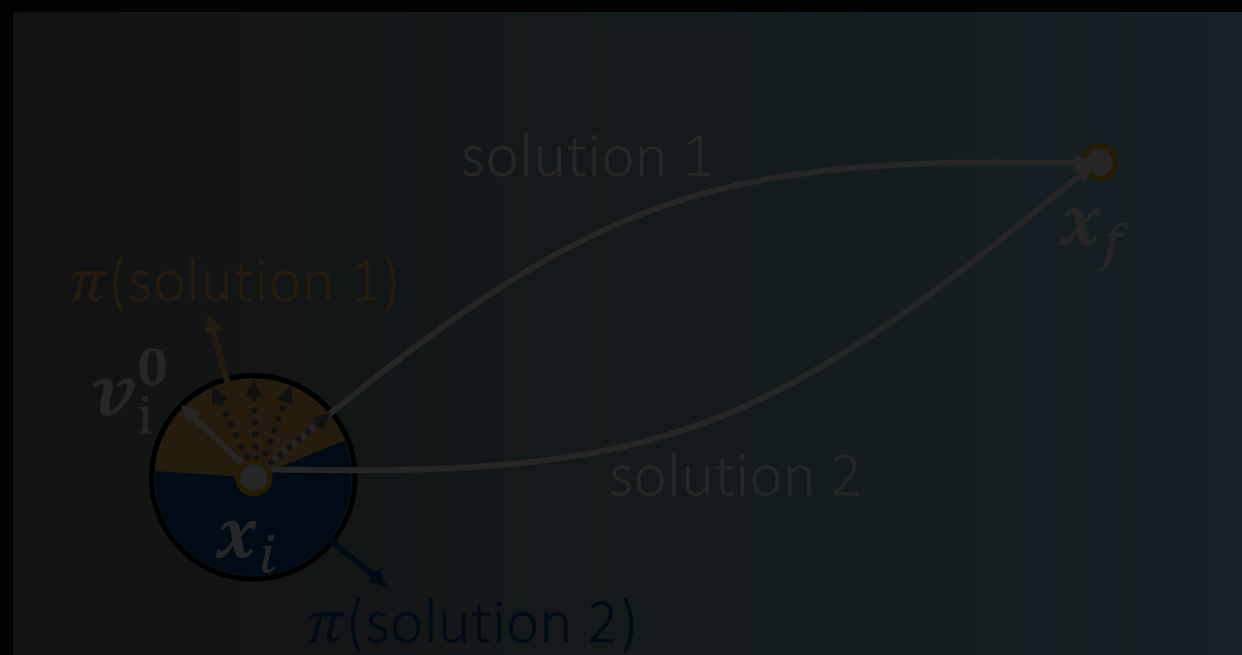
3. acceleration techniques



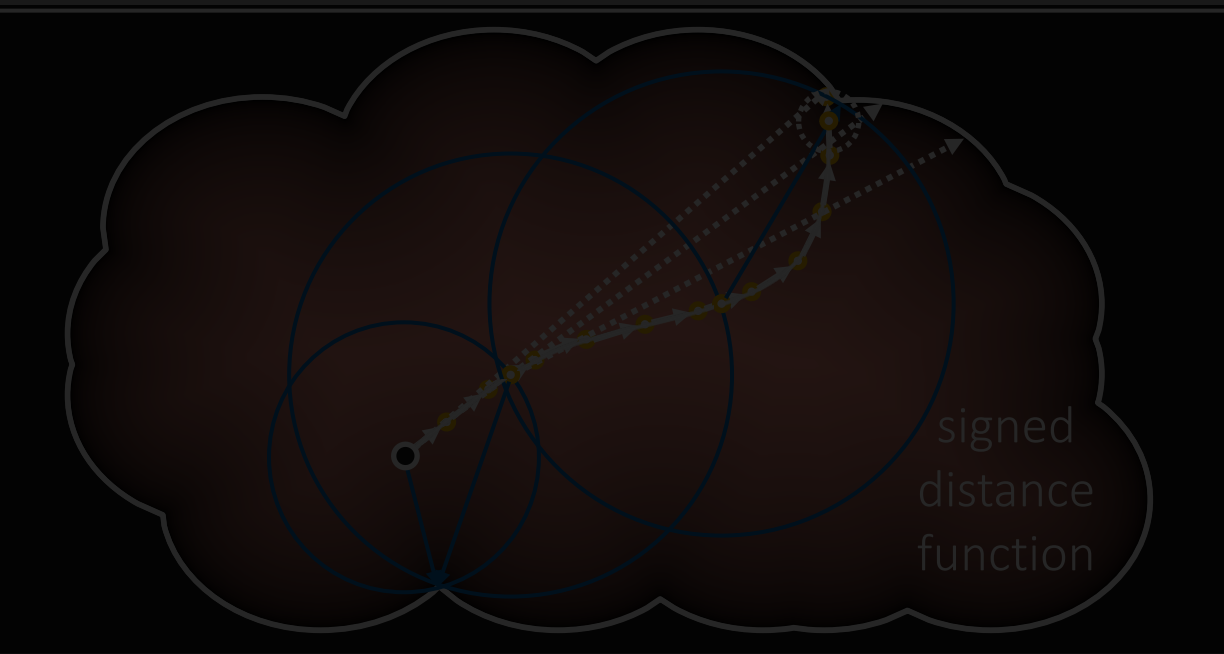
4. experiments



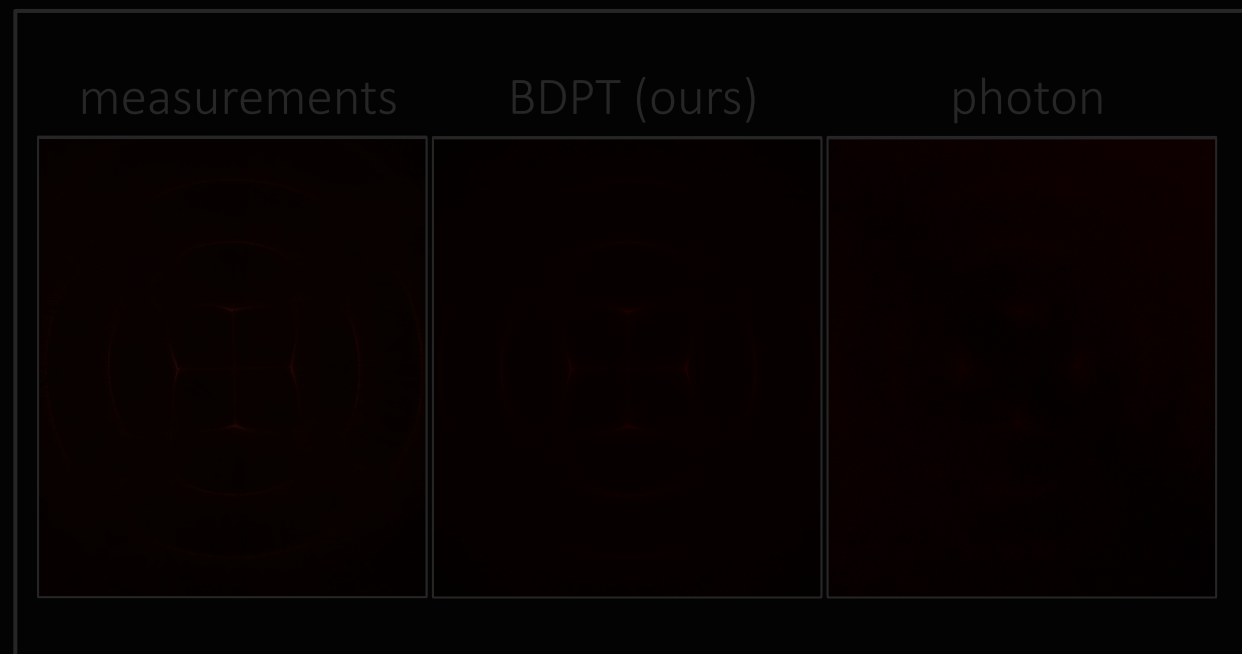
1. background on refractive radiative transfer equation



2. direct connections: our solution to unbiased rendering

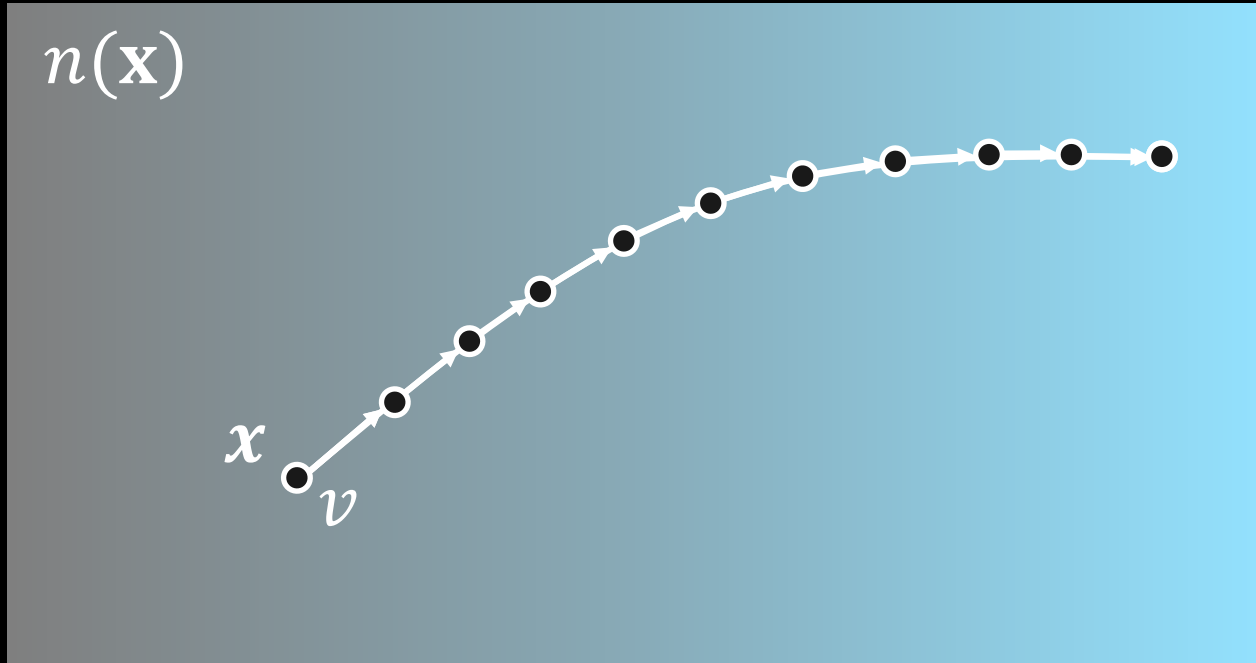


3. acceleration techniques



4. experiments

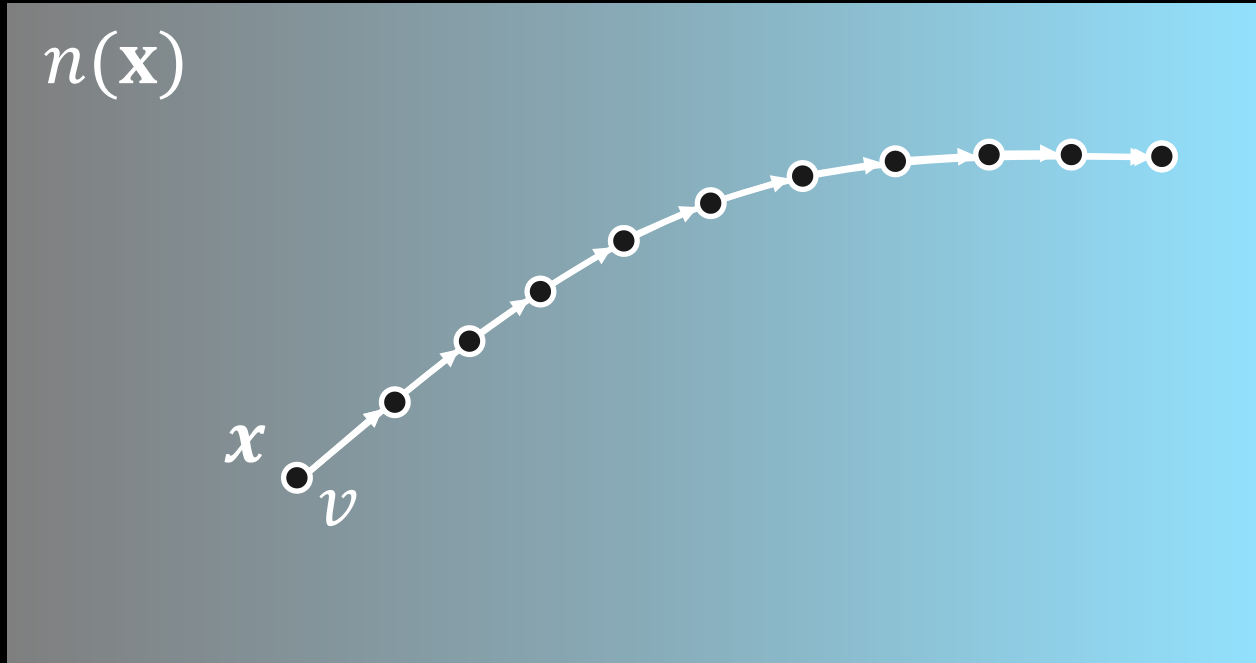
continuous refraction and no scattering



Hamilton's equations for refractive ray tracing

$$\frac{d\mathbf{v}}{ds} = \nabla_{\mathbf{x}} n(\mathbf{x})$$
$$\frac{d\mathbf{x}}{ds} = \frac{\mathbf{v}}{n(\mathbf{x})}$$

continuous refraction and no scattering



Hamilton's equations for refractive ray tracing

$$\frac{d\mathbf{v}}{ds} = \nabla_{\mathbf{x}} n(\mathbf{x})$$

solved using symplectic integration

$$\frac{d\mathbf{x}}{ds} = \frac{\mathbf{v}}{n(\mathbf{x})}$$

scattering and no continuous refraction



radiative transfer equation (RTE)

$$\frac{dL}{ds} = \sigma_a L_e - (\sigma_a + \sigma_s)L + \frac{\sigma_s}{4\pi} \int f_s(\omega', \omega) L d\omega'$$

scattering and no continuous refraction

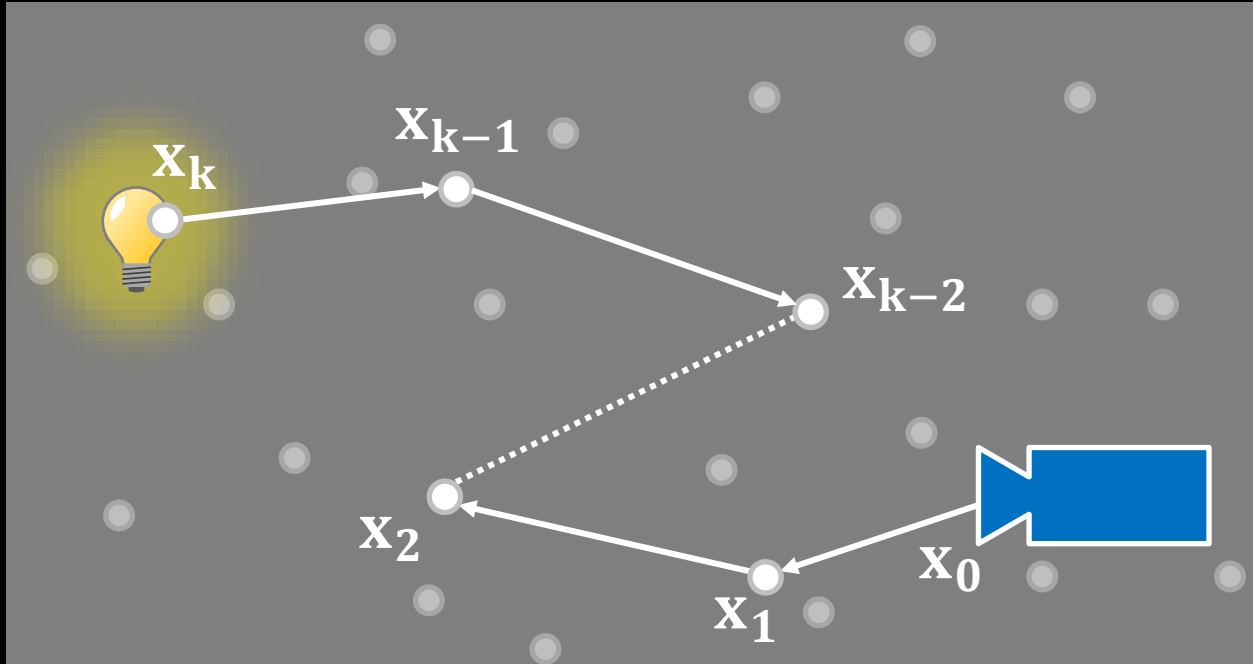


radiative transfer equation (RTE)

$$\frac{dL}{ds} = \sigma_a L_e - (\sigma_a + \sigma_s)L + \frac{\sigma_s}{4\pi} \int f_s(\omega', \omega) L d\omega'$$

solved using Monte Carlo integration

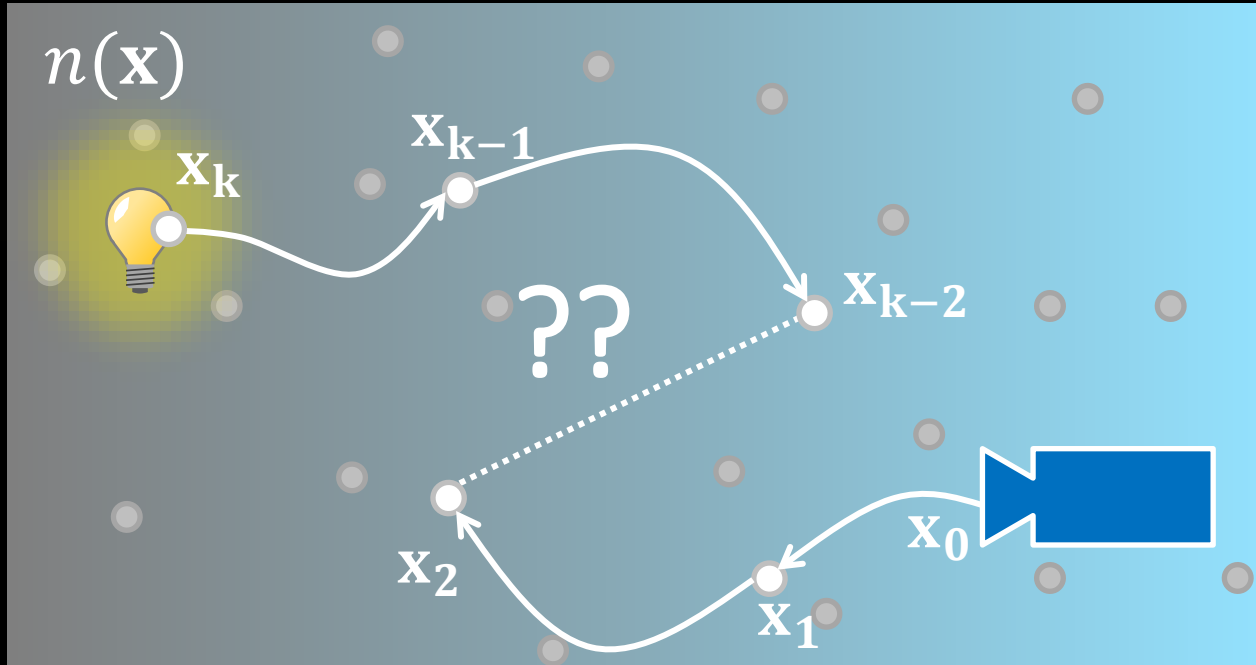
scattering and no continuous refraction



bidirectional path tracing (BDPT):

1. trace a random sensor subpath
2. trace a random emitter subpath
3. join vertices with a straight line

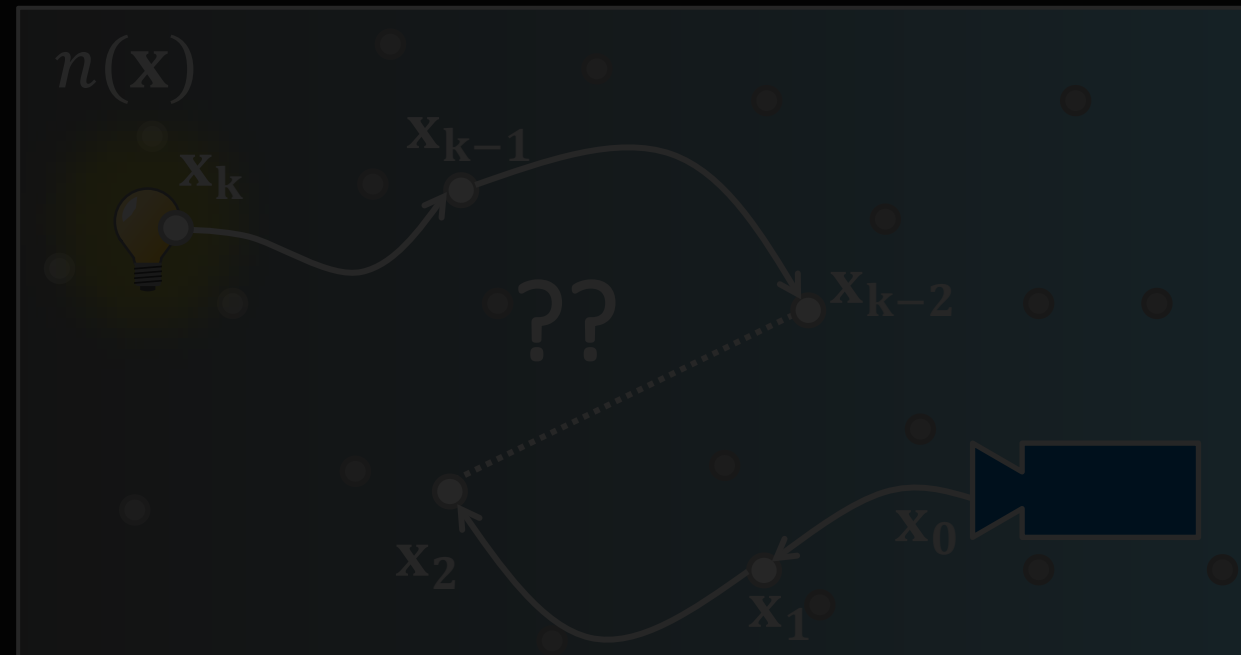
continuous refraction and scattering



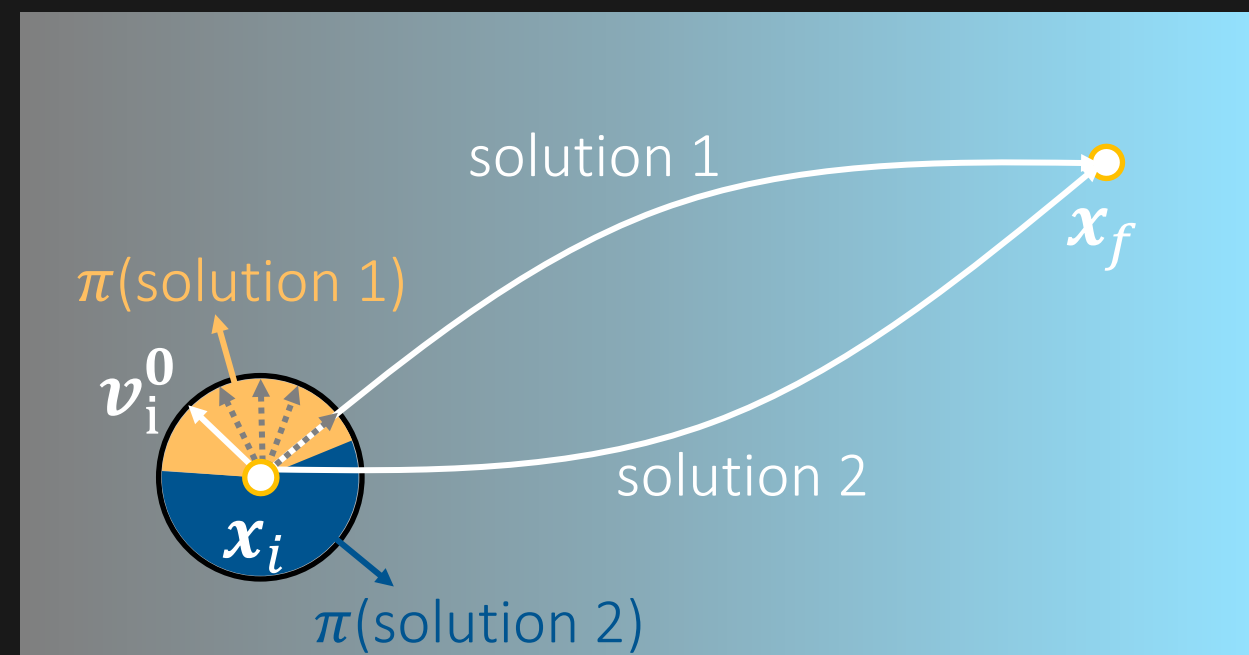
bidirectional path tracing (BDPT):

1. trace a random sensor subpath
use refractive ray tracing
2. trace a random emitter subpath

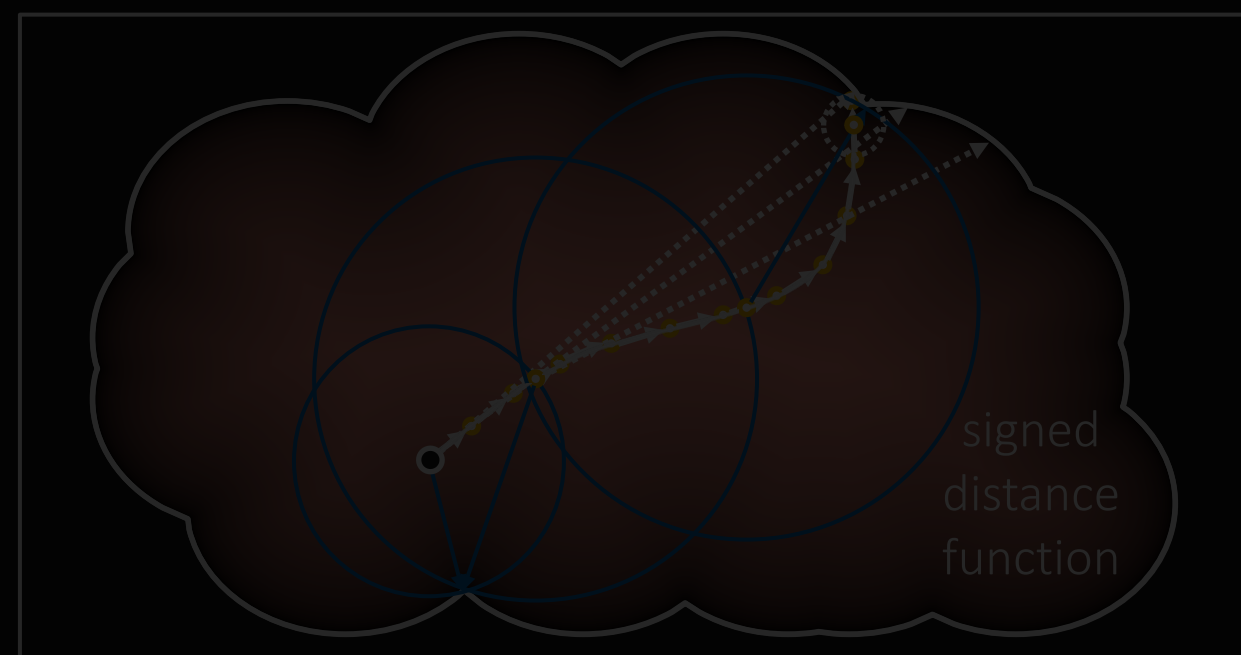
3. join vertices with a ~~straight line~~ curve



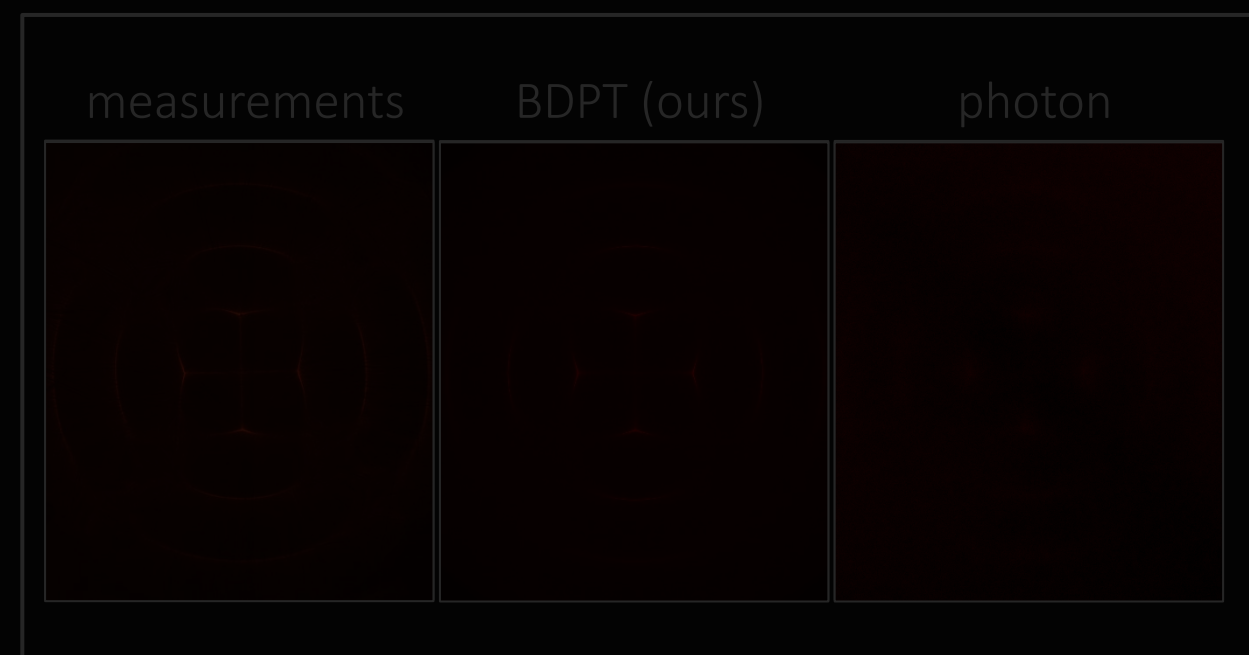
1. background on refractive radiative transfer equation



2. direct connections: our solution to unbiased rendering



3. acceleration techniques



4. experiments

direct connections



we have to solve this:

$$\frac{d\mathbf{v}}{ds} = \nabla_{\mathbf{x}} n(\mathbf{x}), \quad \frac{d\mathbf{x}}{ds} = \frac{\mathbf{v}}{n(\mathbf{x})}$$

boundary conditions: $\mathbf{x}_i, \mathbf{x}_f$

boundary value problem (BVP)

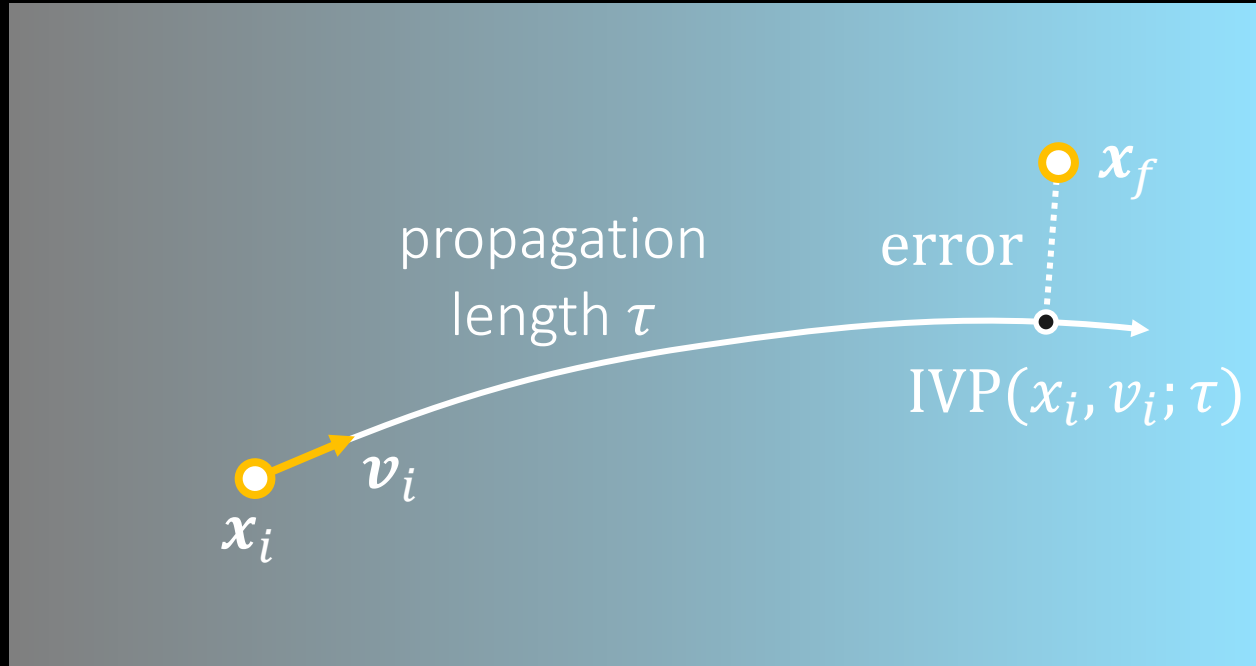
we know how to solve this:

$$\frac{d\mathbf{v}}{ds} = \nabla_{\mathbf{x}} n(\mathbf{x}), \quad \frac{d\mathbf{x}}{ds} = \frac{\mathbf{v}}{n(\mathbf{x})}$$

boundary conditions: $\mathbf{x}_i, \mathbf{v}_i$

initial value problem (IVP),
a.k.a. refractive ray tracing

direct connections



$$\text{error}(x_f, x_i, v_i) \equiv \min_{\tau} \|x_f - \text{IVP}(x_i, v_i; \tau)\|^2$$

we have to solve this:

$$\frac{d\mathbf{v}}{ds} = \nabla_{\mathbf{x}} n(\mathbf{x}), \quad \frac{d\mathbf{x}}{ds} = \frac{\mathbf{v}}{n(\mathbf{x})}$$

boundary conditions: $\mathbf{x}_i, \mathbf{x}_f$

boundary value problem (BVP)

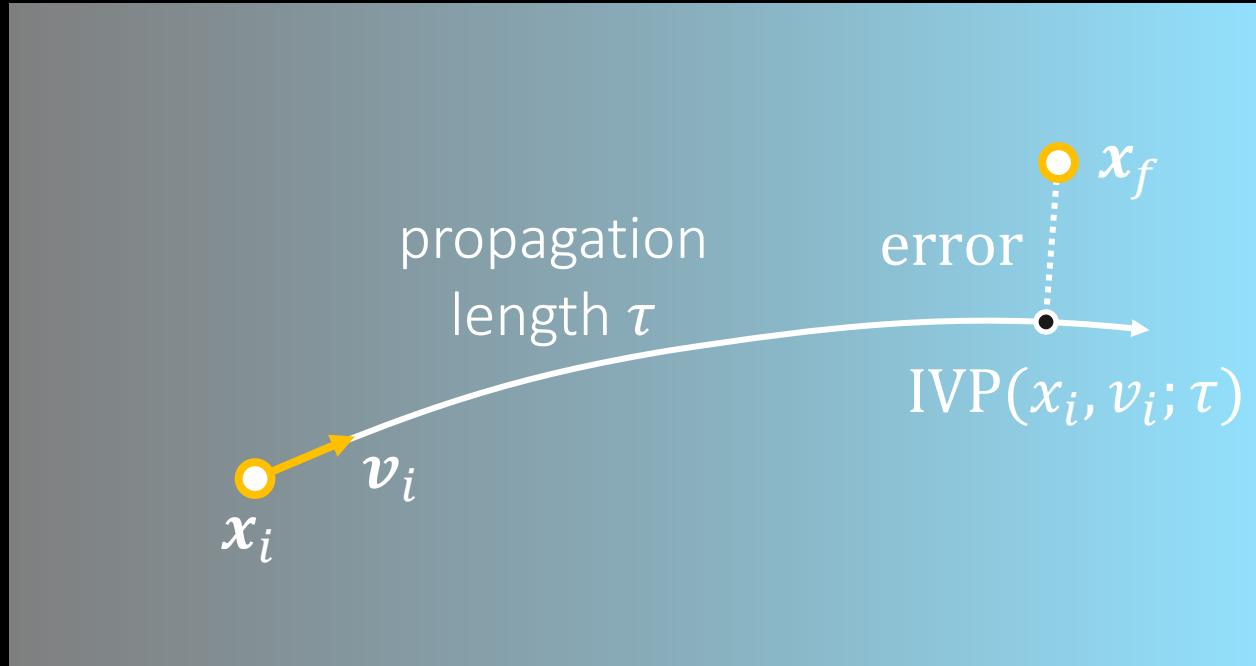
we know how to solve this:

$$\frac{d\mathbf{v}}{ds} = \nabla_{\mathbf{x}} n(\mathbf{x}), \quad \frac{d\mathbf{x}}{ds} = \frac{\mathbf{v}}{n(\mathbf{x})}$$

boundary conditions: $\mathbf{x}_i, \mathbf{v}_i$

initial value problem (IVP),
a.k.a. refractive ray tracing

direct connections



we have to solve this:

$$\min_{v_i} \text{error}(x_f, x_i, v_i)$$

boundary conditions: x_i, x_f

boundary value problem (BVP)

we know how to solve this:

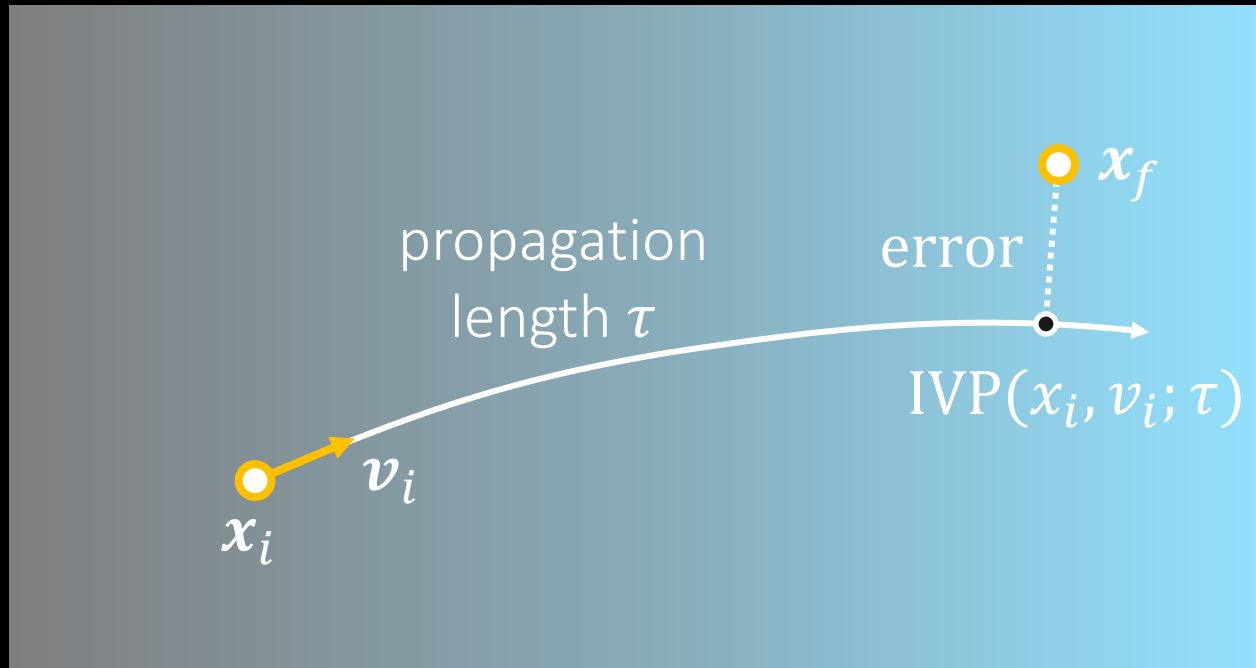
$$\frac{d\mathbf{v}}{ds} = \nabla_{\mathbf{x}} n(\mathbf{x}), \quad \frac{d\mathbf{x}}{ds} = \frac{\mathbf{v}}{n(\mathbf{x})}$$

boundary conditions: x_i, v_i

$$\text{error}(x_f, x_i, v_i) \equiv \min_{\tau} \|x_f - \text{IVP}(x_i, v_i; \tau)\|^2$$

initial value problem (IVP),
a.k.a. refractive ray tracing

direct connections



differentiable

$$\text{error}(x_f, x_i, v_i) \equiv \min_{\tau} \|x_f - \text{IVP}(x_i, v_i; \tau)\|^2$$

we have to solve this:

$$\min_{v_i} \text{error}(x_f, x_i, v_i)$$

boundary conditions: x_i, x_f

boundary value problem (BVP)

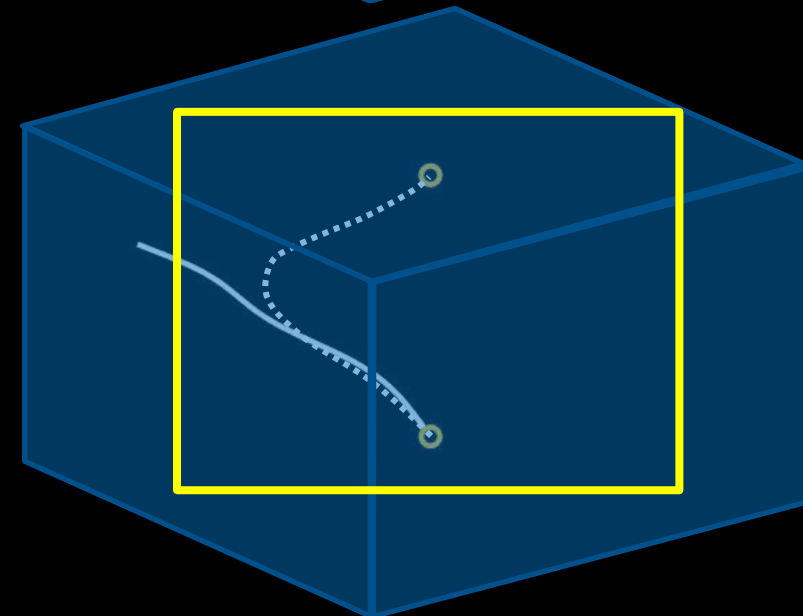
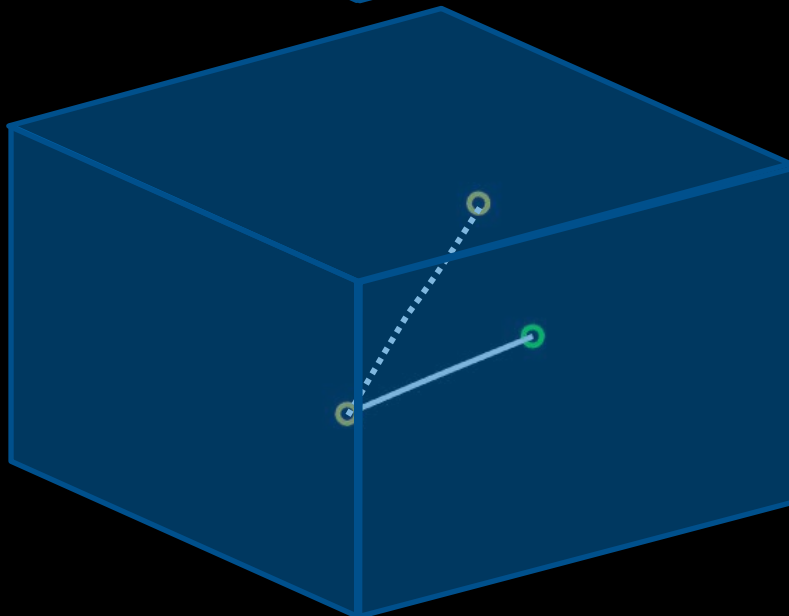
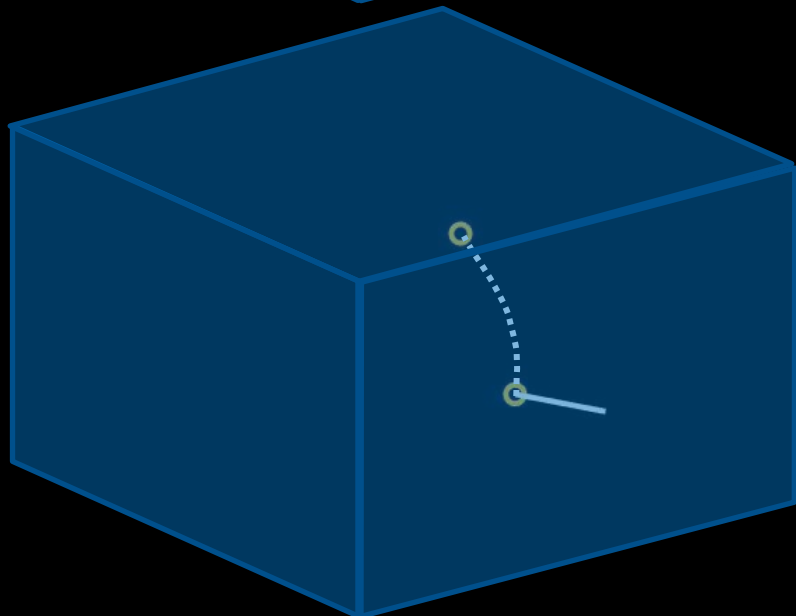
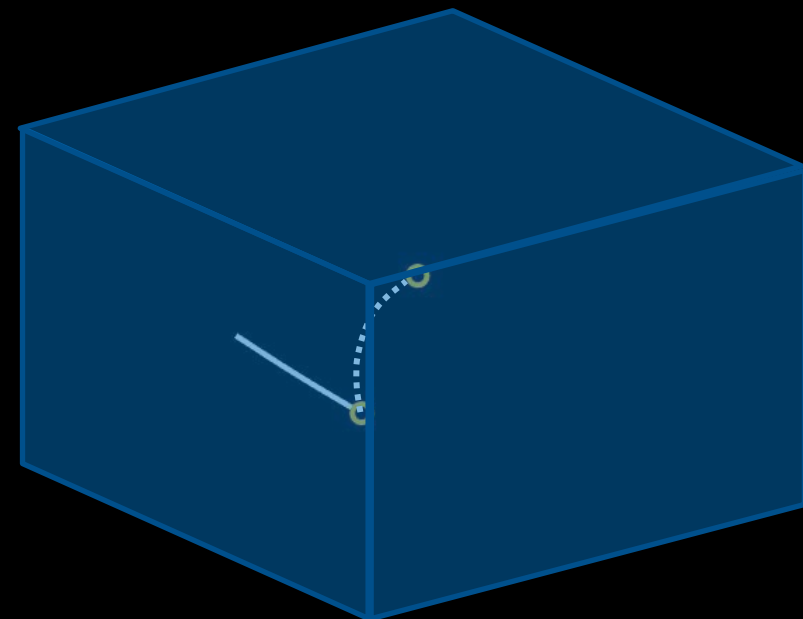
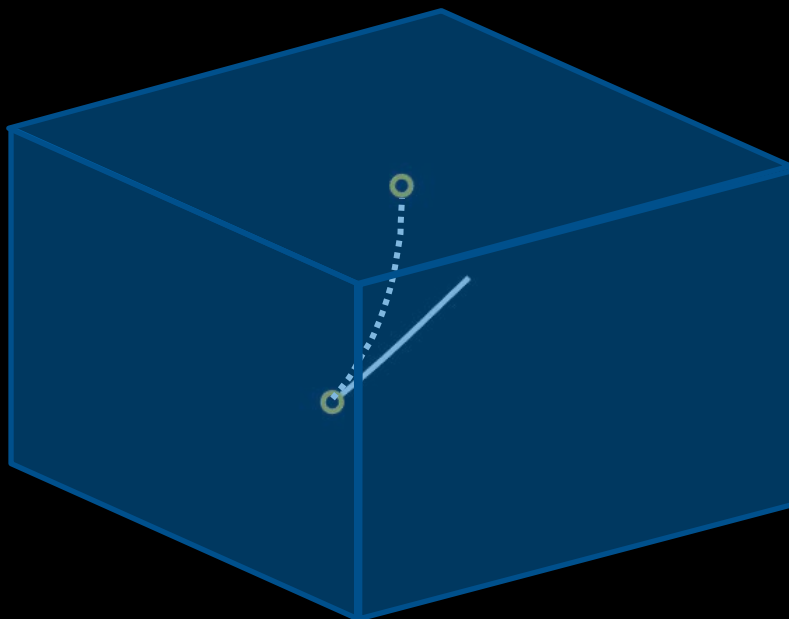
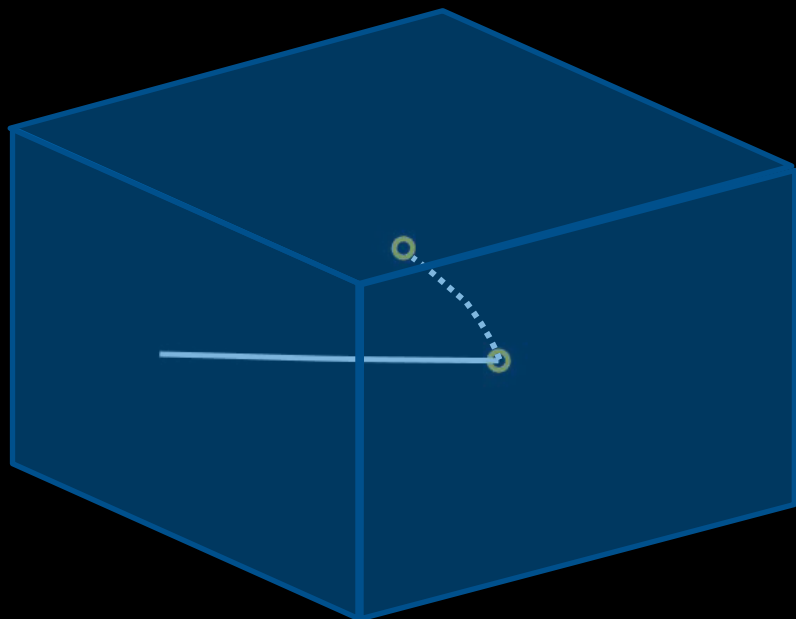
differentiable

$$\frac{dv}{ds} = \nabla_x n(x), \quad \frac{dx}{ds} = \frac{v}{n(x)}$$

boundary conditions: x_i, v_i

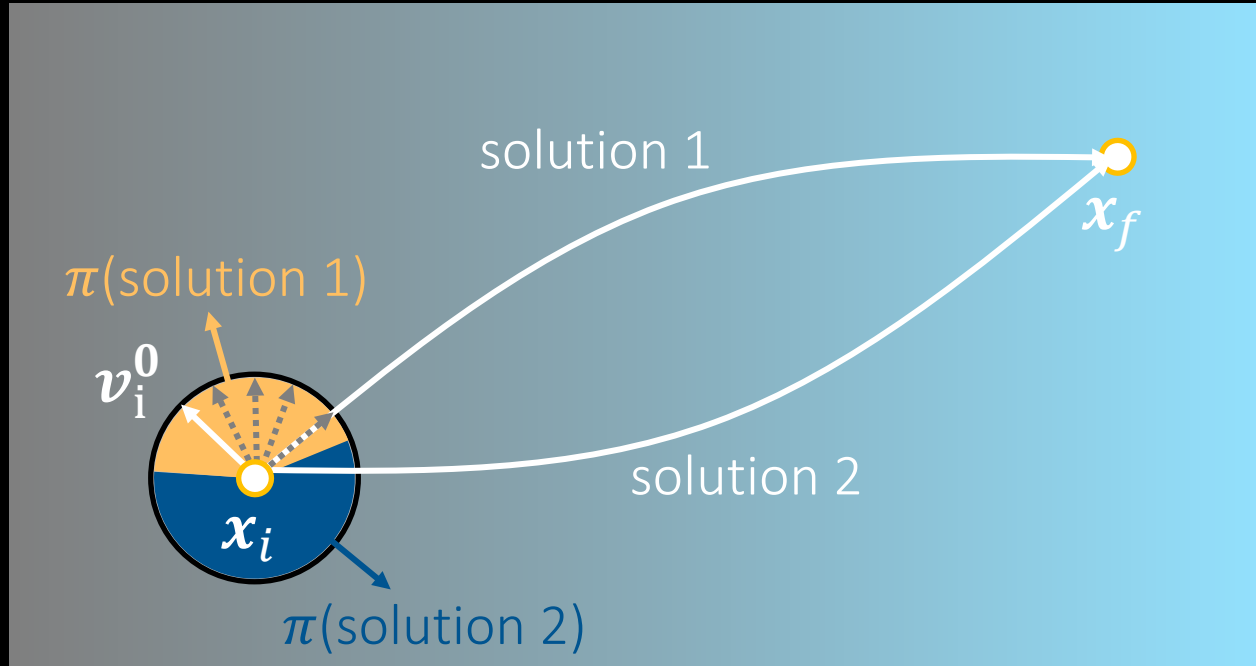
initial value problem (IVP),
a.k.a. refractive ray tracing

direct connections



multiple direct connections

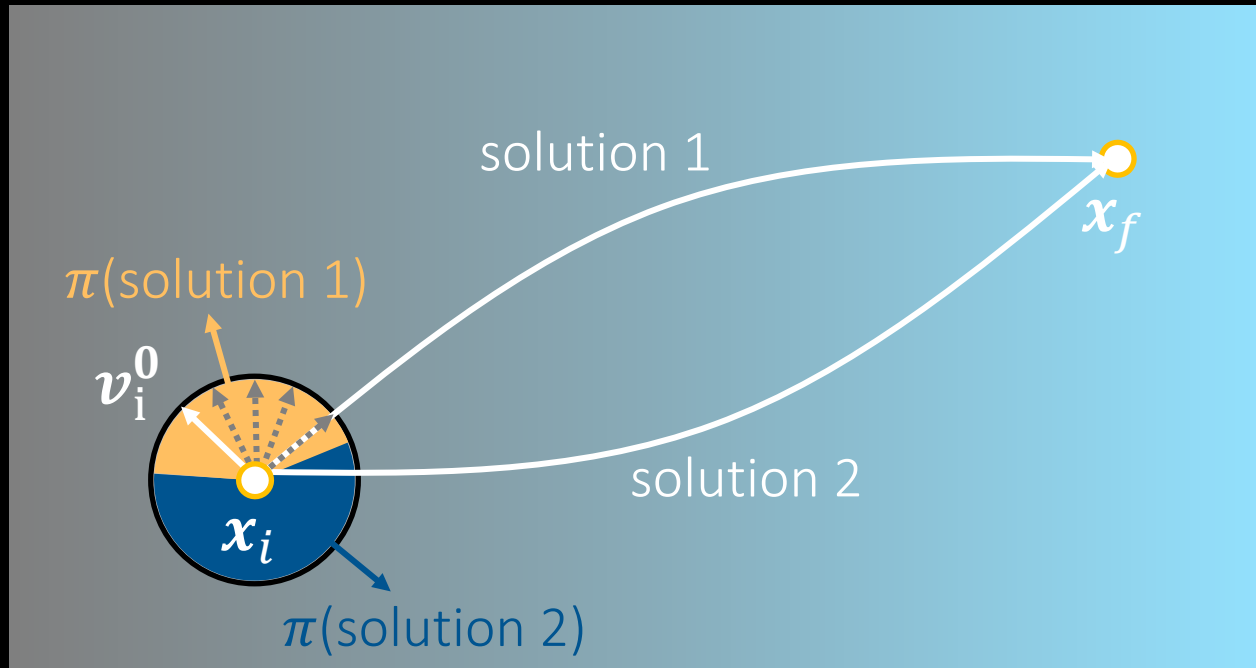
$$\text{total throughput} = \sum_{\text{all solutions}} \text{throughput}(\text{solution})$$



approach 1:
exhaustively enumerate all solutions

multiple direct connections

$$\text{total throughput} = \sum_{\text{all solutions}} \text{throughput}(\text{solution})$$



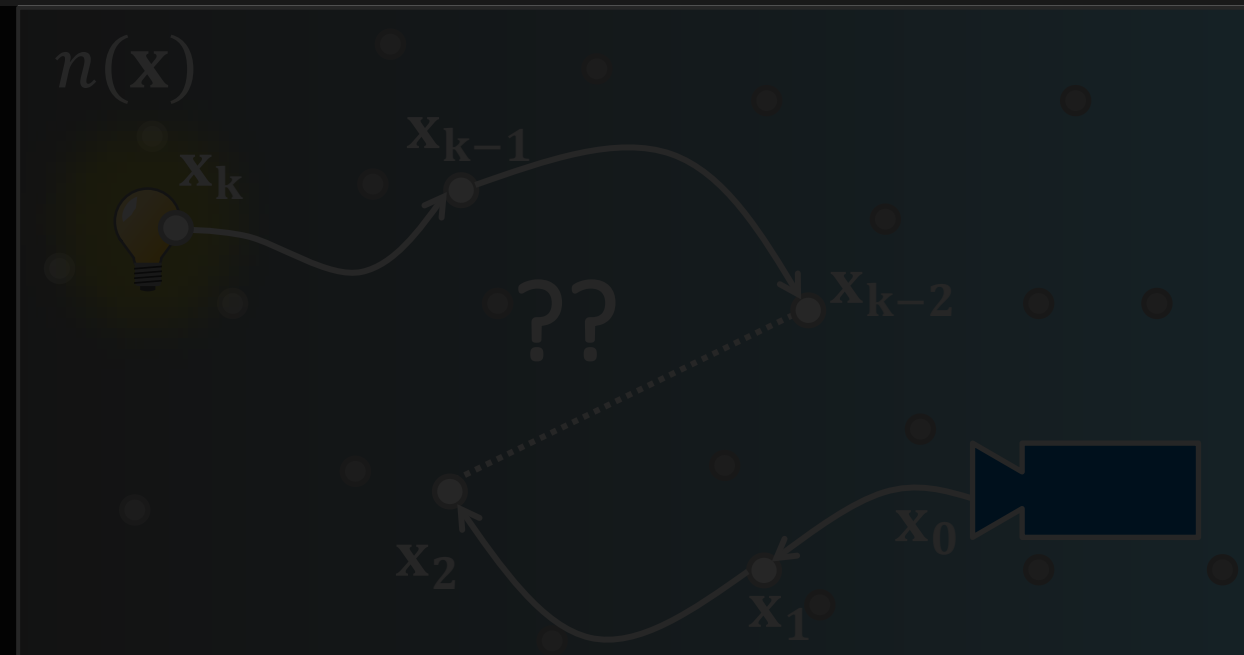
approach 1: impractical
exhaustively enumerate all solutions

approach 2:
unbiased single-sample Monte Carlo

1. randomly sample initial direction
2. solve BVP
3. form estimate

$$\text{total throughput} \approx \frac{\text{throughput}(\text{solution})}{\text{probability}(\text{solution})}$$

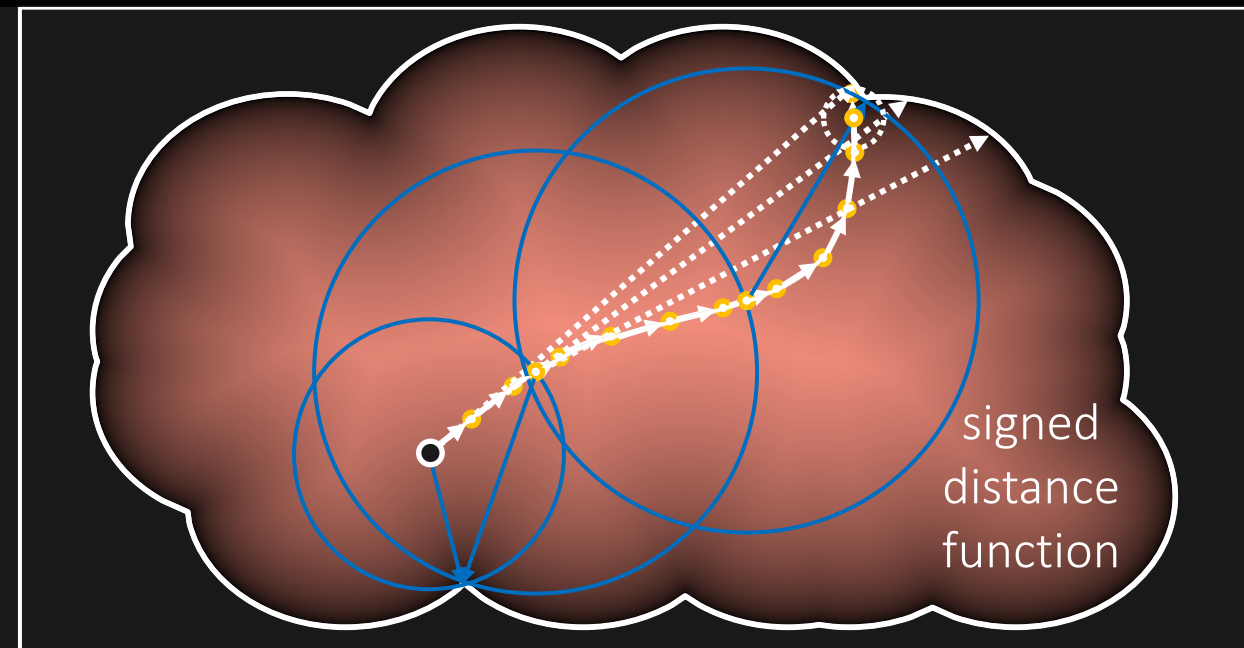
set of initial directions that converge to the solution



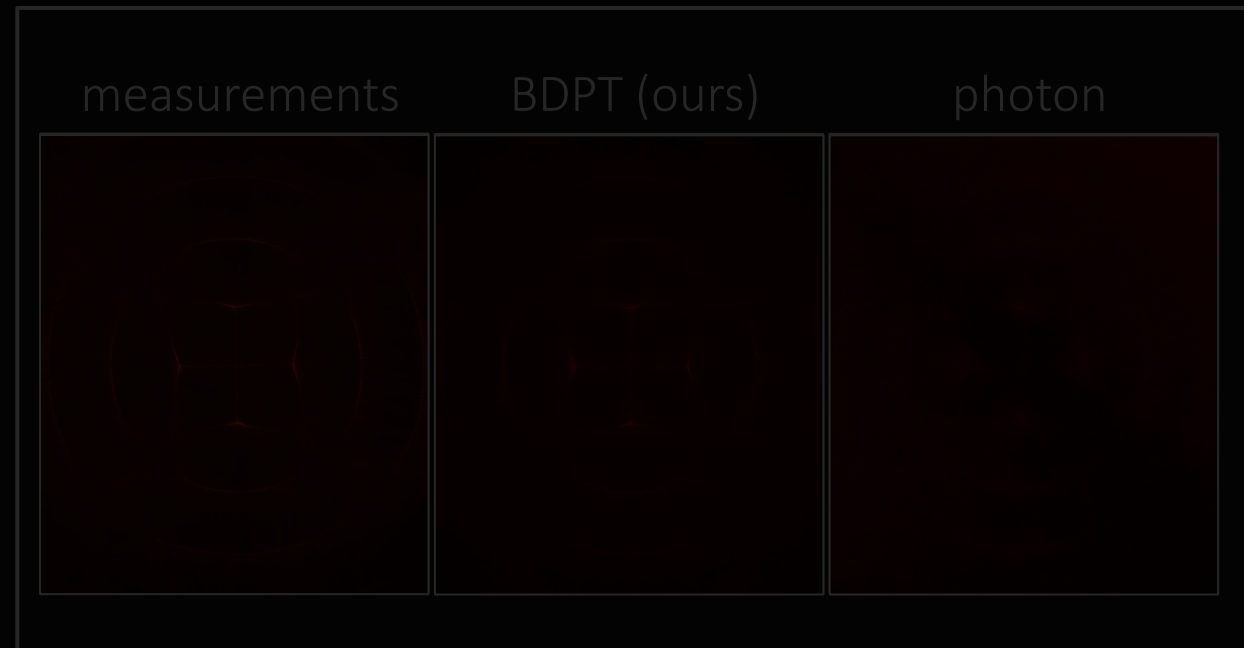
1. background on refractive radiative transfer equation



2. direct connections: our solution to unbiased rendering



3. acceleration techniques



4. experiments

acceleration: sphere tracing

standard ray tracing

ray-mesh
intersection test

A diagram illustrating standard ray tracing. A white cloud-like shape represents a mesh. A ray, shown as a solid line with an arrow, originates from a white circle on the left and points towards a white circle on the right. A dotted line extends from the ray's path to the intersection point on the cloud's boundary.

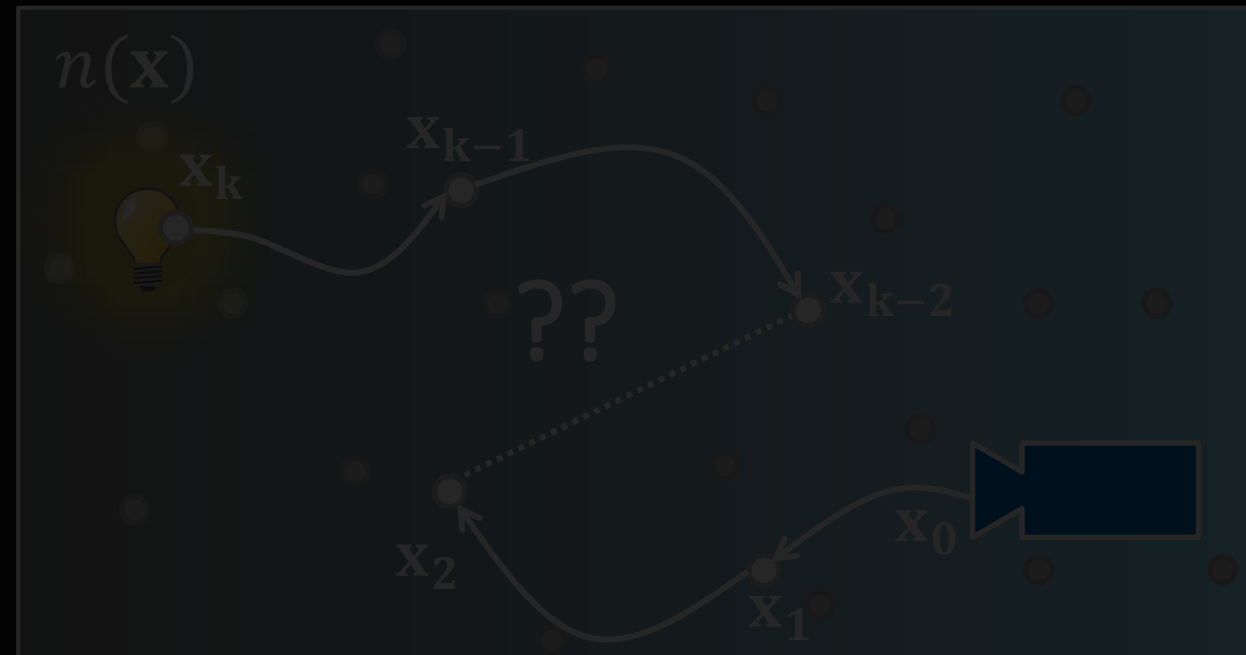
refractive ray tracing

switch to
standard tests

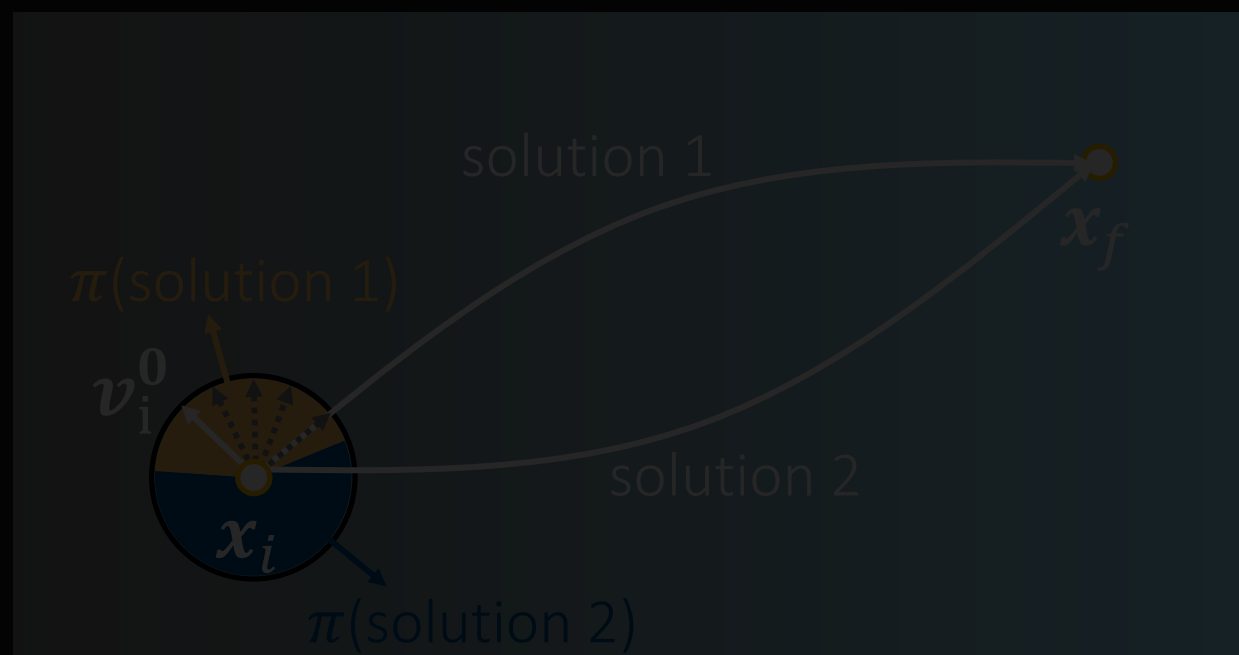
A diagram illustrating refractive ray tracing. A white cloud-like shape is filled with a dark red gradient. Several blue circles of varying sizes are overlaid on the cloud, representing spheres. A ray, shown as a solid line with an arrow, originates from a white circle on the left and passes through the spheres. The ray's path is marked with yellow dots. At the intersection with a sphere, the ray refracts. A dotted line shows the original path, and a solid line shows the refracted path. The text "switch to standard tests" is positioned above the final intersection point. The text "signed distance function" is positioned below the spheres.

signed
distance
function

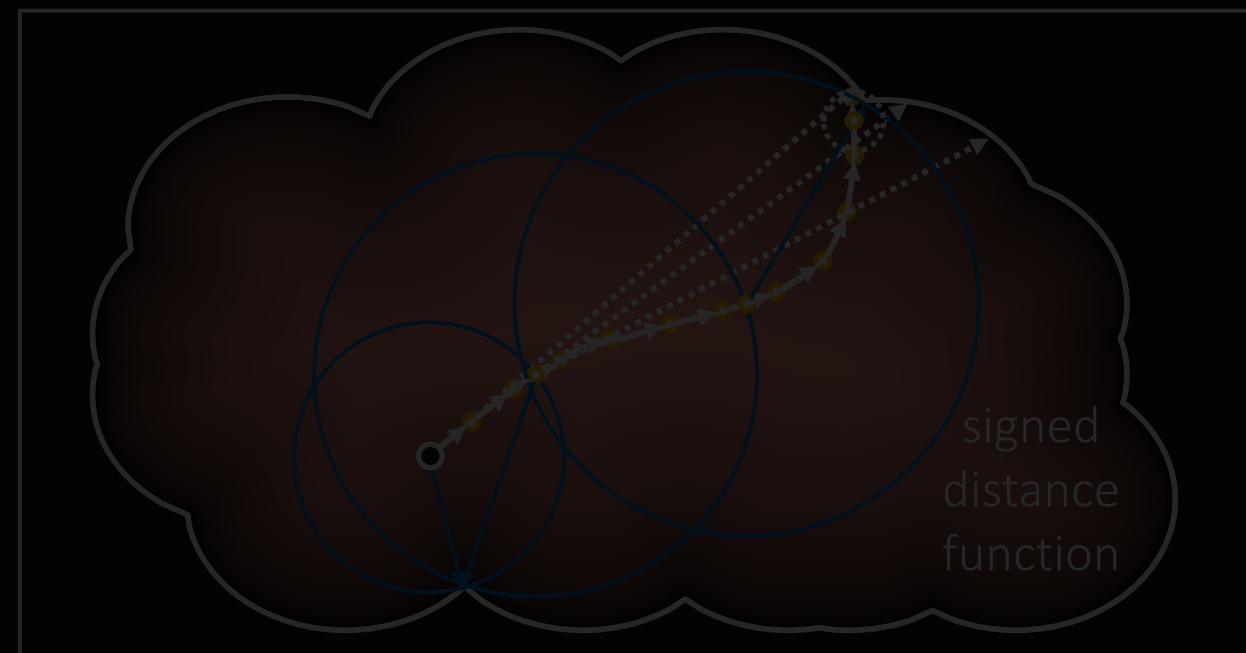
does not introduce bias



1. background on refractive radiative transfer equation



2. direct connections: our solution to unbiased rendering



3. acceleration techniques

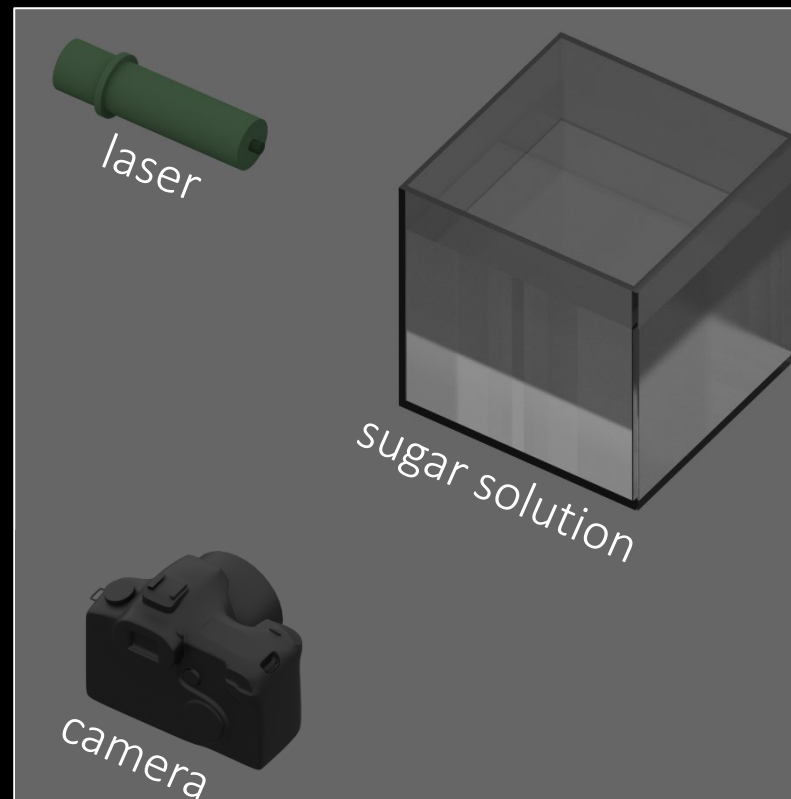


4. experiments

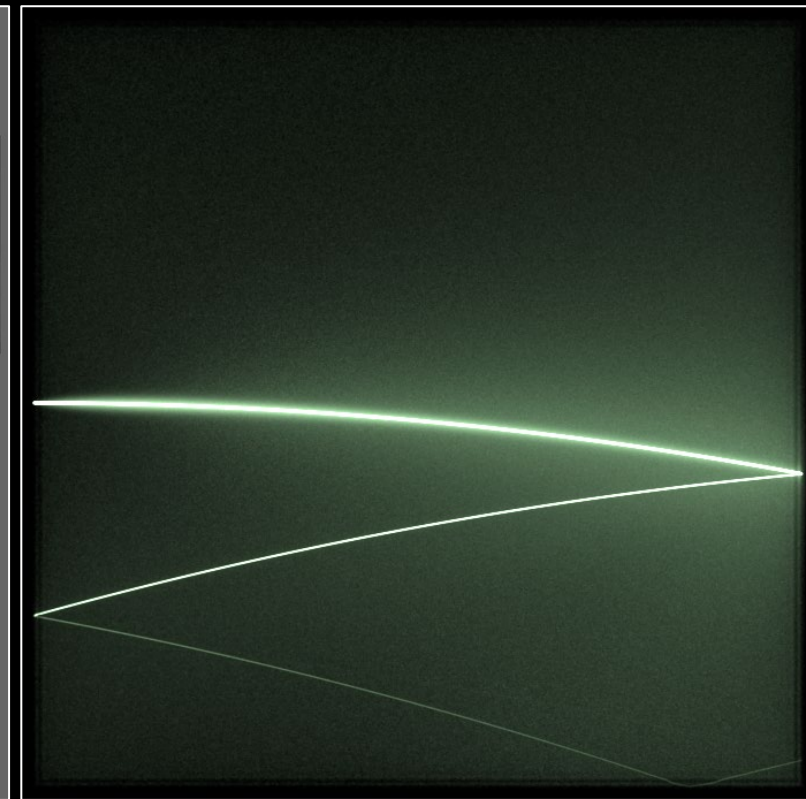
continuously refractive media and scattering



real scene

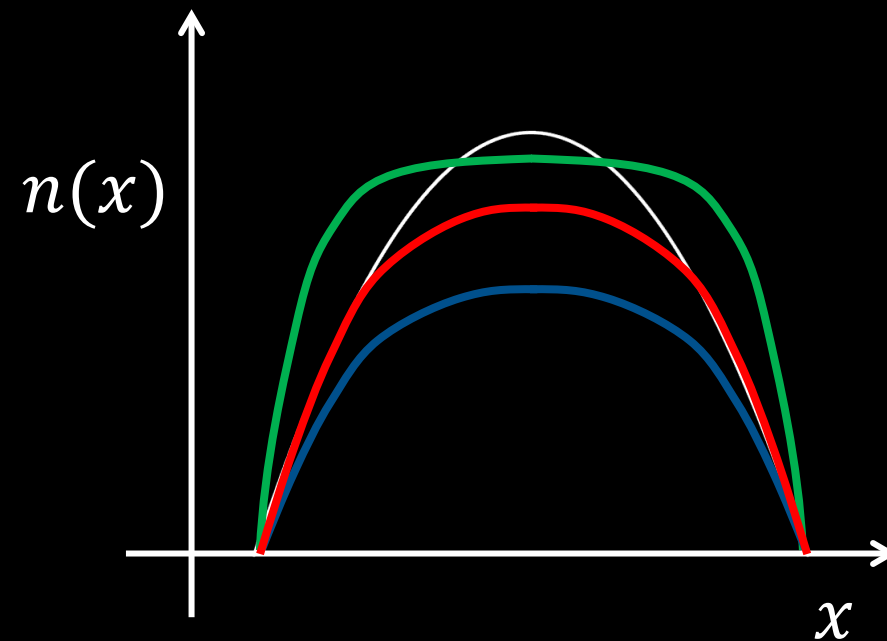
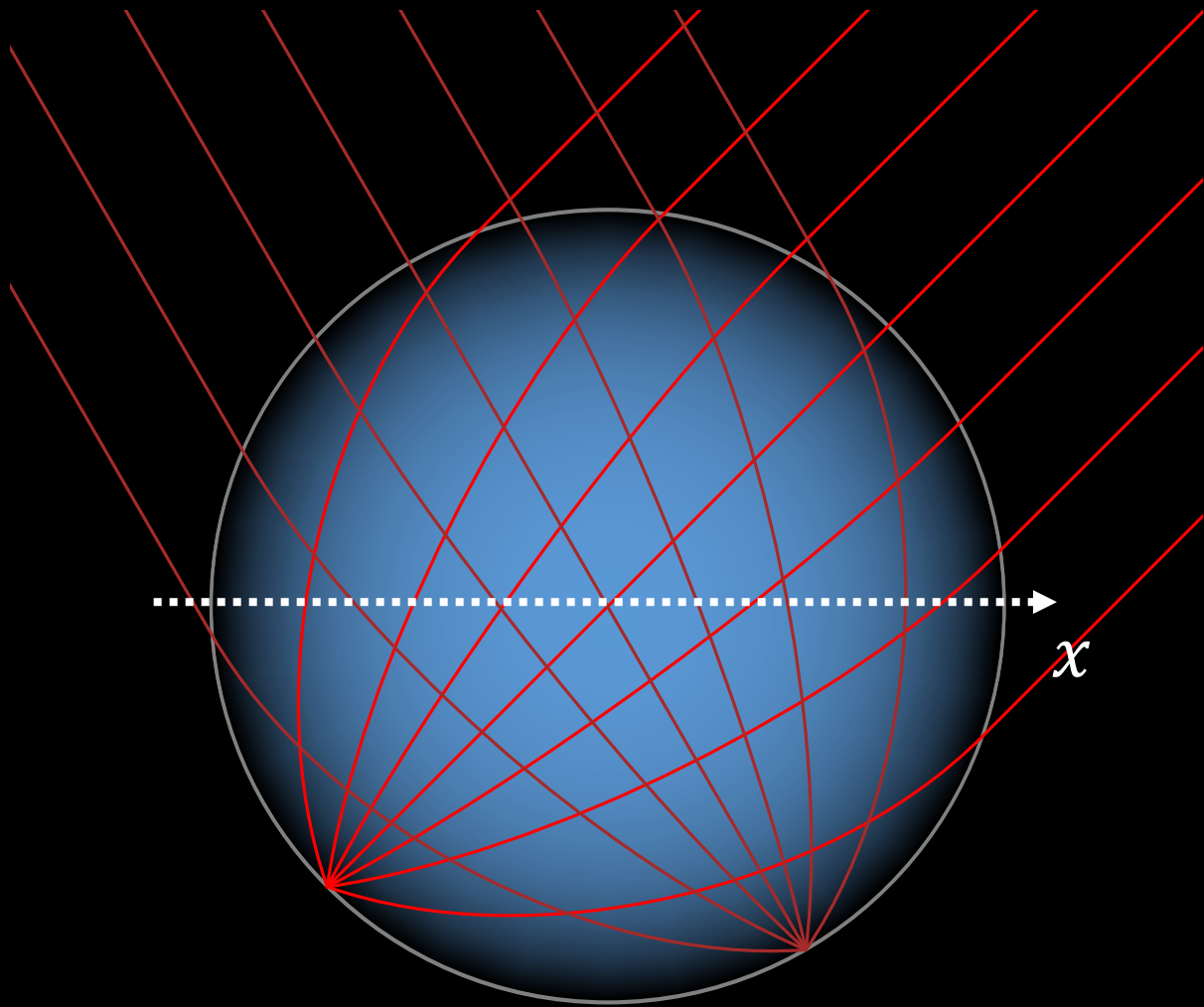


set up

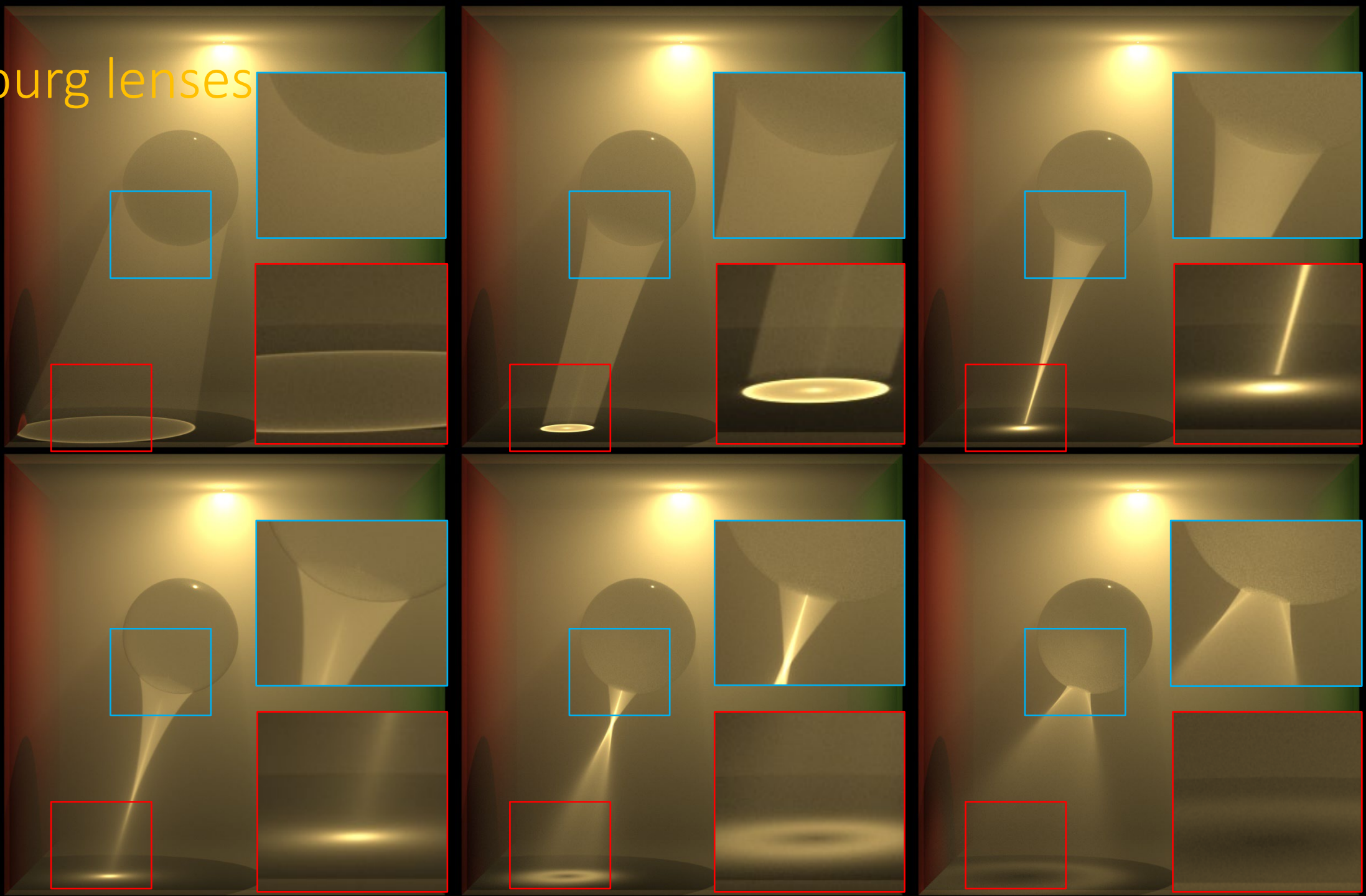


light propagation

Luneburg lenses



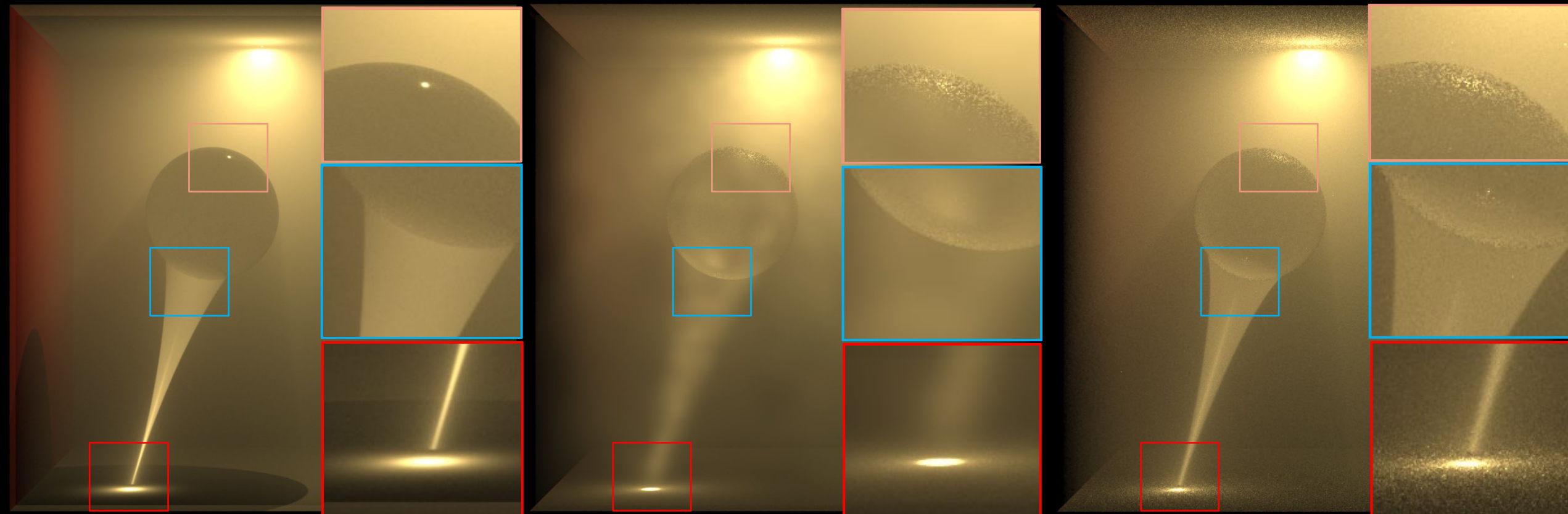
Luneburg lenses



power
equal to
standard
lens ←

rendering
time: 10 mins

comparison with photon mapping



BDPT (ours)

photon mapping
(default parameters)

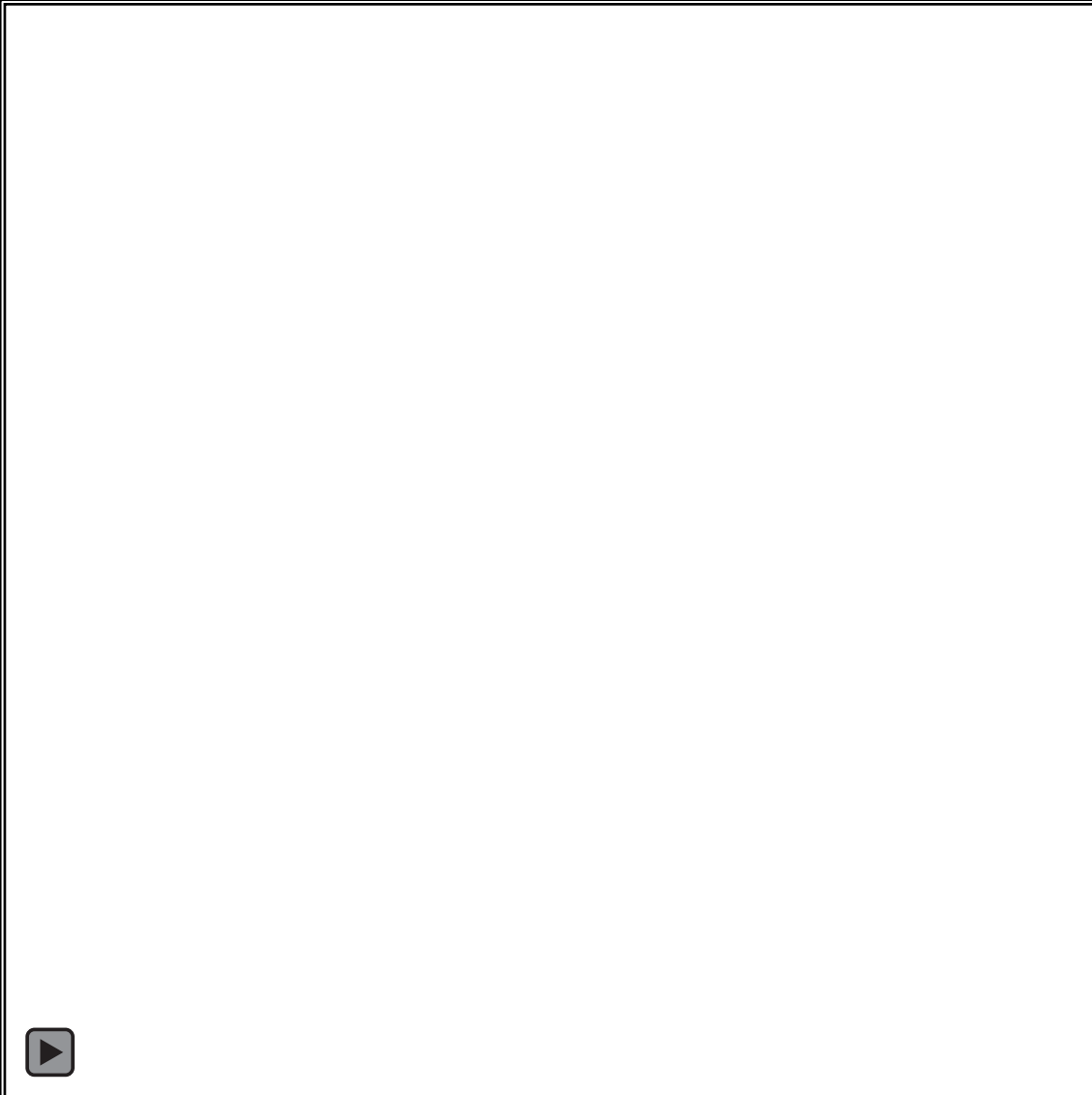
photon mapping
(optimized parameters)

rendering time: 10 min

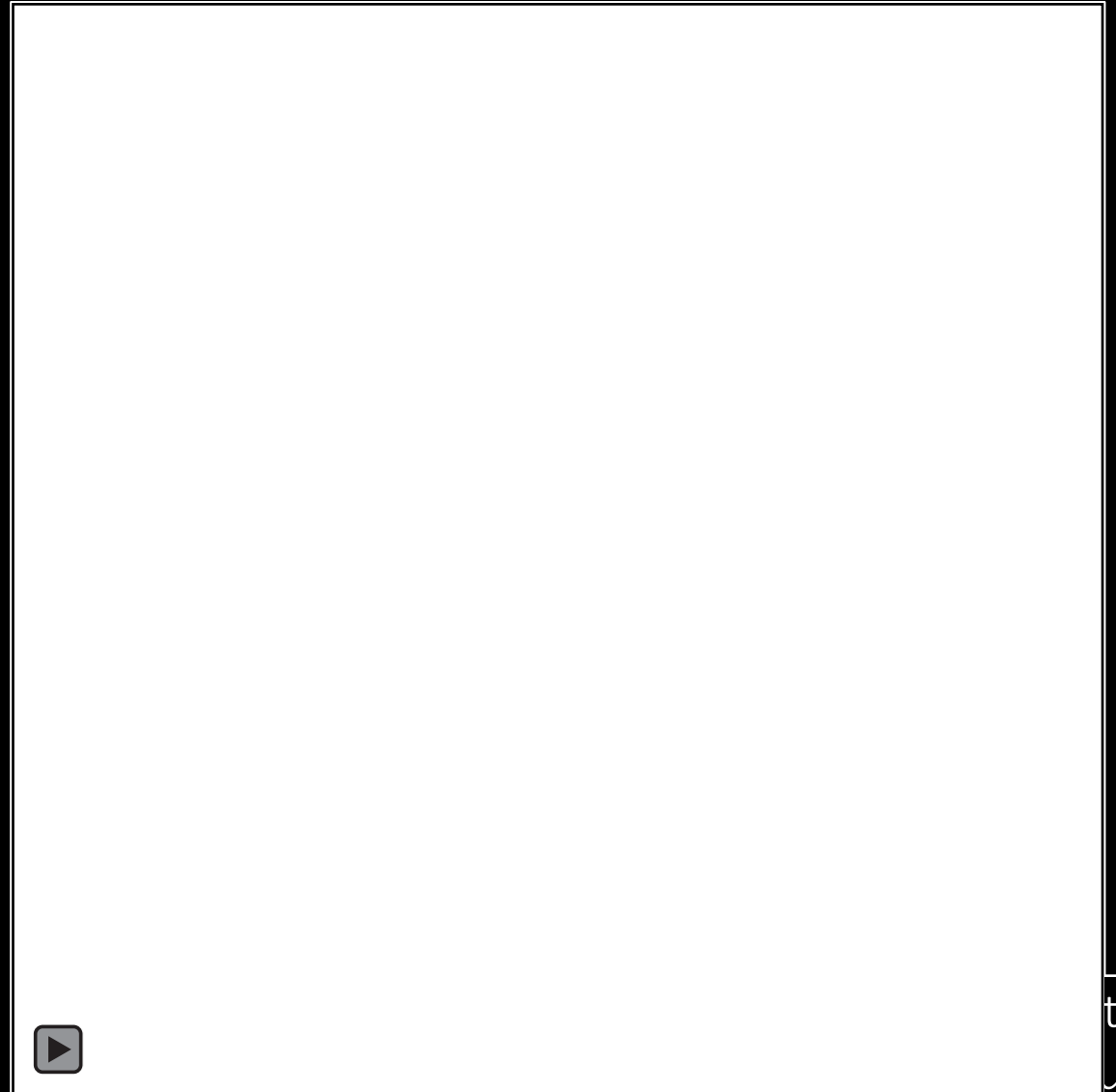
BDPT is 5x faster than photon mapping

transient rendering (videos)

constant refractive index



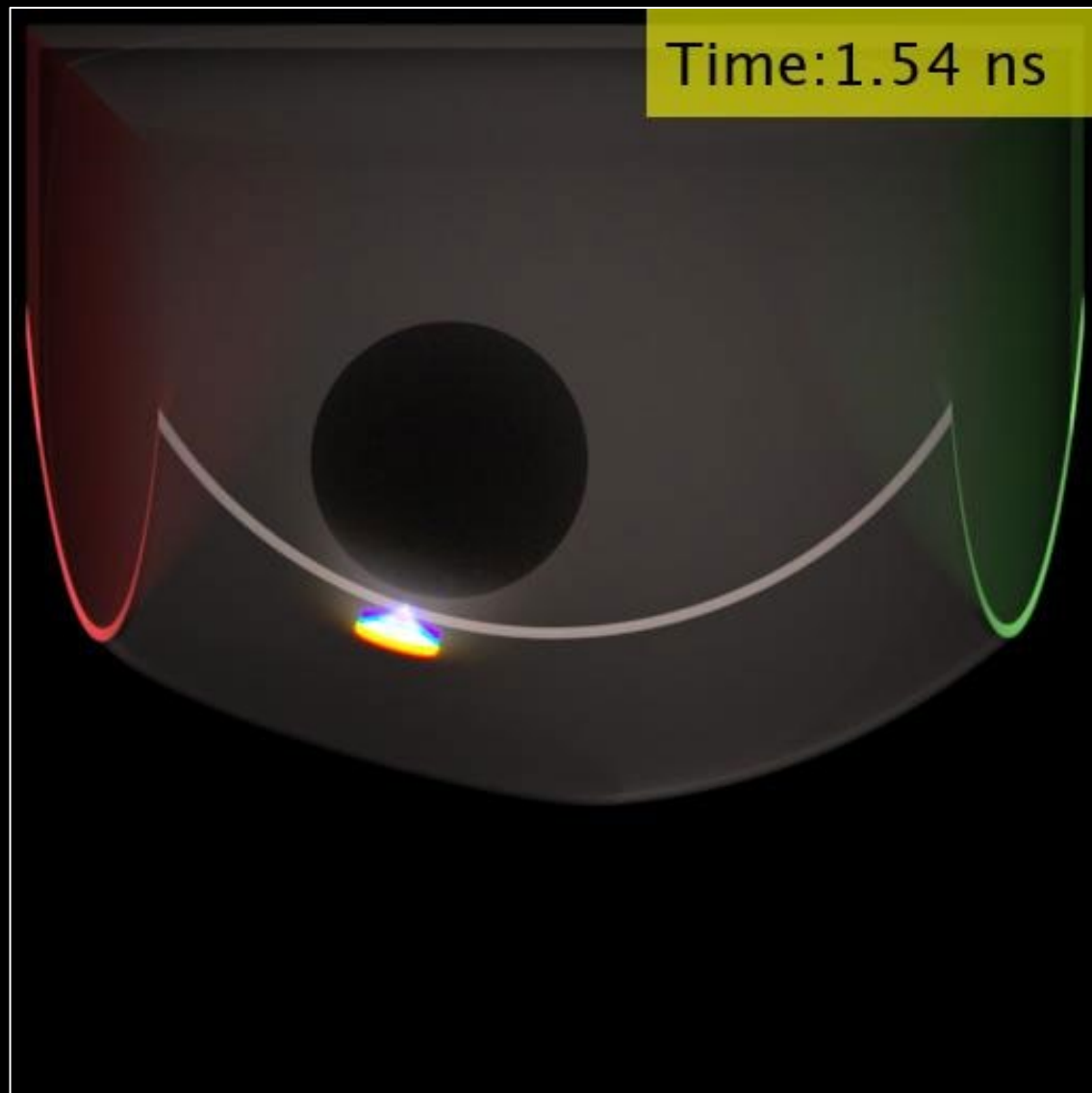
continuous refractive index



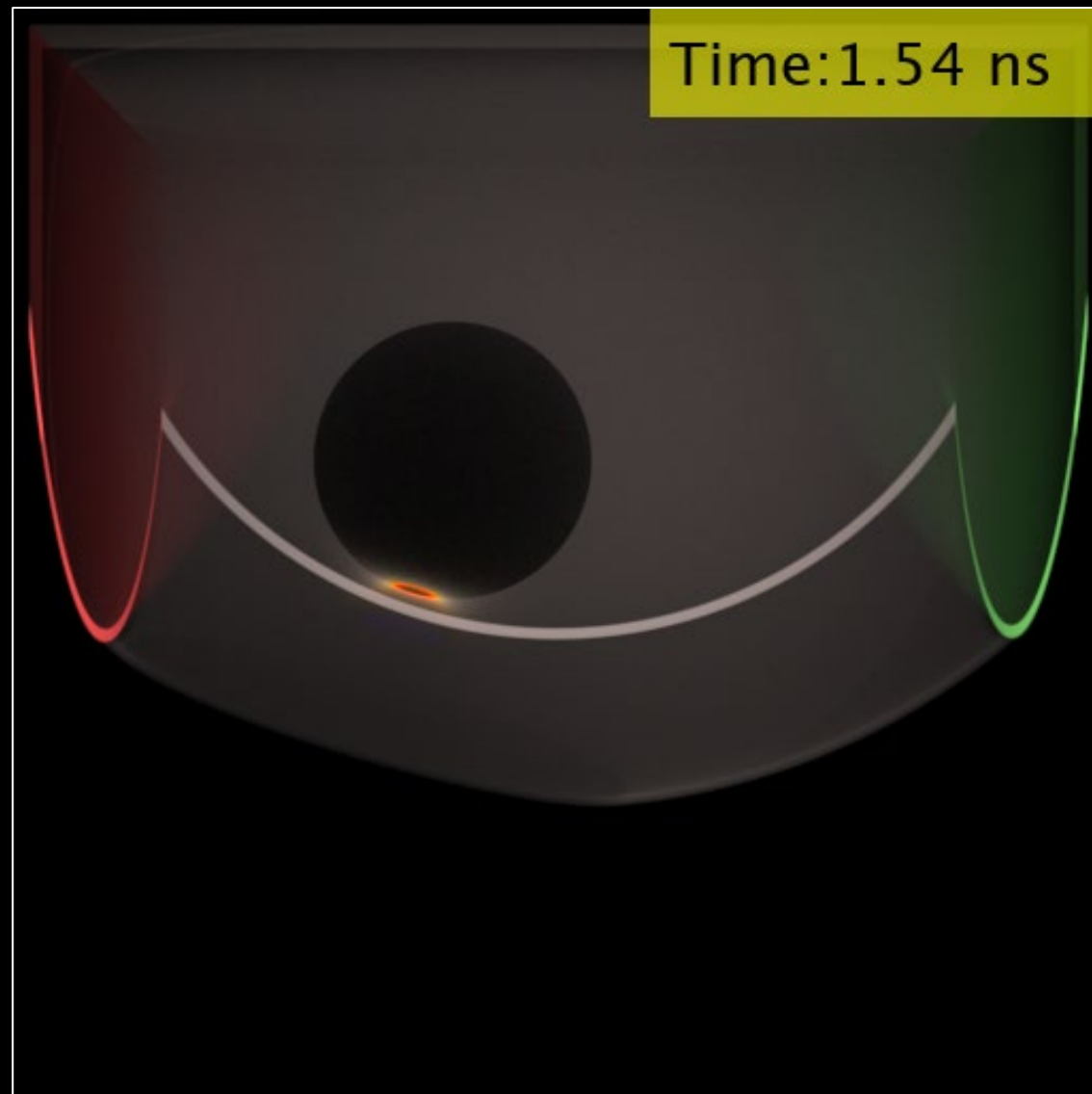
time:
urs

transient rendering

constant refractive index



continuous refractive index

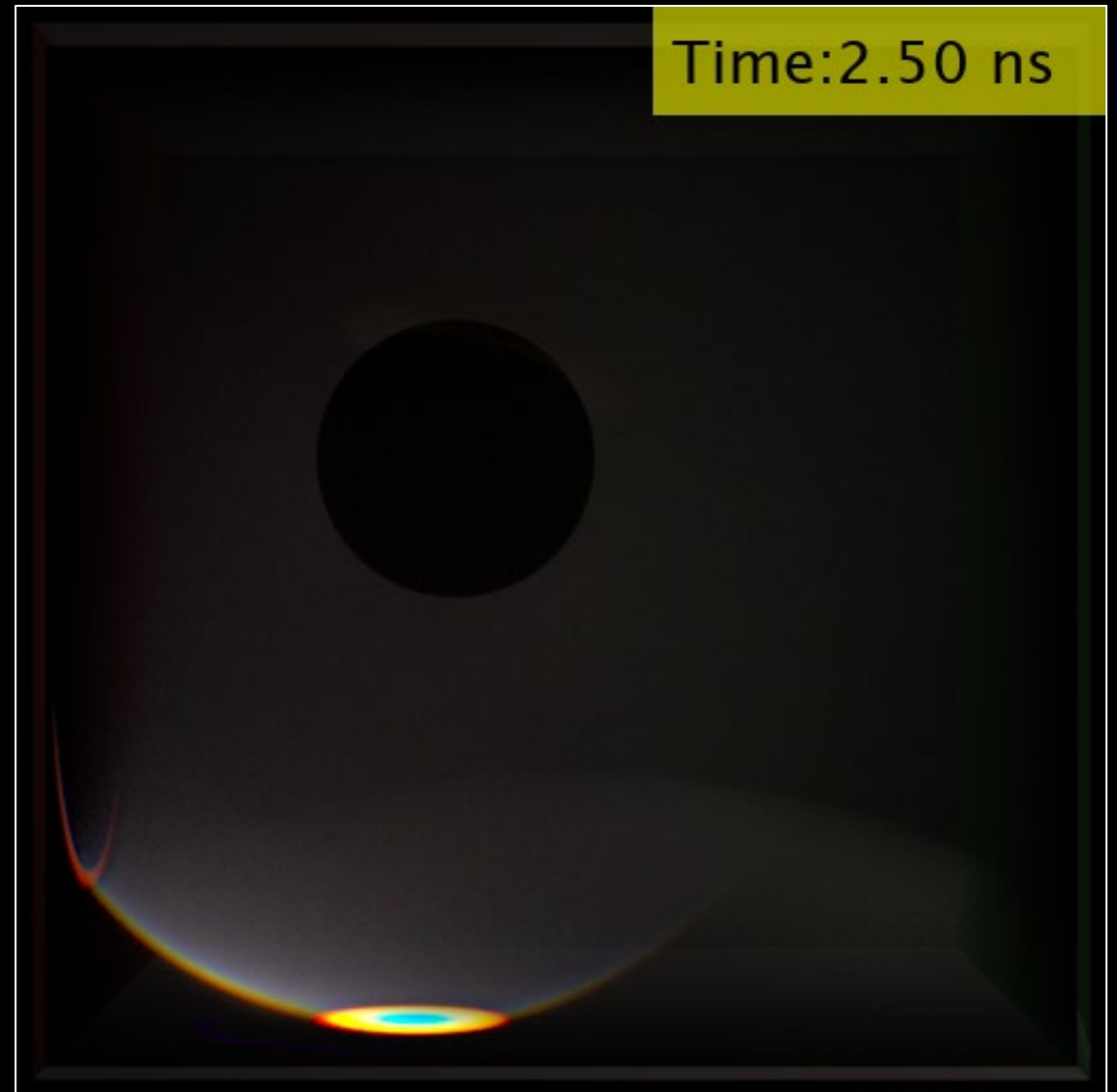


transient rendering

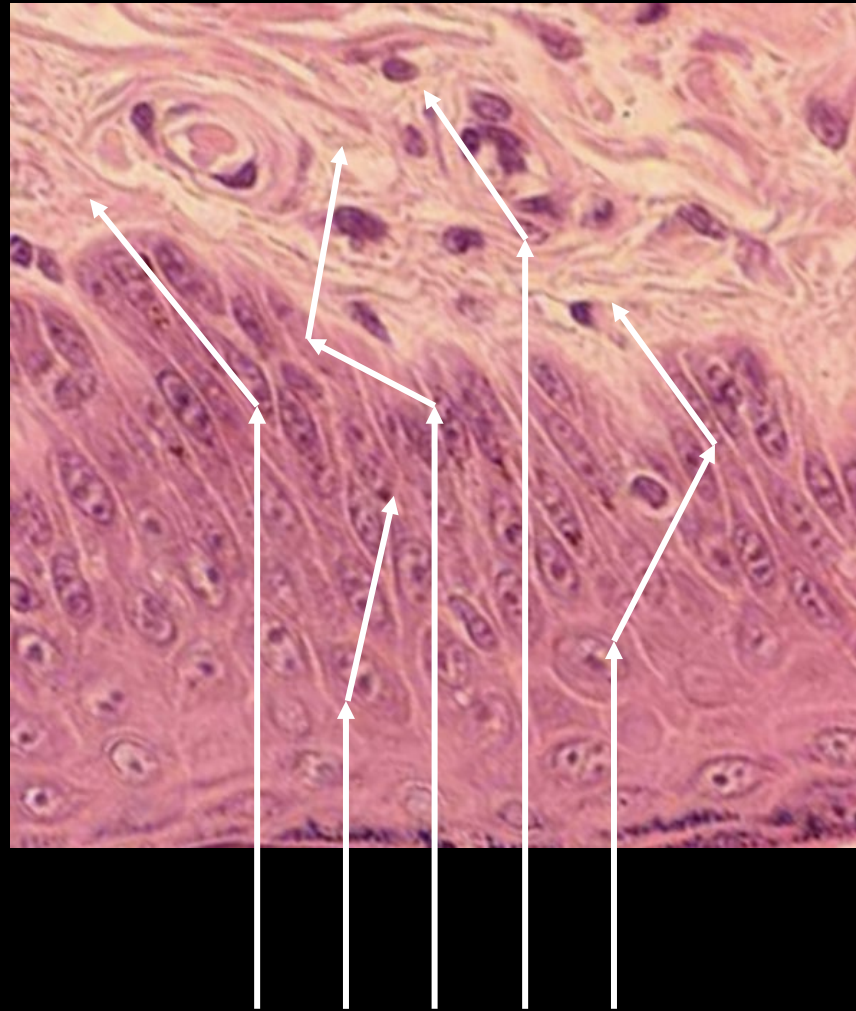
constant refractive index



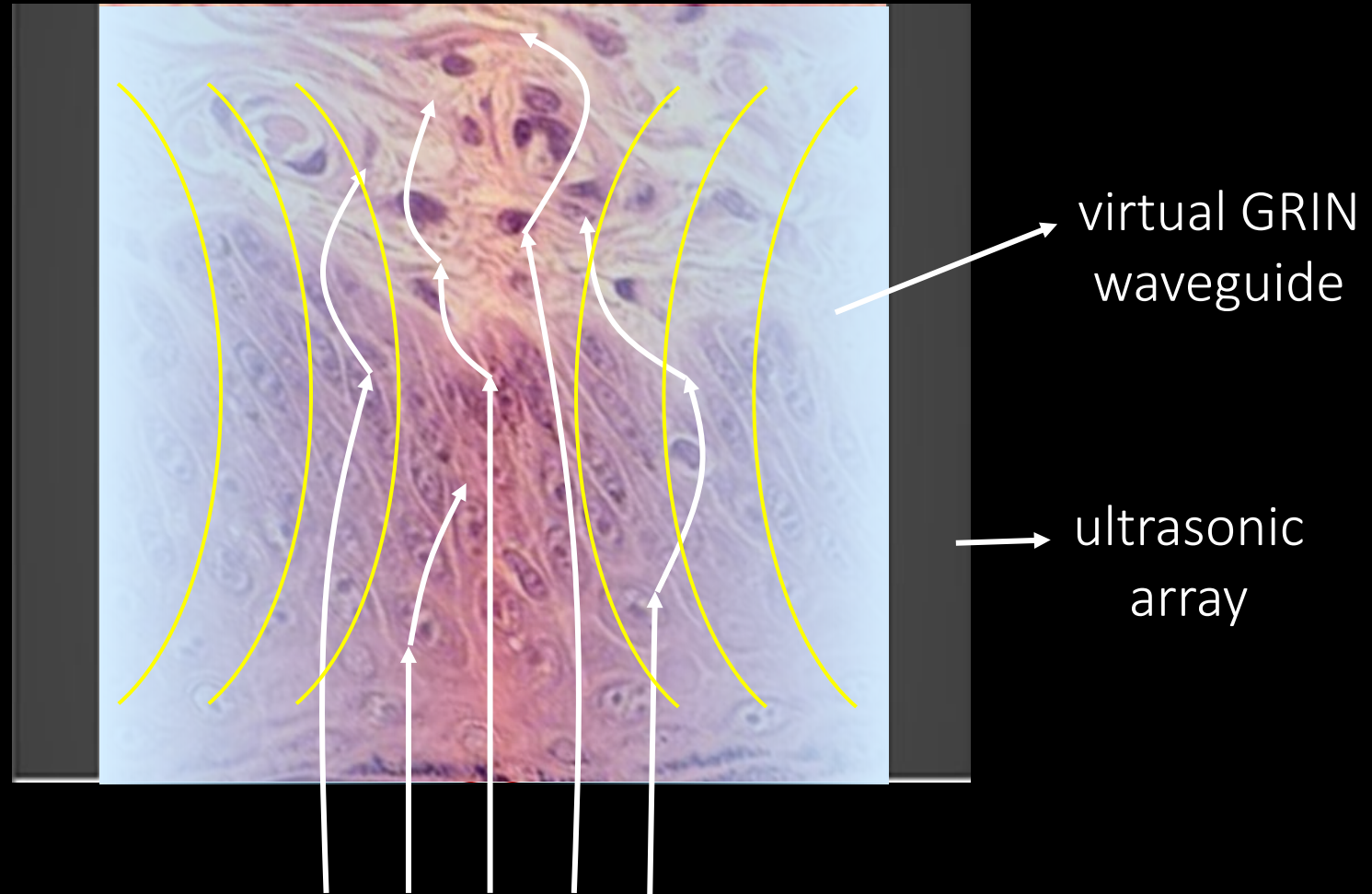
continuous refractive index



virtual ultrasonic waveguides

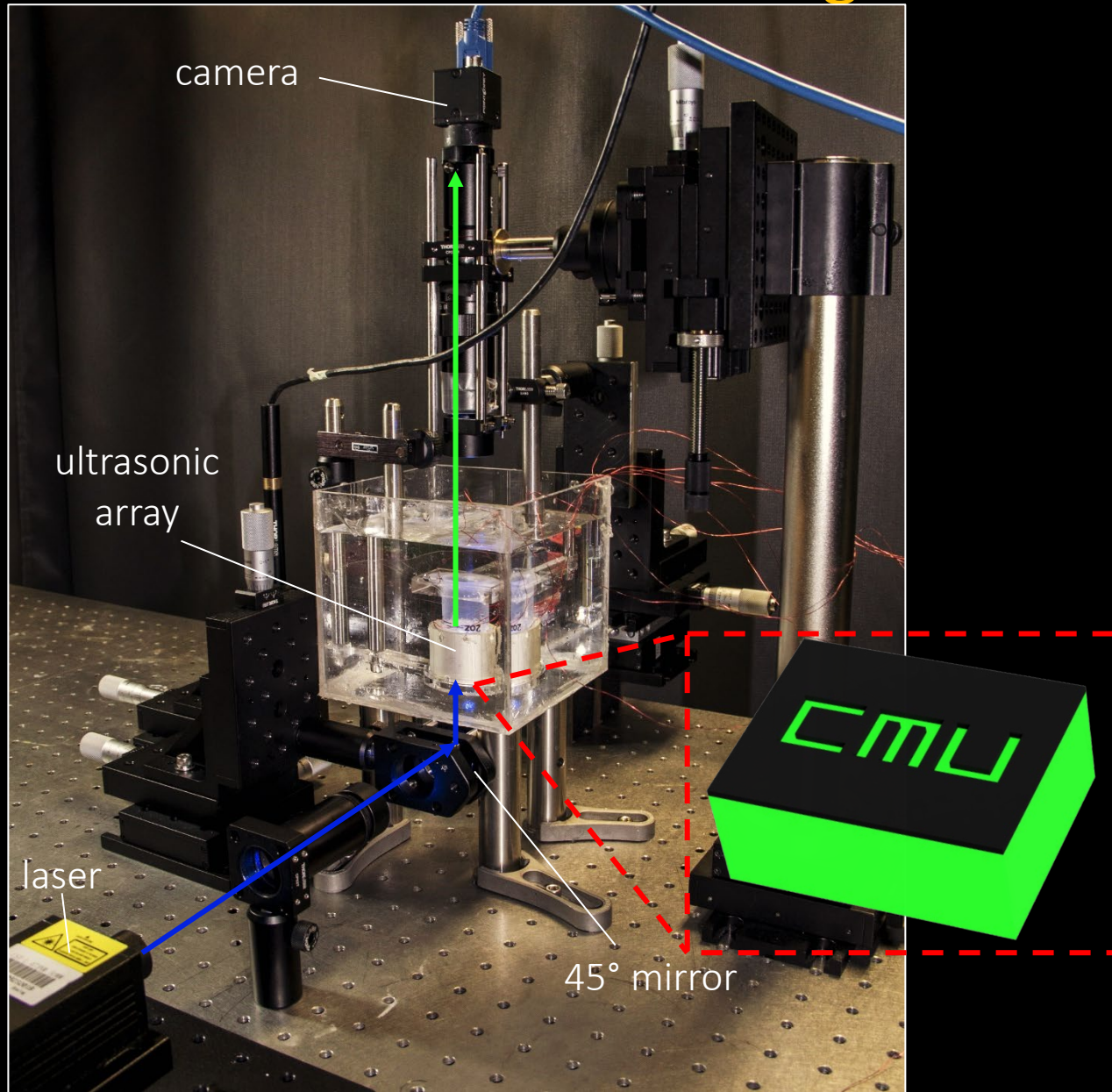


virtual ultrasonic waveguides

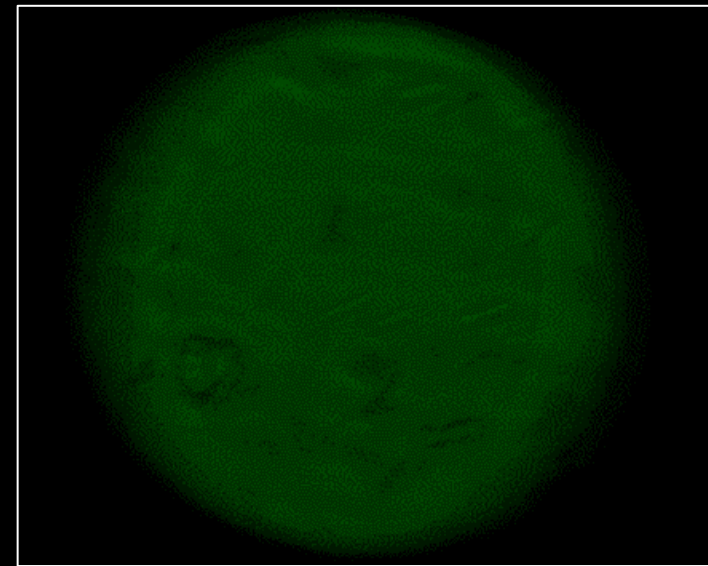


Chamanzar et al. "Ultrasonic sculpting of virtual optical waveguides in tissue". Nature communications, 2019
Scopelliti et al. "Ultrasonically sculpted virtual relay lens for in situ microimaging". Light: Science and Applications, 2019
Karimi et al. "In situ 3D reconfigurable ultrasonically sculpted optical beam paths". Optics express, 2019

virtual ultrasonic waveguides



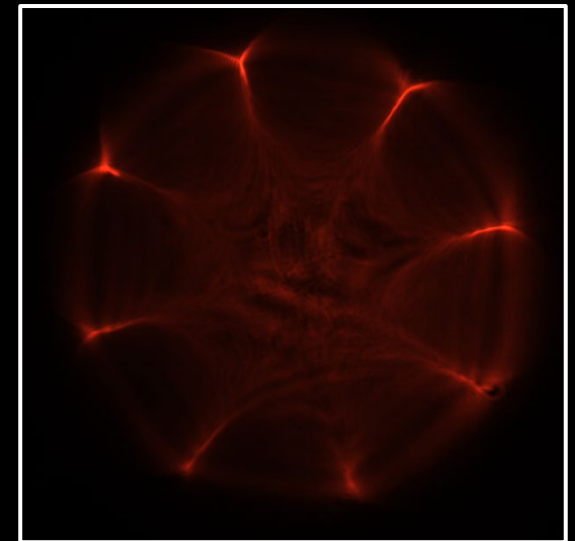
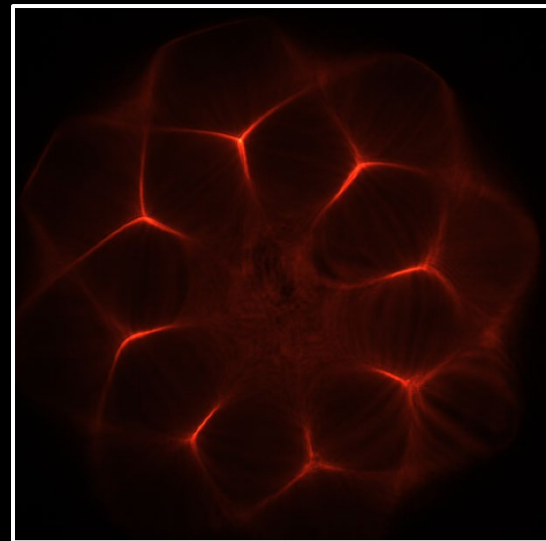
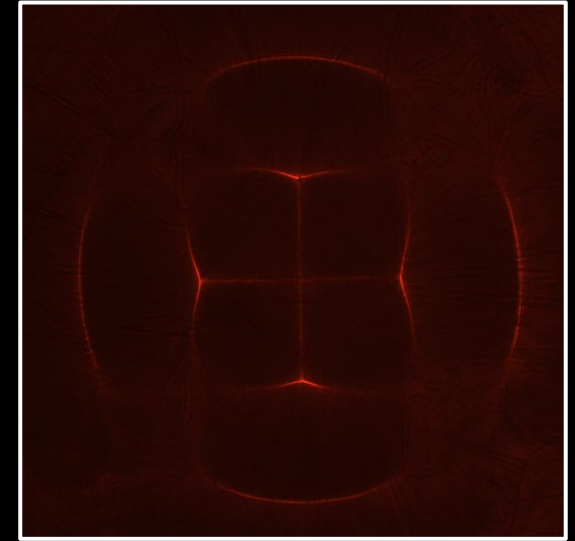
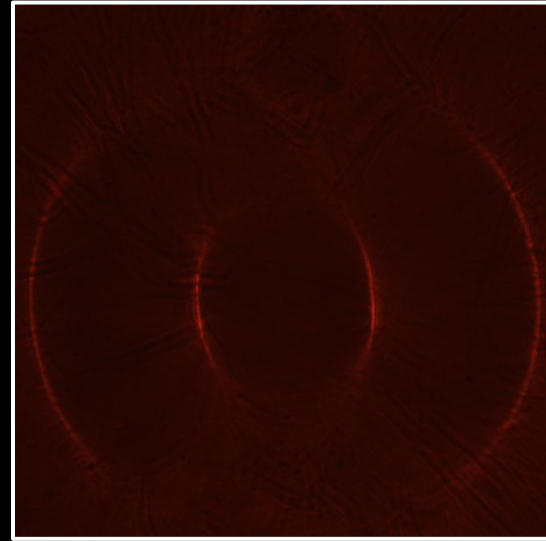
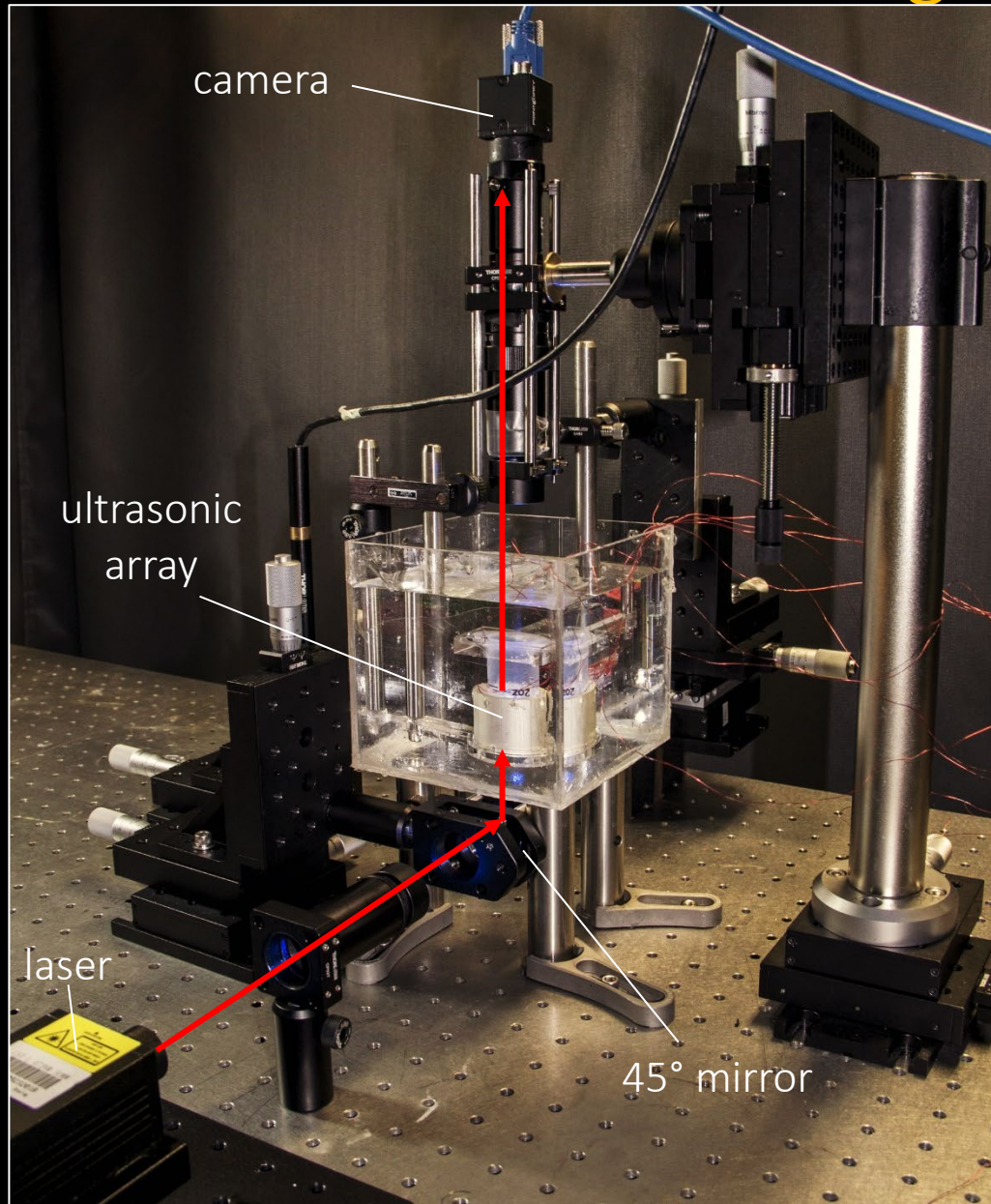
no waveguide



virtual waveguide

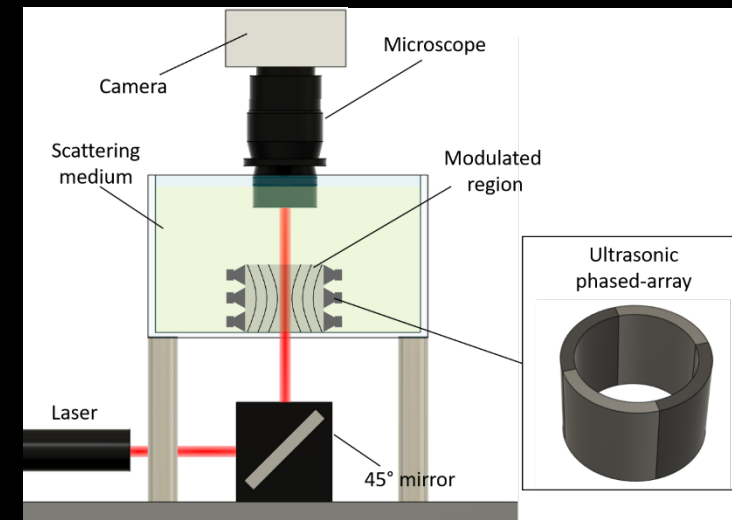


virtual ultrasonic waveguides



Rendering acousto-optics

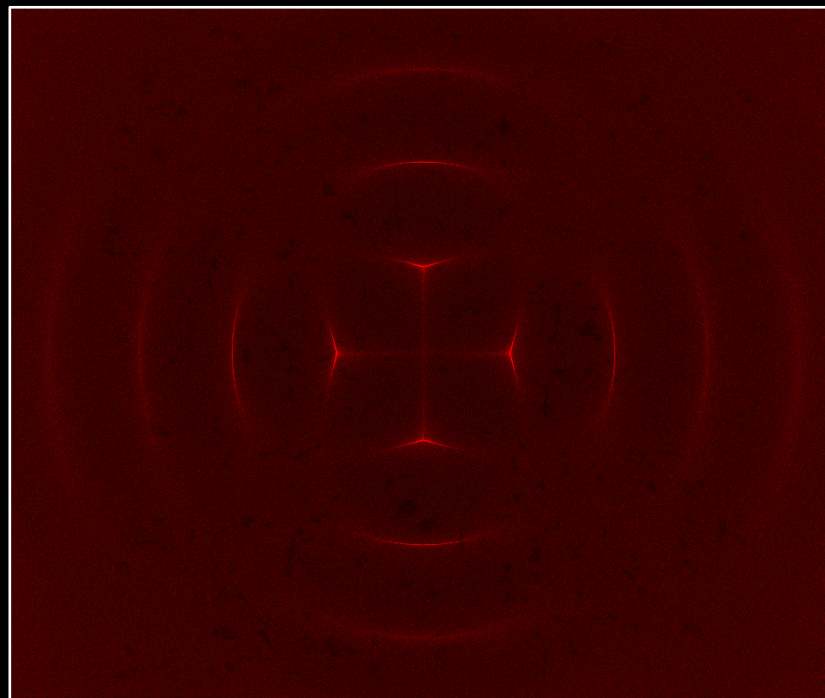
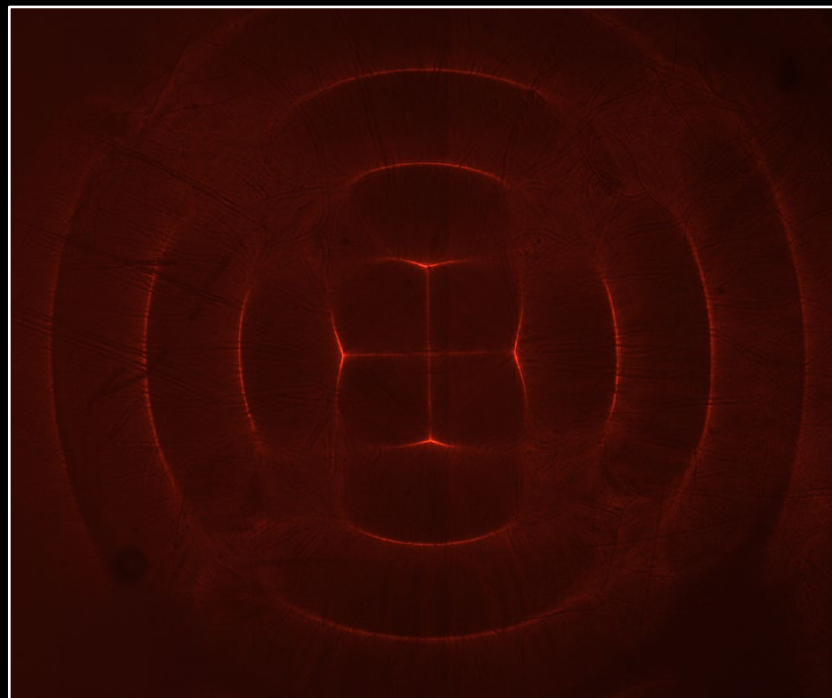
setup for ultrasonic lensing in scattering



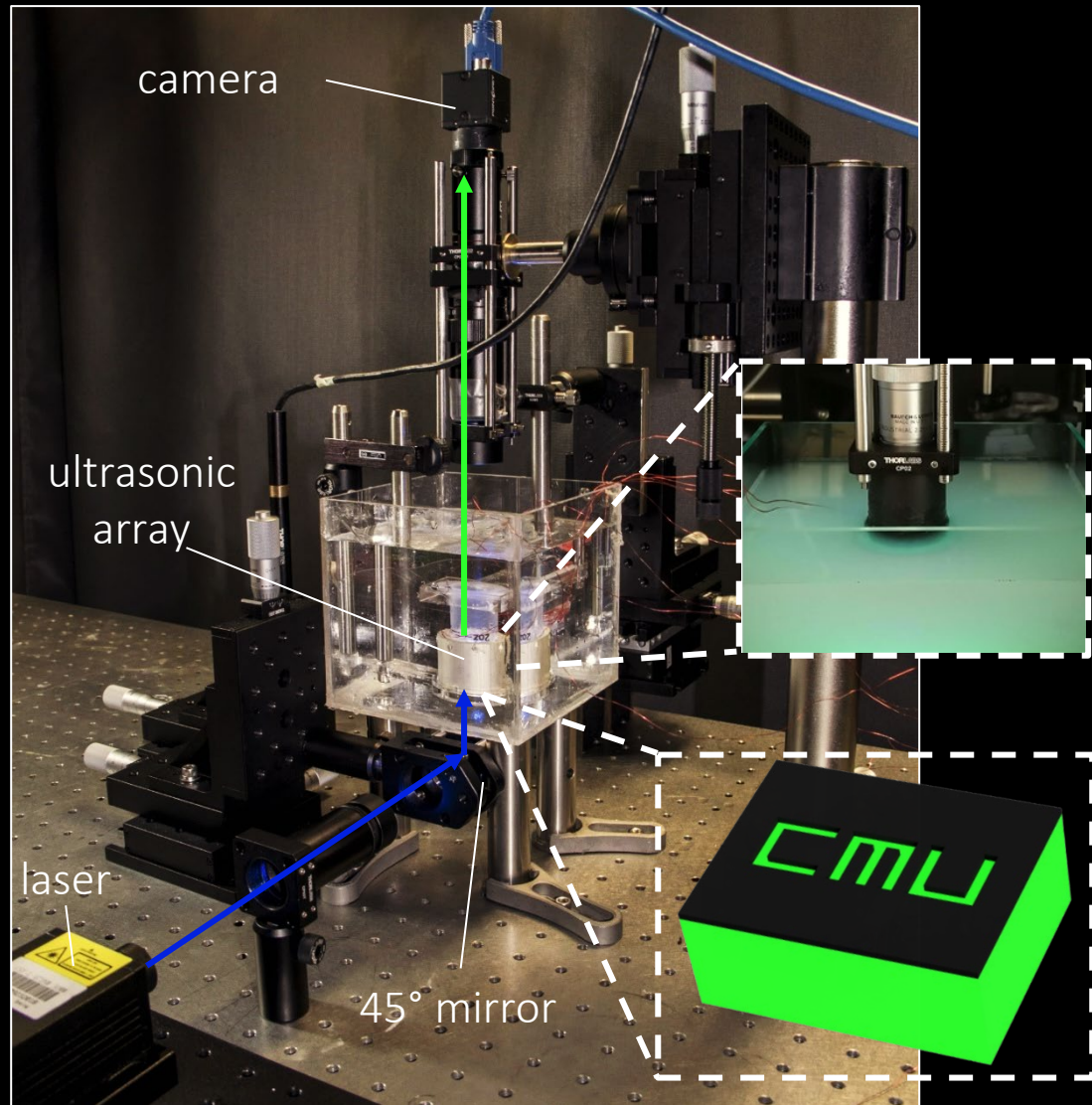
real capture

our algorithm

previous algorithm



Ultrasonic light guiding inside tissue



High-dimensional, highly-non-linear design problem:

- ultrasound frequency
- ultrasound voltage
- shape of waveguides
- placement of transducers
- sensor size
- and more...

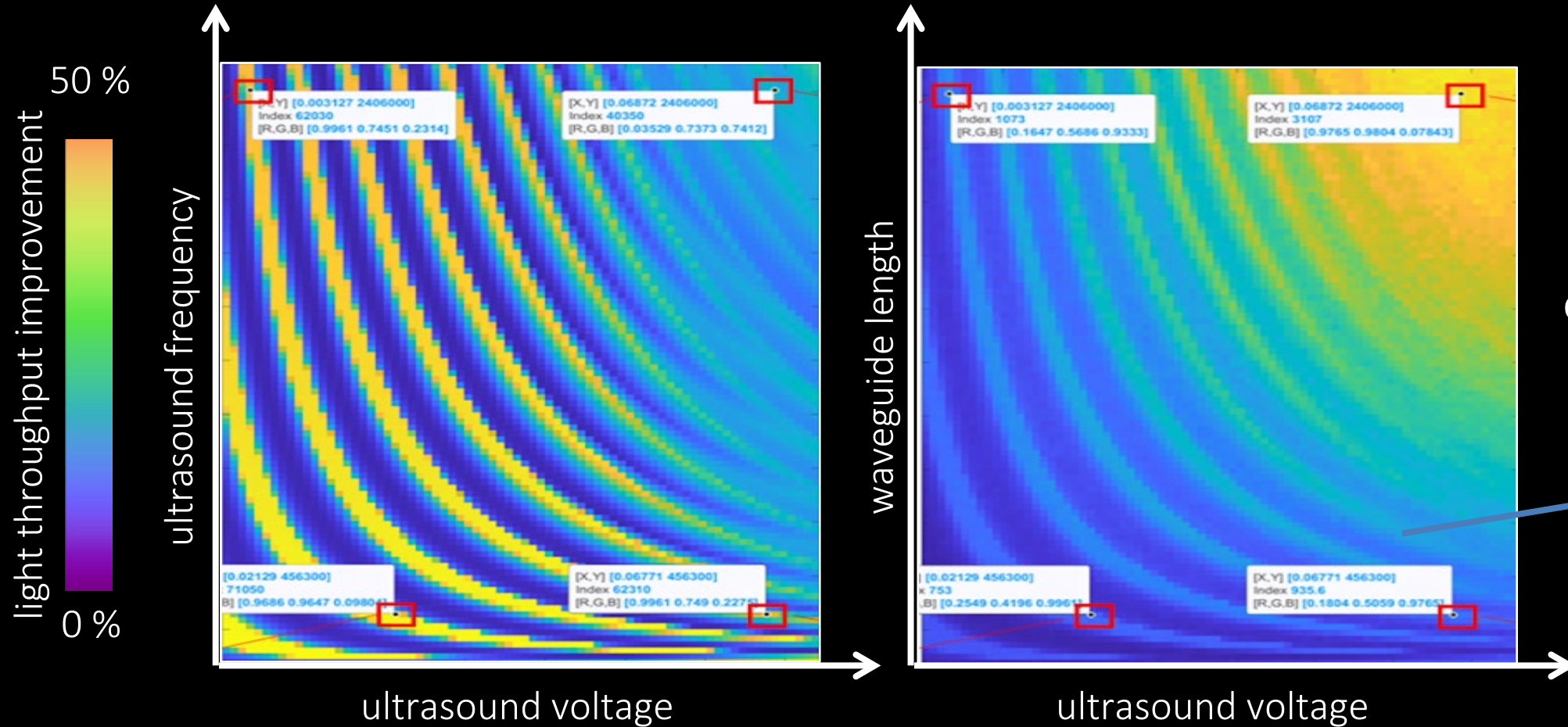
Guiding performance strongly affected by different parameter values

Painstaking experiments:

- several hours of work to test one set of parameter values

Optimizing ultrasonic GRIN waveguides

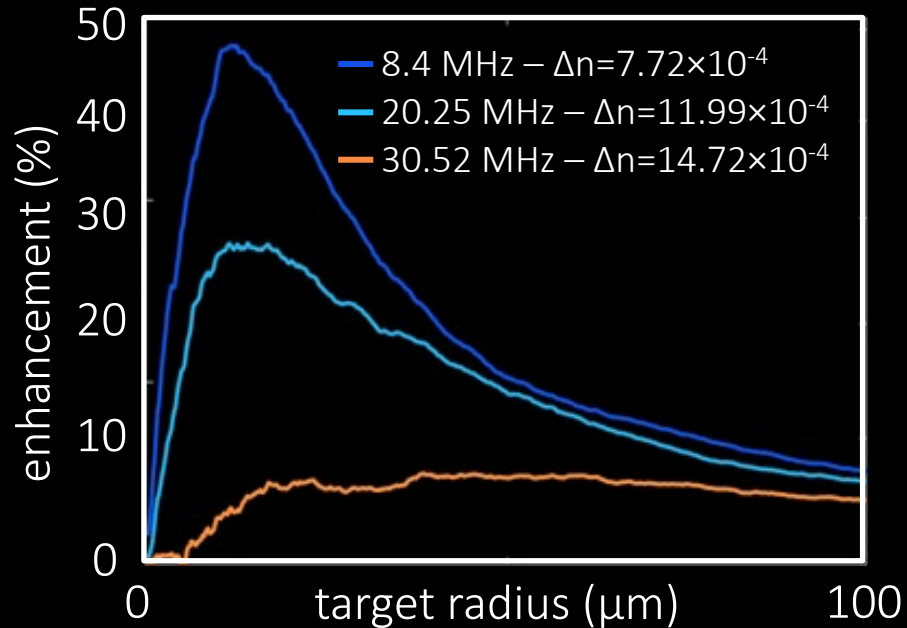
- Hundreds of thousands of virtual experiments.



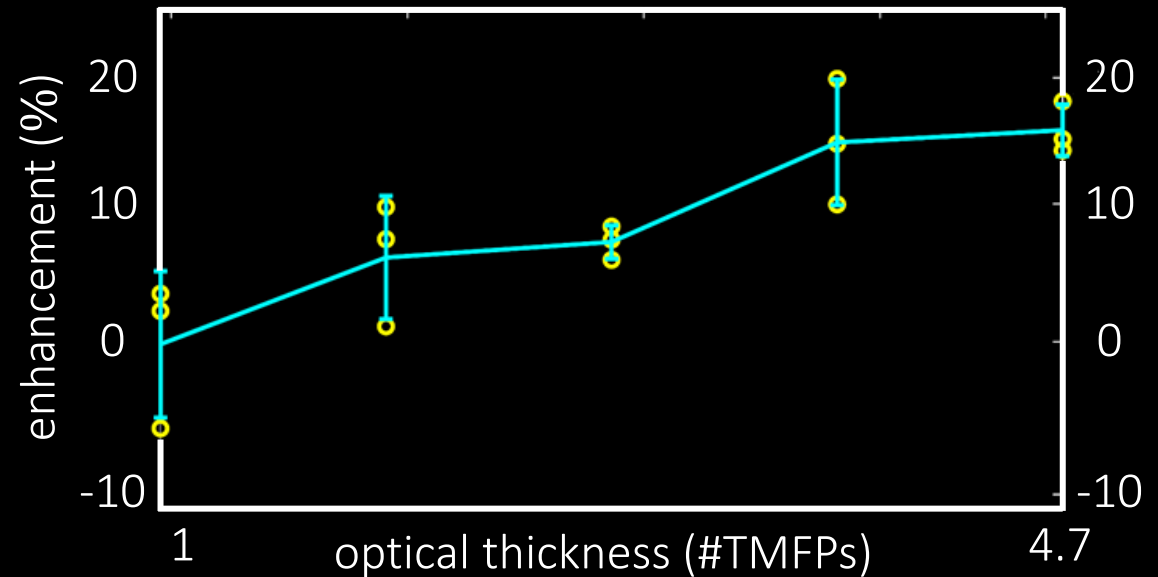
Each dot on these graphs would have been a real experiment taking a PhD student a full day's work

Improved light guiding in human bladder

simulations

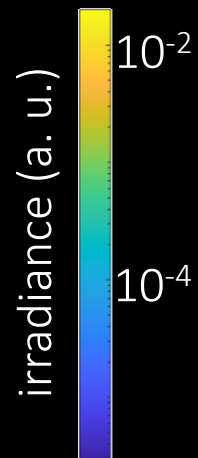
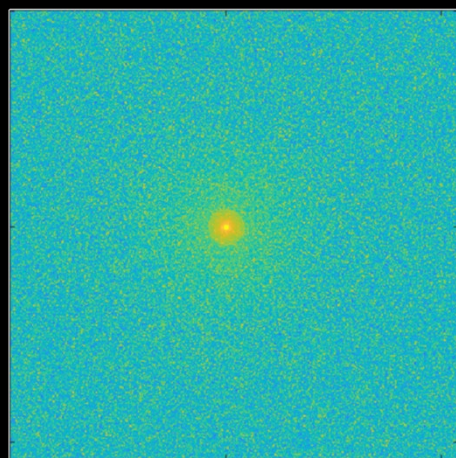
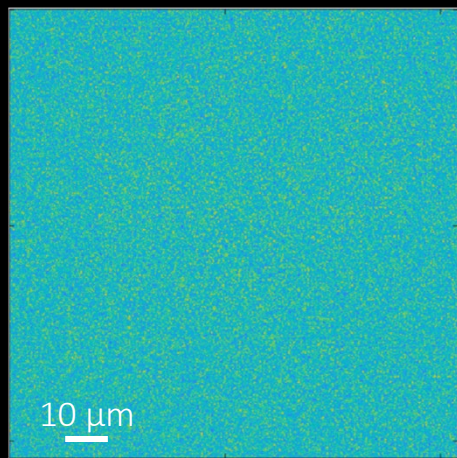


real data



ideal lens

GRIN waveguide

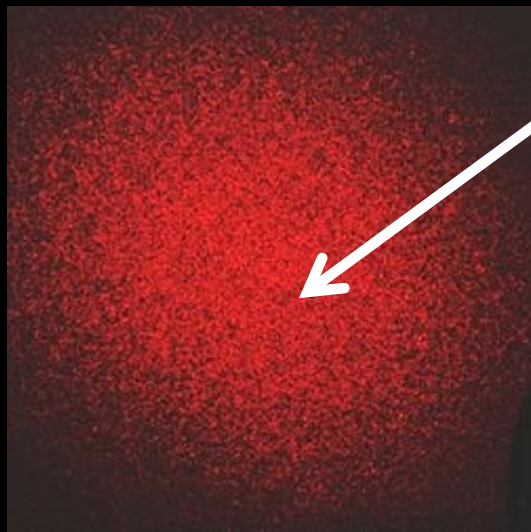


Improved light guiding performance by

- 200% compared to unoptimized waveguides
- 50% compared to external optics

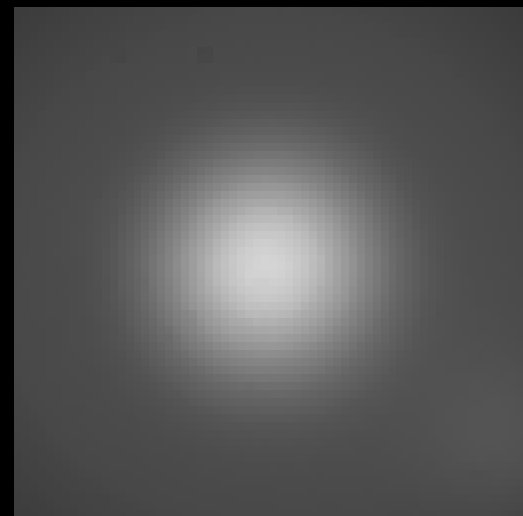
Simulation predictions verified experimentally

Speckle and memory effect



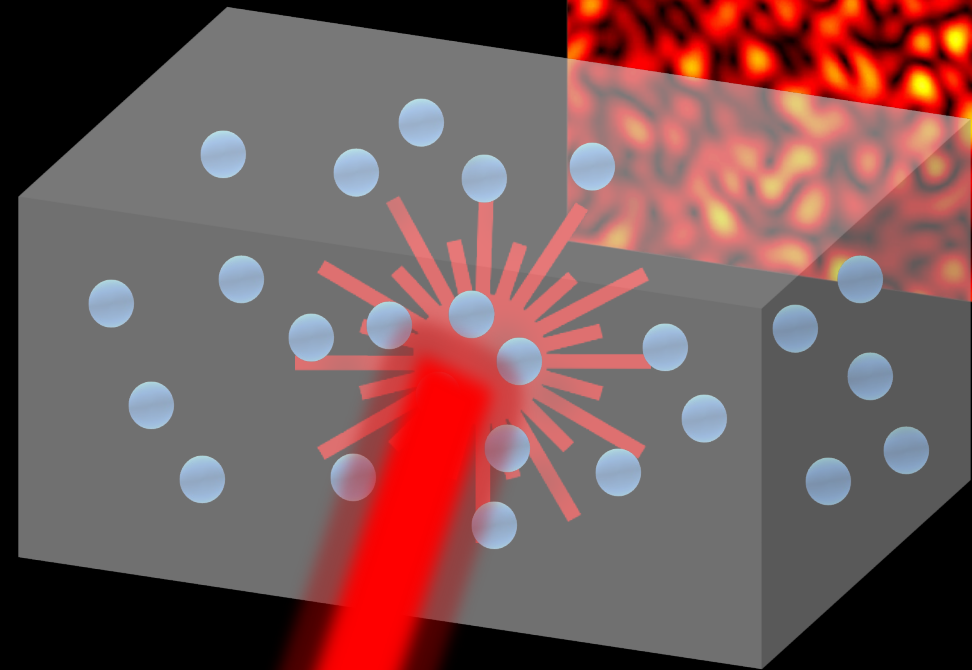
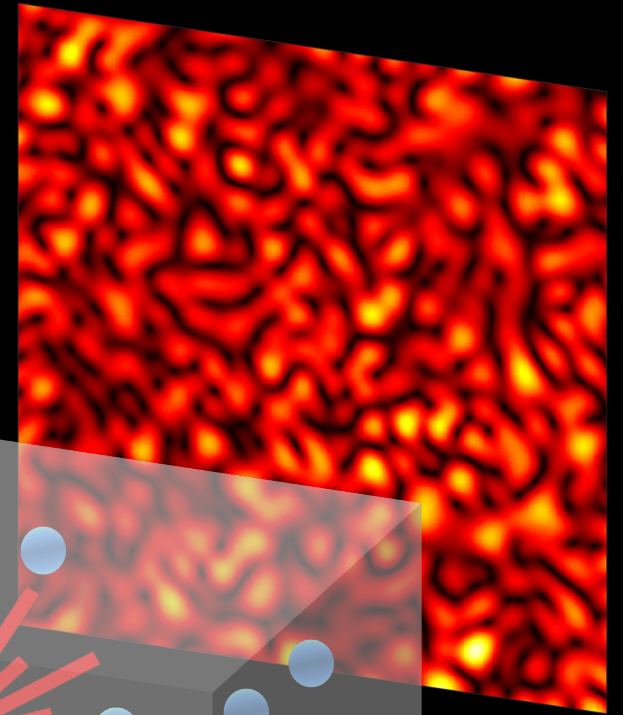
speckle: noise-like pattern

what real laser images look like



what standard rendered images look like

projected speckle image



laser beam

scattering volume



Applications and Related Work

SCIENTIFIC REPORTS

OPEN **Memory-effect based deconvolution microscopy for super-resolution imaging through scattering media**

Eitan Edrei & Giuliano Scarcelli

High-resolution imaging through turbid media is a fundamental challenge of optical sciences that has attracted a lot of attention in recent years for its wide range of potential applications. Here, we demonstrate that the resolution of imaging systems looking behind a highly scattering medium can be improved below the diffraction-limit that uses a deconvolution image processing and thus it does not require iterative focusing, scanning or phase retrieval procedures. We show that this newly established ability of direct imaging through turbid media provides fundamental and practical advantages such as three-dimensional refocusing and unambiguous object reconstruction.

Imaging performances of traditional optical systems quickly degrade with increasing scattering^{1,2}, so that in the diffusive regime only low resolution optical images can be obtained^{3,4}. However, recently, novel strategies such as phase conjugation, scattering-matrix inversion, ultrasonic encoding and the so-called 'memory effect' have revolutionized this field showing high resolution imaging and focusing behind turbid media up to several scattering lengths⁵⁻¹⁰. In many of these studies, the ability to image through turbid media is facilitated by additional information gathered on the scattering medium, for example, placing a 'guide star' in the object plane, iterative algorithms have been used to correct for the aberrations induced by the medium¹¹, or we use the fundamental information gathered on the scattering medium, for example, placing a 'guide star' in the object plane. Here, we use the fundamental information gathered on the scattering medium, for example, placing a 'guide star' in the object plane. Here, we use the fundamental information gathered on the scattering medium, for example, placing a 'guide star' in the object plane. Here, we use the fundamental information gathered on the scattering medium, for example, placing a 'guide star' in the object plane.

LOOKING THROUGH WALLS AND AROUND CORNERS

Isaac FREUND

Department of Physics, Bar-Ilan University, Ramat-Gan, Israel

It is shown theoretically that under appropriate conditions a visual scattering optical barrier can be made to serve as a thin lens which projects a real, paraxial image of objects lying behind the barrier. Preliminary experimental results verify the validity of the underlying assumptions. The described method which verifies the validity of the underlying assumptions. The described method which verifies the validity of the underlying assumptions. The described method which verifies the validity of the underlying assumptions.

1. Introduction

With the advent of radar half a century ago, detection of visually opaque barriers, such as dense cloud cover, randomness in size and position of water droplets which leads to substantial scattering of the coherent electromagnetic radiation, has become a central theme of radar. This study of coherent propagation through random media became an important part of the British Admiralty. Some of the earliest theoretical studies were carried out by Cyril Domb while seconded to the Royal Air Force. As always, the problems attacked early on by Domb were to form later on the basis of his very first publications. As always, the problems attacked early on by Domb were to form later on the basis of his very first publications. As always, the problems attacked early on by Domb were to form later on the basis of his very first publications.

ARTICLES

PUBLISHED ONLINE: 29 JUNE 2015 | DOI: 10.1038/NPHYS3373

Translation correlations in anisotropic scattering media

Benjamin Judkewitz^{1,2*}, Roarke Horstmeyer^{2*}, Ivo M. Vellekoop³, Ioannis N. Papadimitrakis⁴ and Changhuei Yang²

Controlling light propagation across scattering media by wavefront shaping holds great promise for communications and imaging applications. But, finding the right shape for the wavefront is a challenge because the transmission matrix of a scattering medium is not known. Here, we demonstrate a method for imaging through scattering media by exploiting the inherent angular correlation of the scattered light. We show that significant transmission correlations in thick scattering media at zero distance are directional.

Focusing light through strongly scattering media is an important goal in optical imaging and communication. Long considered impossible, recent advances in the field of wavefront shaping¹⁻³ changed this view by demonstrating that diffuse light can be focused through inhomogeneous media—as long as the correct input wavefront is used. With direct optical access to the target plane, the correct wavefront can be obtained by iterative optimization⁴, phase conjugation⁵, or by measuring the transmission matrix^{6,7}. In many cases, nonlinear⁸, fluorescent⁹, kinematic¹⁰, acousto-optic¹¹ and photo-acoustic¹² guide stars can be used as reference beacons. However, these techniques provide wavefront information for only one target location at a time. Although transmission matrices can be sampled quickly with a photo-acoustic approach¹³, this method requires absorbing samples. As a result, many samples within a transmission matrix can be sampled only sparsely. Correlations between input and output scattered wavefronts (that is, the transmission matrix) is not known. Here, we demonstrate a method for imaging through scattering media by exploiting the inherent angular correlation of the scattered light. We show that significant transmission correlations in thick scattering media at zero distance are directional.

ARTICLES

PUBLISHED ONLINE: 31 AUGUST 2014 | DOI: 10.1038/NPHOTON.2014.189

Non-invasive single-shot imaging through scattering layers and around corners via speckle correlations

Ori Katz^{1,2*}, Pierre Heidmann¹, Mathias Fink¹ and Sylvain Gigan^{1,2}

Optical imaging through and inside complex samples is a difficult challenge with important applications in many fields. The fundamental problem is that inhomogeneous samples such as biological tissue randomly scatter and diffuse light, preventing the formation of diffraction-limited images. Despite many recent advances, no current method can perform non-invasive imaging through strongly scattering layers and around corners via speckle correlations.

Object **Scattering medium** **Camera image**

O S $I = O * S$

reconstruction

A schematic of the experimental setup is presented in Fig. 1. An object is hidden at a distance u behind a highly scattering medium of thickness L . The object is illuminated by a spatially incoherent, narrow-band source, and a high-resolution camera that is placed at a distance v on the other side of the medium records the pattern of the scattered light that has diffused through the scattering medium. Although the raw recorded camera image (Fig. 1b), its autocorrelation (Fig. 1c) is essentially identical to the object's autocorrelation (Fig. 1d) and thus can be reconstructed by exploiting the inherent angular correlation of the scattered light.

LETTER

Non-invasive imaging through opaque scattering layers

Ebert G. van Putten^{1,2*}, Christian Illume¹, Ad Legendijk^{1,2}, Willem L. Vos³ & Allard P. Mosk¹

Optical imaging techniques, such as optical coherence tomography, are essential diagnostic tools in many fields of science and technology. However, present techniques require either a detector¹ or a nonlinear process behind the scattering layer. Here we report a non-invasive imaging method that allows non-invasive imaging of a fluorescent object hidden behind an opaque scattering layer. We scan the angle of incidence of the total fluorescence of the object from the front surface of the scattering layer. As a proof of concept, we obtain the image of a fluorescent object, compared to a typical human cell, through an opaque optical diffuser, and an image of a fluorescent object, compared to a typical human cell, through an opaque optical diffuser, and an image of a fluorescent object, compared to a typical human cell, through an opaque optical diffuser.

ARTICLES

Correlation resolution enhancement of fluorescence imaging

Ebert G. van Putten^{1,2*}, Jacopo Bertolotti^{1,3}, Ad Legendijk¹, Allard P. Mosk¹

Fluorescence imaging is essential in nanoscience and biological sciences. Due to the diffraction limit, imaging systems can only resolve structures larger than 200 nm. Here, we introduce a new imaging method that enhances the resolution by using a high-index scattering medium as an imaging lens. We achieve a wide field of view. We develop a new image reconstruction algorithm that converges to a wide field of view. We develop a new image reconstruction algorithm that converges to a wide field of view. We develop a new image reconstruction algorithm that converges to a wide field of view.

Simulating speckles

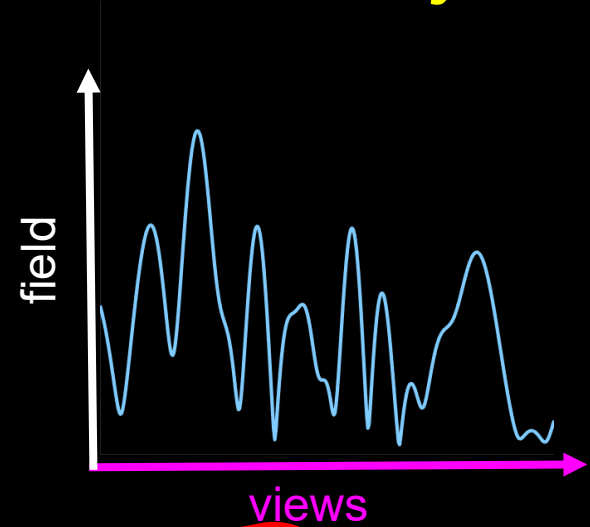
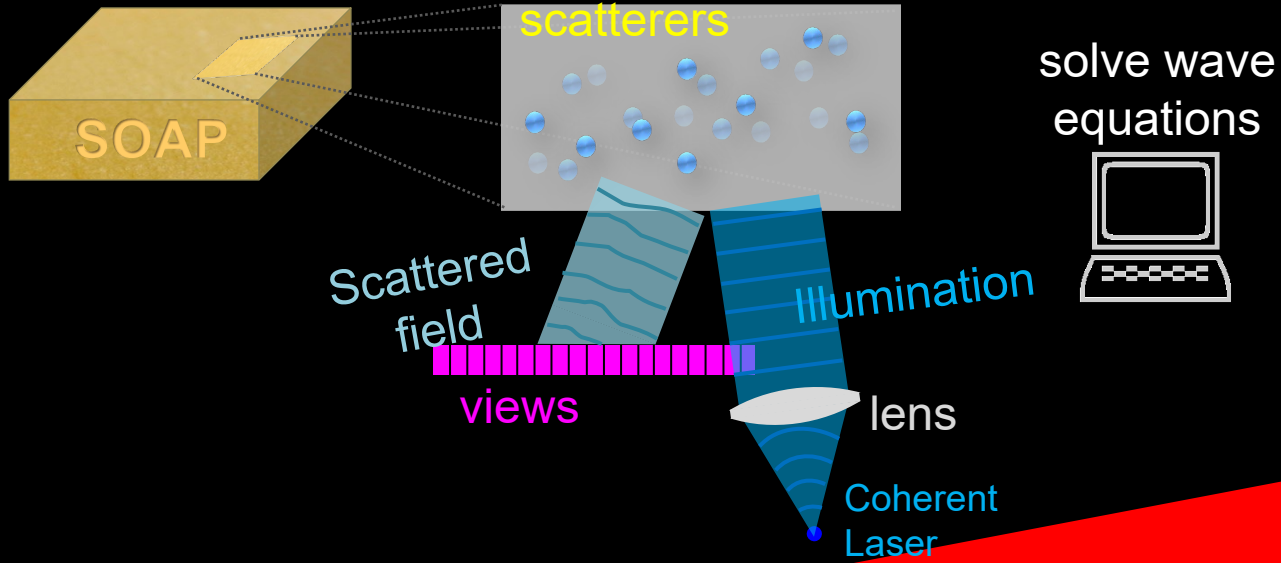
inefficient



Specify exact (sub-wavelength) position of scatterers



In graphics we describe materials by **statistical** bulk parameters, as the **density** of scatterers



Wave equation solvers

- Differential equation F
- Integral equation (e.g.,

Slow
Practical only for tiny or optically thin media

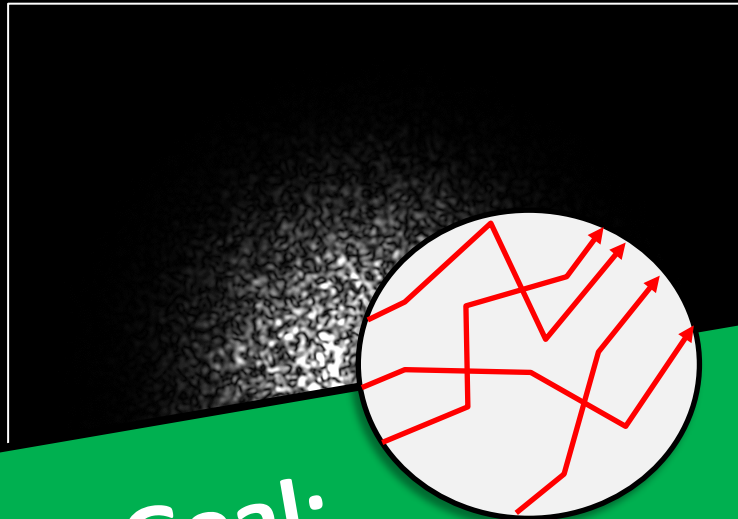


For simplicity: **Flatland**
Scattering medium is 2D
Sensor is 1D
Speckle pattern is 1D

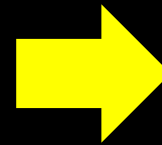
Monte Carlo (MC) Simulation of Speckles

MC Advantage:

1. **Fast**
2. input is scatterer **density** rather than exact scatterer locations

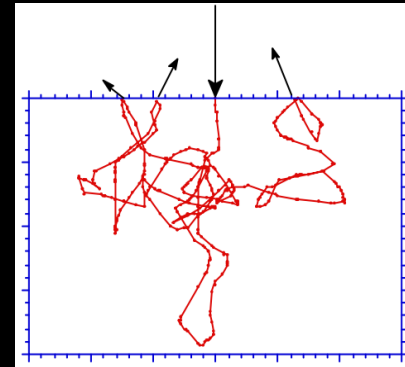


Our Goal:
Extend efficient MC tools
to evaluate speckles and
their coherent statistics



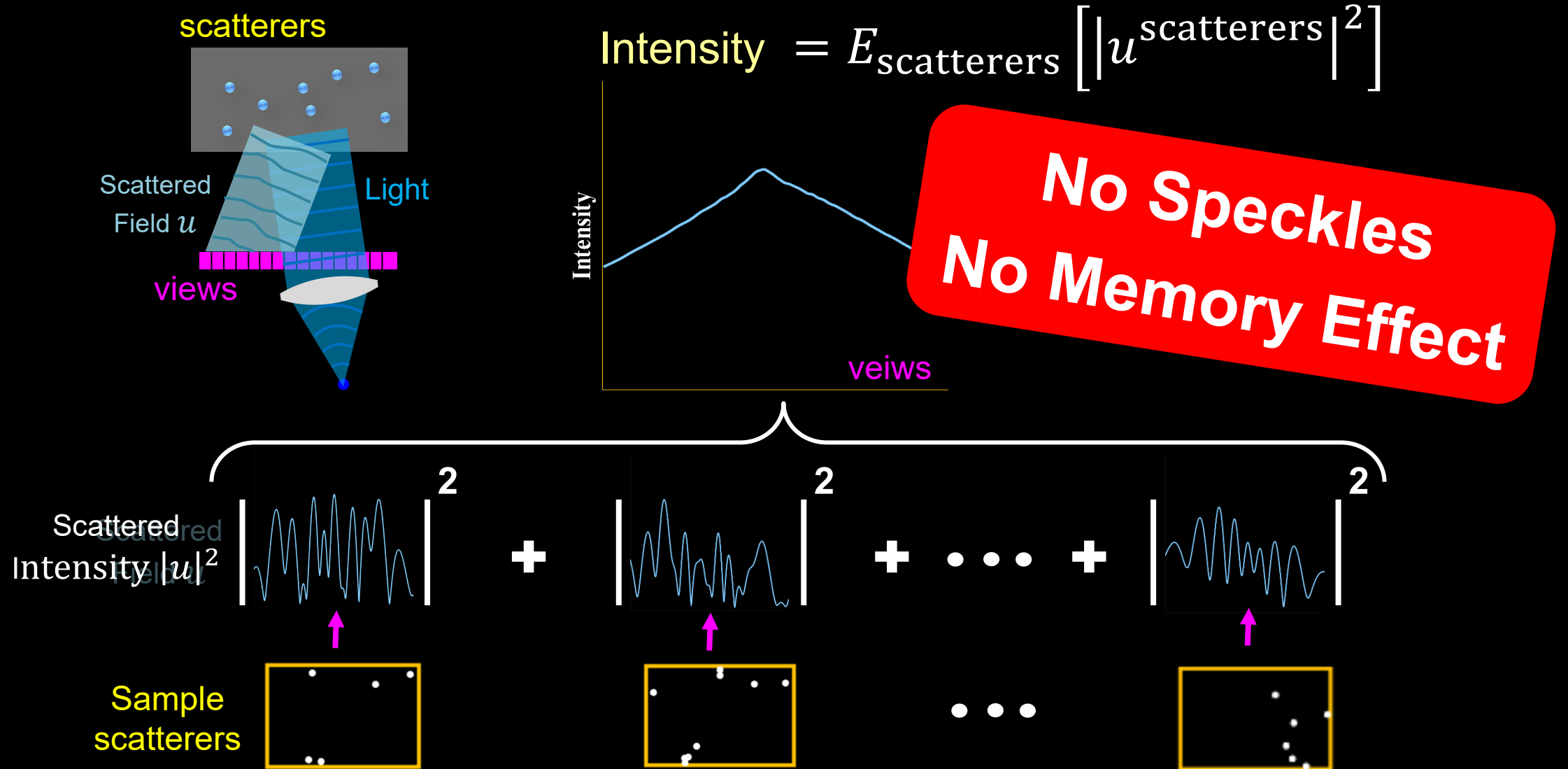
Standard intensity MC

Smooth, no speckles



Monte Carlo Modeling of Light
Transport in Multi-layered Tissues,
Wang & Jacques, 1992

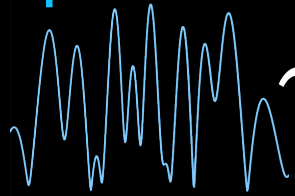
Wave Solution v.s. Monte Carlo



MC requires the scatterers density – no need for exact positions

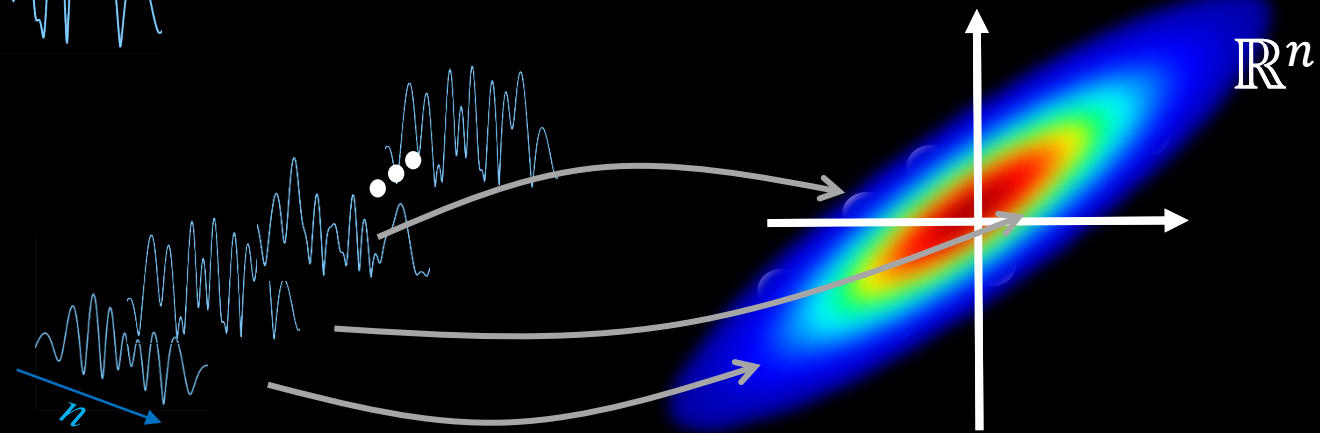
Speckle Statistics

Speckles



$$\sim \mathcal{N} (\text{Mean, Covariance})$$

Sufficient Statistics

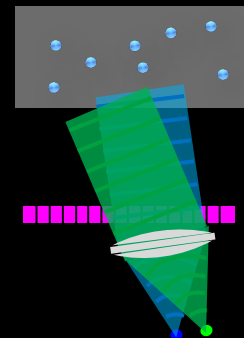
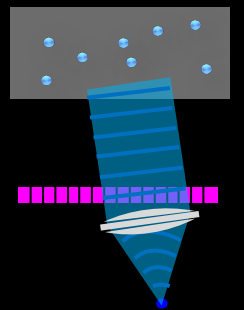


1st moment

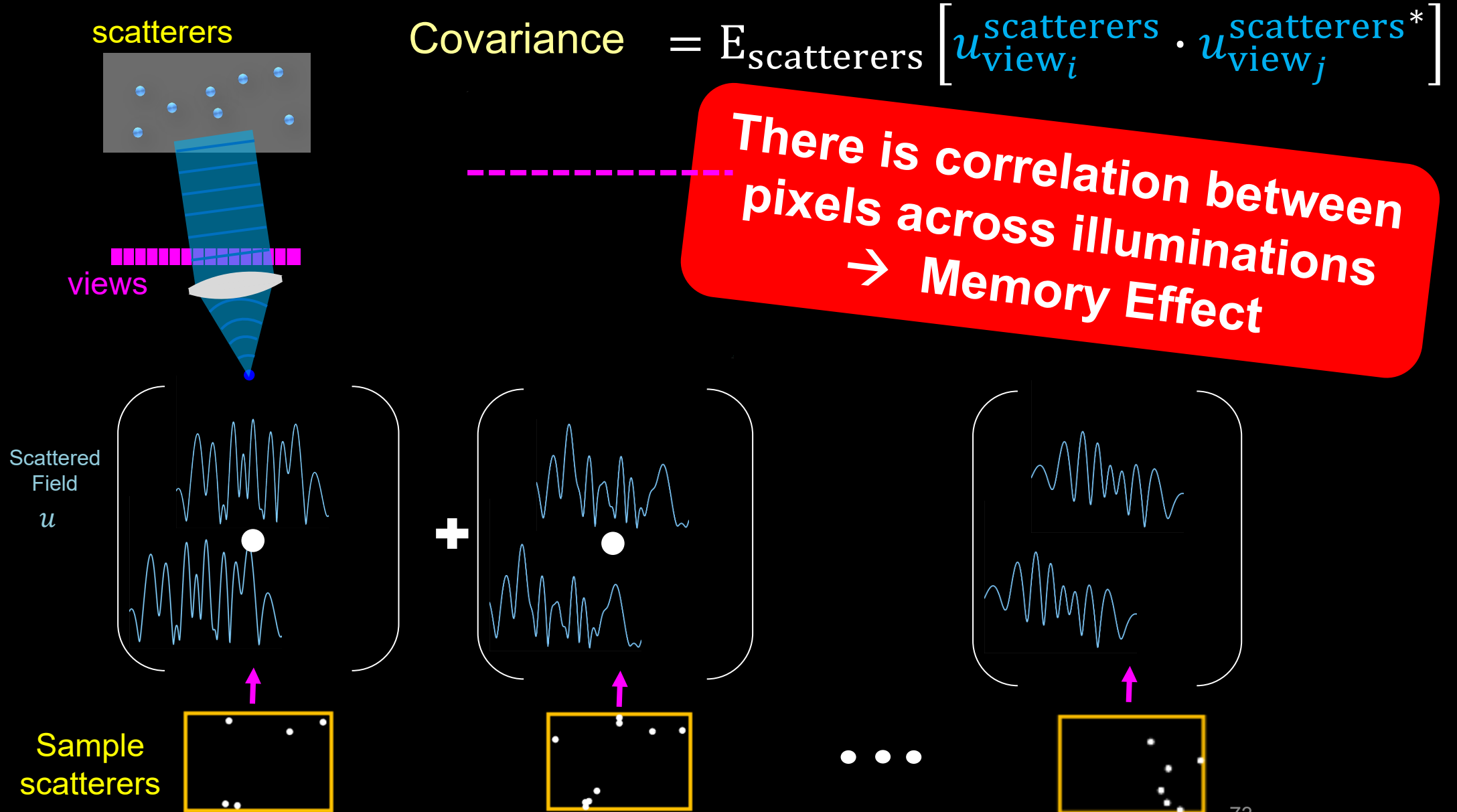
~~$$\text{Intensity Mean} = E_{\text{scatterers}} [|u_{\text{scatterers}}|^2] \Rightarrow \text{Incoherent Summation}$$~~

Cross-Illumination

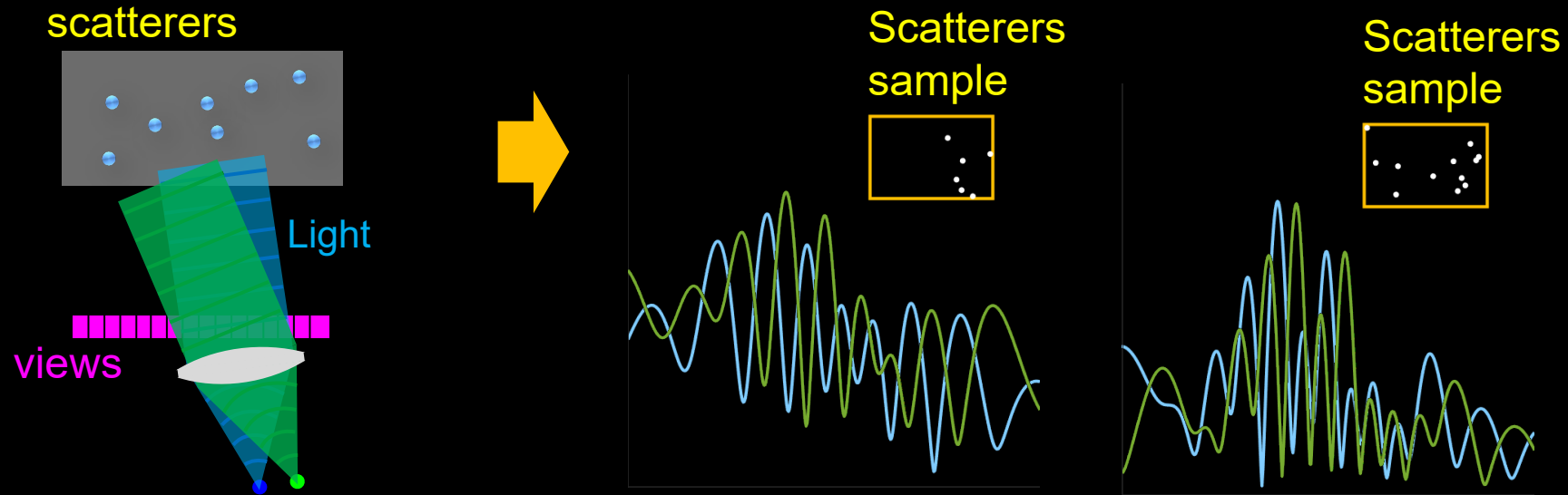
$$\text{Field Covariance} = E_{\text{scatterers}} [u_{\text{view}_i}^{\text{light}_1, \text{scatterers}} \cdot u_{\text{view}_j}^{\text{light}_2, \text{scatterers}*}]$$



2nd Moment - Covariance



Cross-illumination statistics



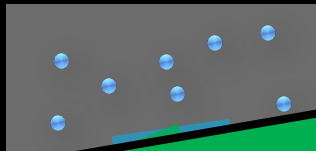
Memory Effect:

tilting illumination results in highly correlated shifted speckles

Next: Cross Illumination Covariance

Cross-illumination statistics

scatterers



Covariance = $E_{\text{scatterers}}$



path shift = path shift

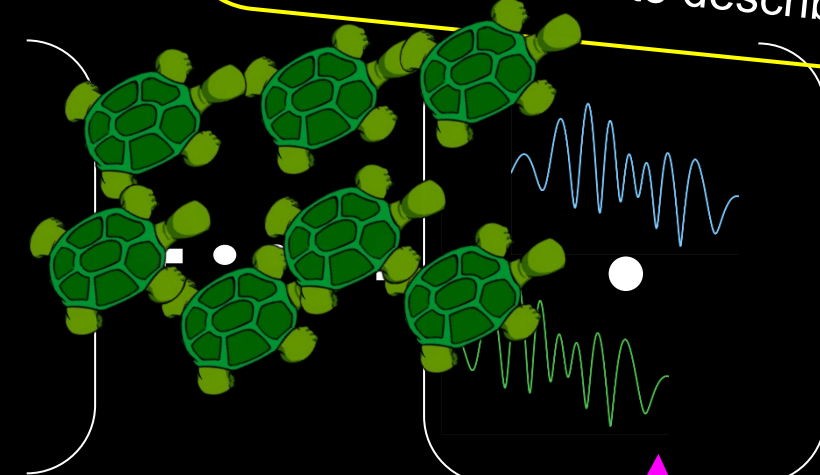
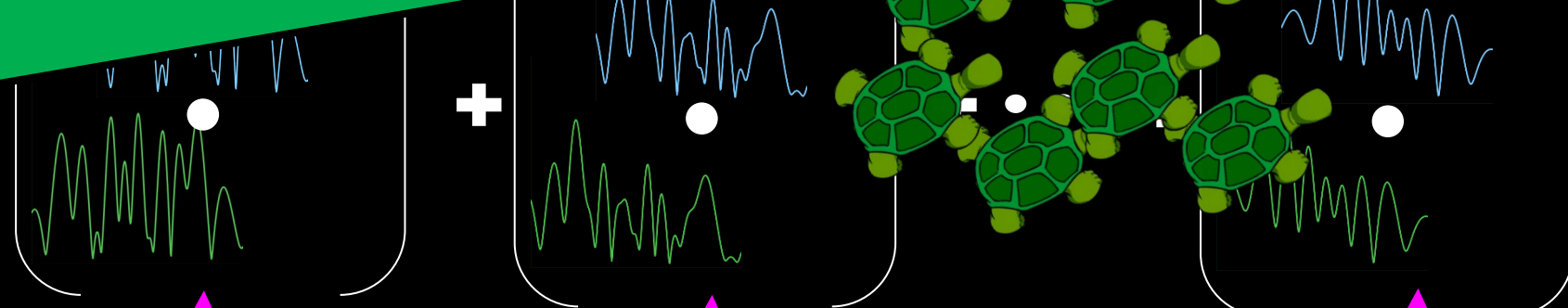
$$\left[\begin{array}{c} \text{light}_1, \text{scatterers} \\ u_{\text{view}_i} \end{array} \cdot \begin{array}{c} \text{light}_2, \text{scatterers}^* \\ u_{\text{view}_j} \end{array} \right]$$

We developed:
Efficient MC
for Speckle Covariance

Speckles are Gaussian:
Mean + Covariance
are sufficient statistics

This is all we need to describe speckles

Scattered Field
 u_{light_2}



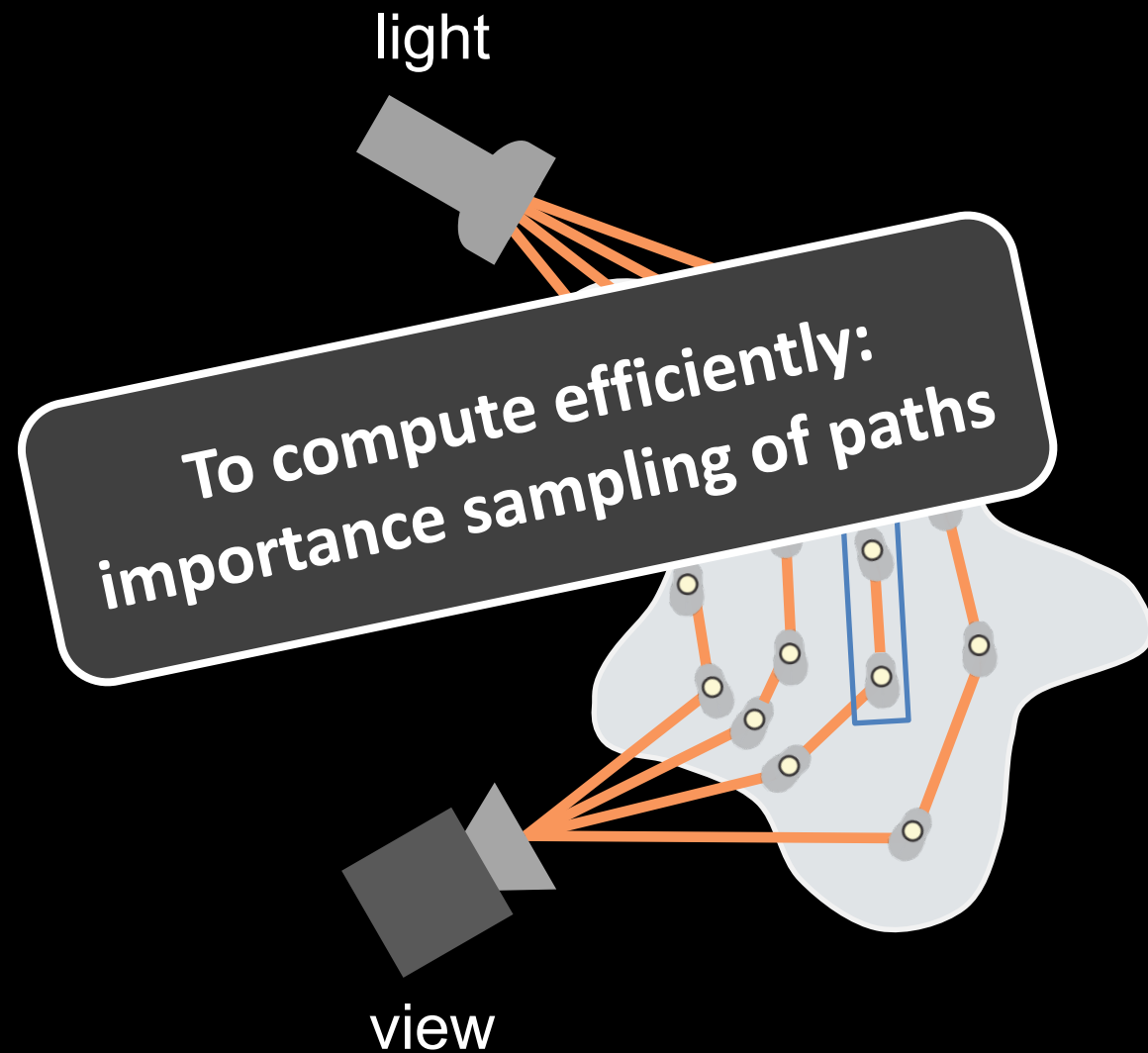
Sample scatterers



...

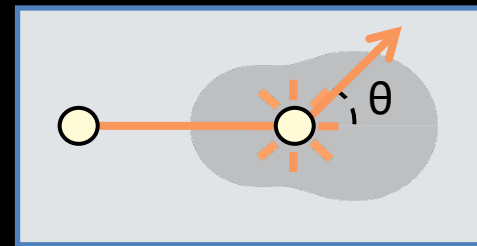


Monte Carlo Rendering 101



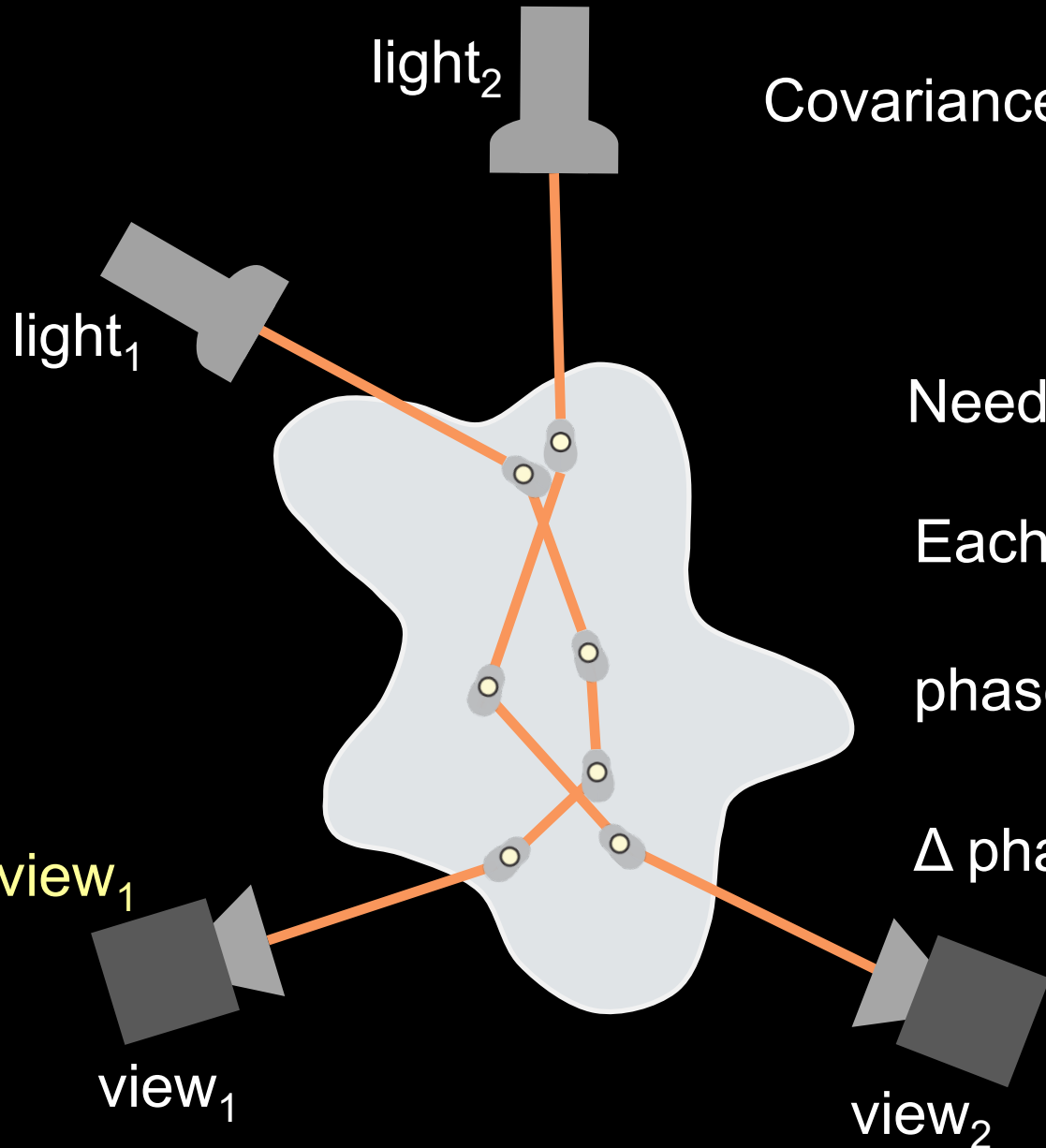
$$\text{Image} = \int_{\text{paths}} f(\text{path})$$

Throughput that acts on each path, depends on the scattering material



volumetric density
(extinction coefficient) $\left[\begin{array}{c} \sigma \\ a \\ p_{\theta} \end{array} \right]$
scattering albedo
phase function

Covariance Rendering



$$\text{Covariance} = \int_{\text{path}_1, \text{path}_2} u(\text{path}_1) \cdot u^*(\text{path}_2)$$

$$u = |u| e^{i \cdot \text{phase}}$$

Need to consider products of **pairs** of paths

Each path contributes a complex number u

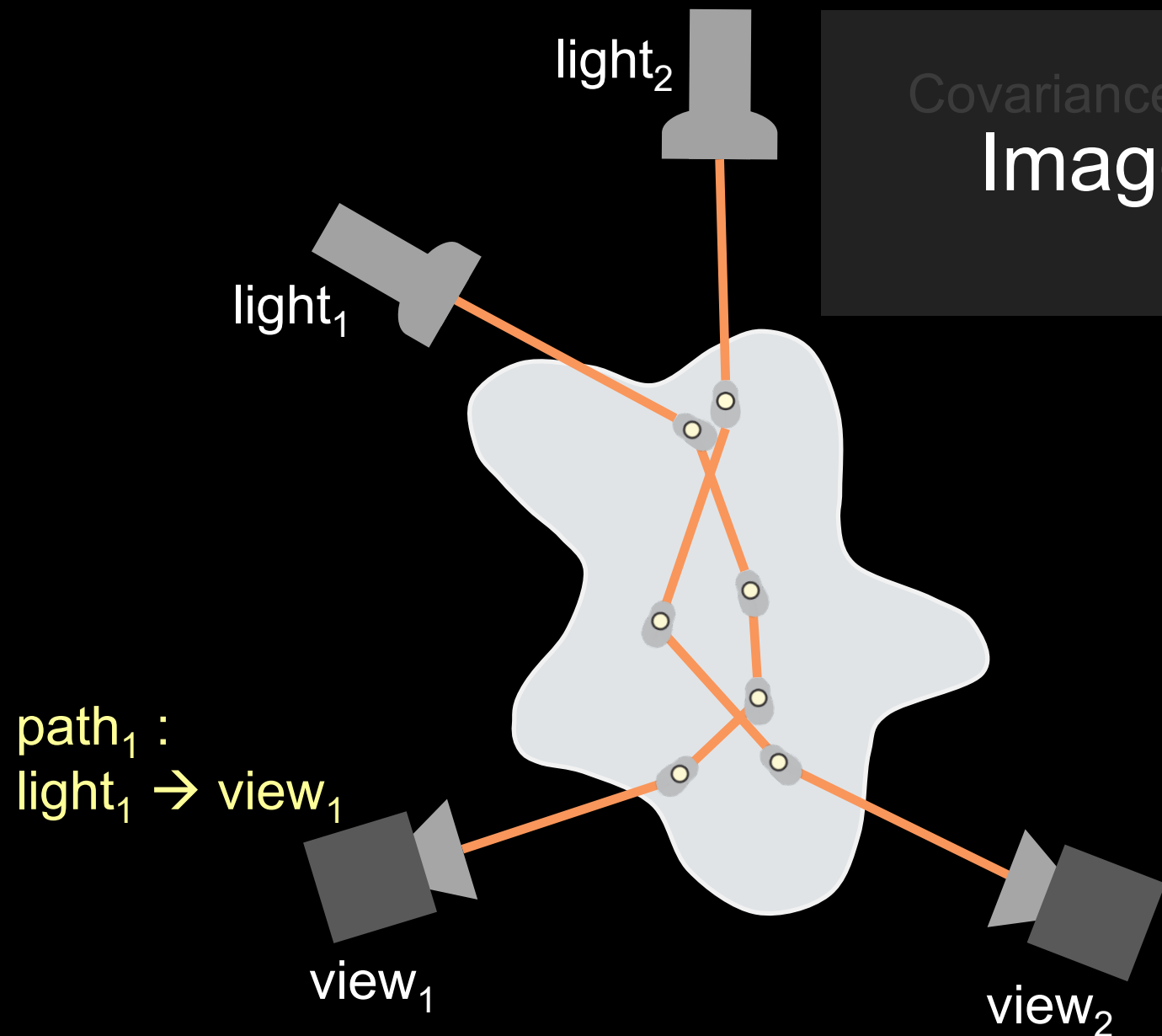
$\text{phase} \propto \text{Length}(\text{path})$

$\Delta \text{phase} \propto \text{Length}(\text{path}_1) - \text{Length}(\text{path}_2)$

$\text{path}_1 :$
 $\text{light}_1 \rightarrow \text{view}_1$

$\text{path}_2 :$
 $\text{light}_2 \rightarrow \text{view}_2$

Covariance Rendering



$$\text{Covariance} = \int_{\text{paths}} u(\text{path}_1) \cdot u^*(\text{path}_2)$$

$$\text{Image} = \int_{\text{paths}} f(\text{path})$$

Real throughout $i \cdot \text{phase}$
 $u = |u| e^{i \cdot \text{phase}}$

$$\text{path}_1 = \text{path}_2$$



Same complex contribution

$$u(\text{path}_1) = u(\text{path}_2)$$



$$\Delta \text{ phase} = 0$$



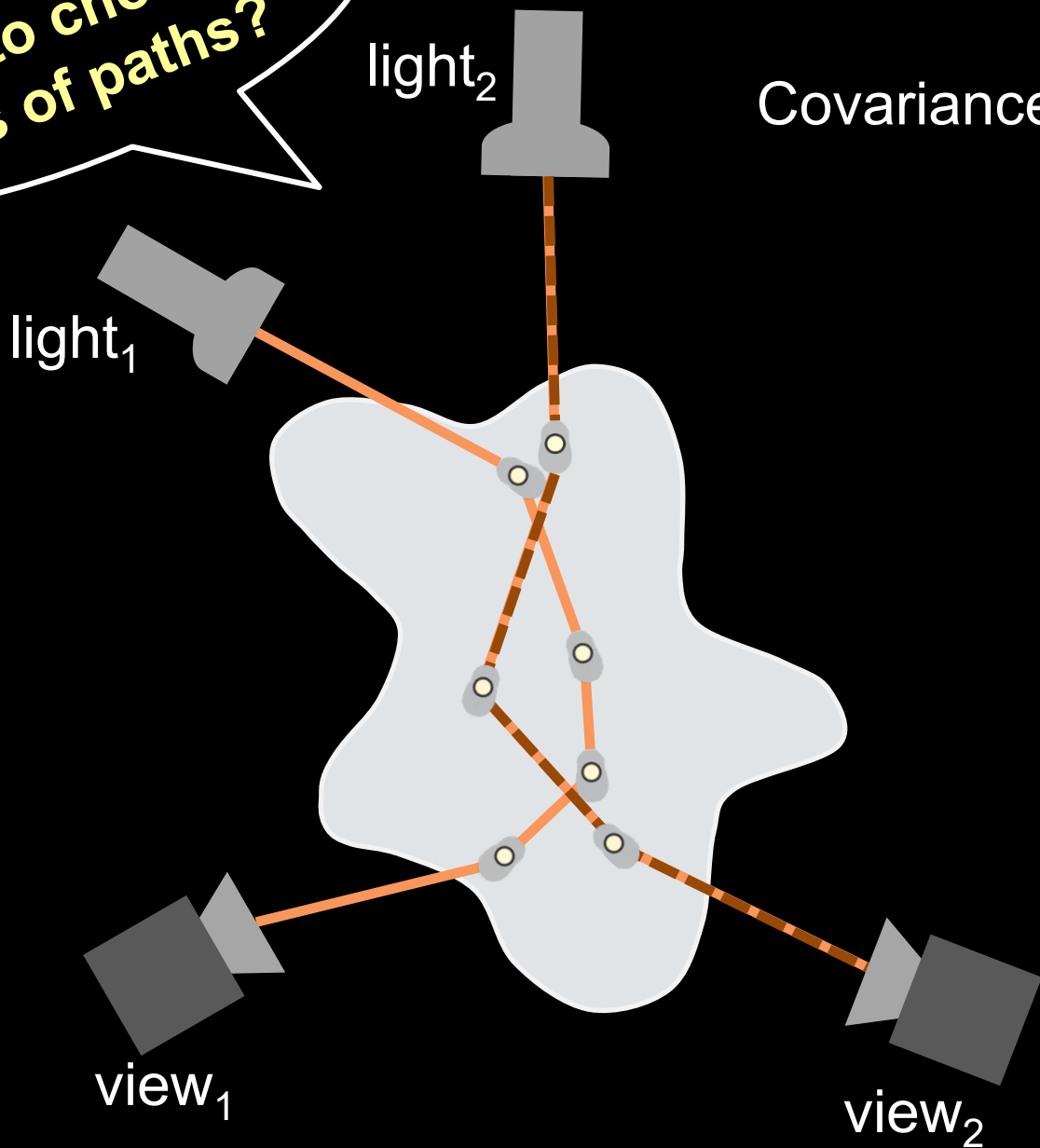
$$\text{path}_2 : u(\text{path}) \cdot u^*(\text{path}) = f(\text{path})$$

$light_2 \rightarrow view_2$

Real

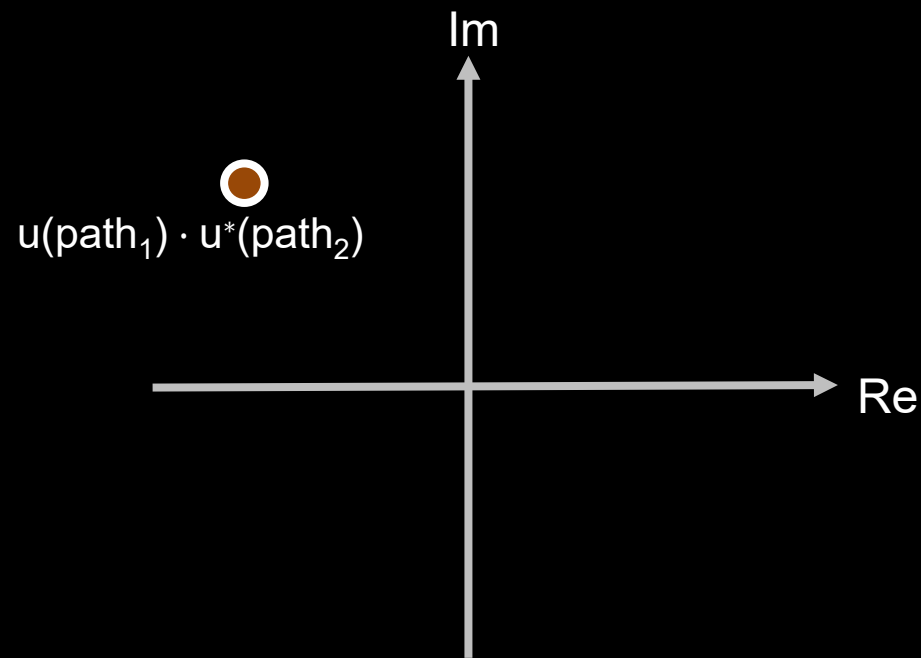
Covariance rendering

How to choose pairs of paths?

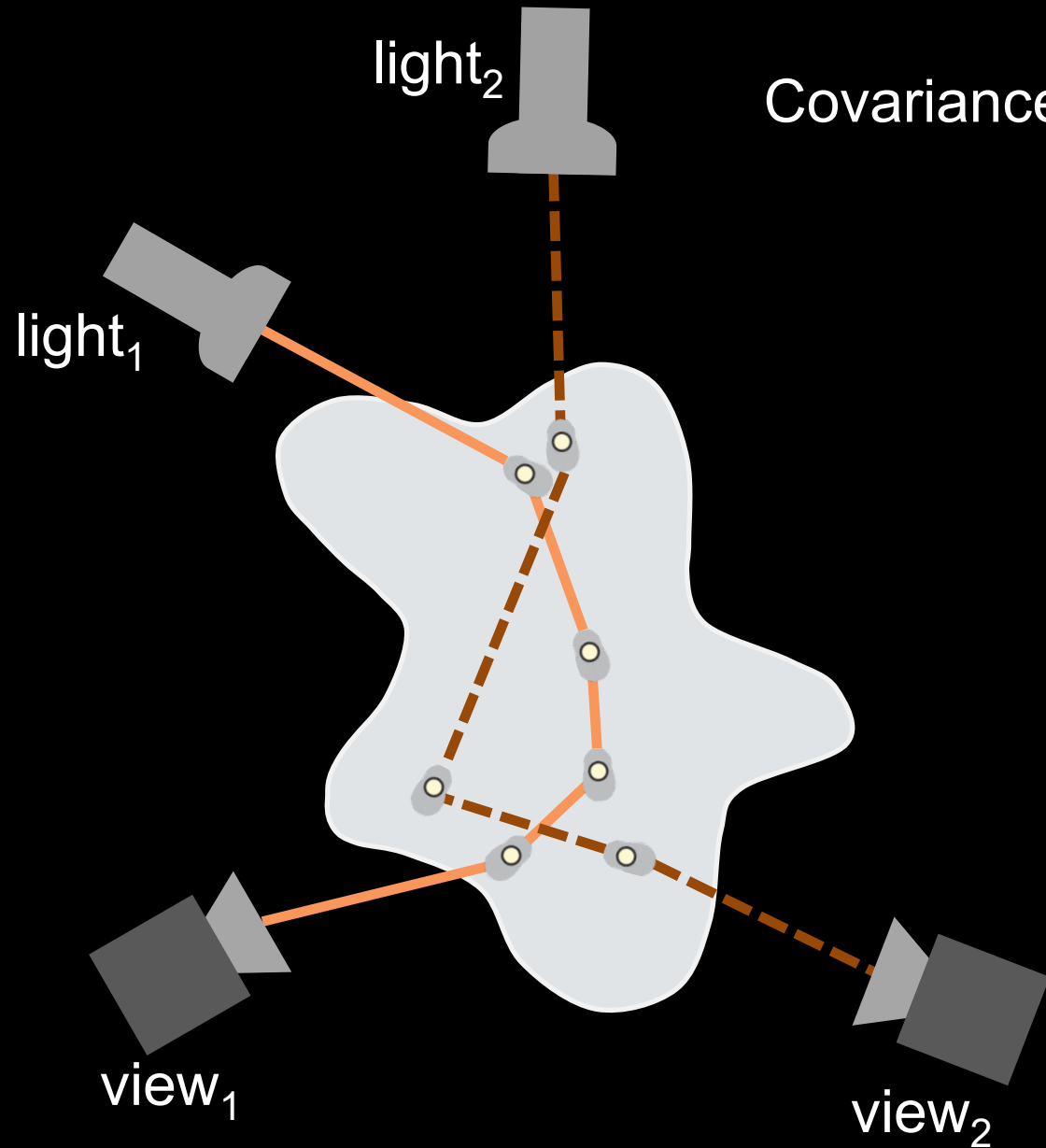


$$\text{Covariance} = \int_{\text{path}_1, \text{path}_2} u(\text{path}_1) \cdot u^*(\text{path}_2)$$

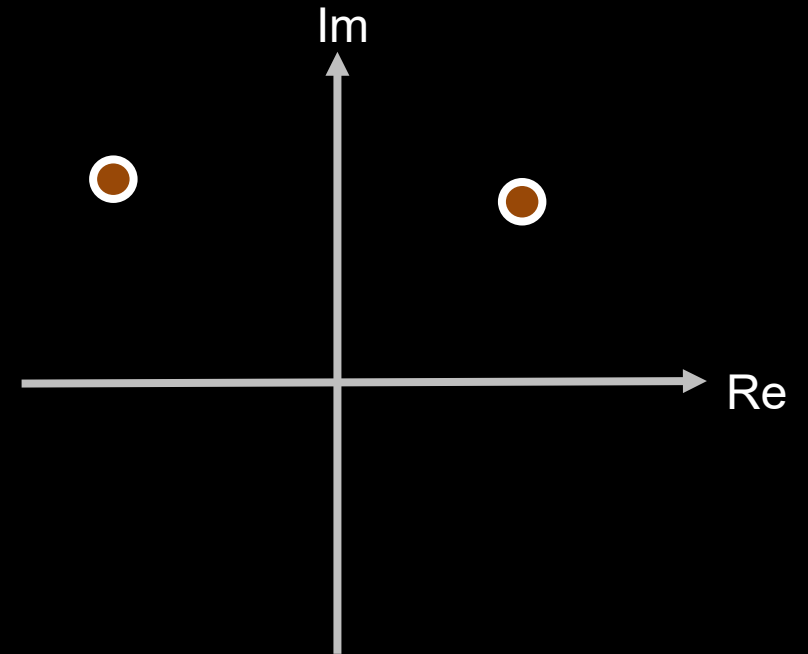
$$u = |u| e^{i \cdot \text{phase}}$$



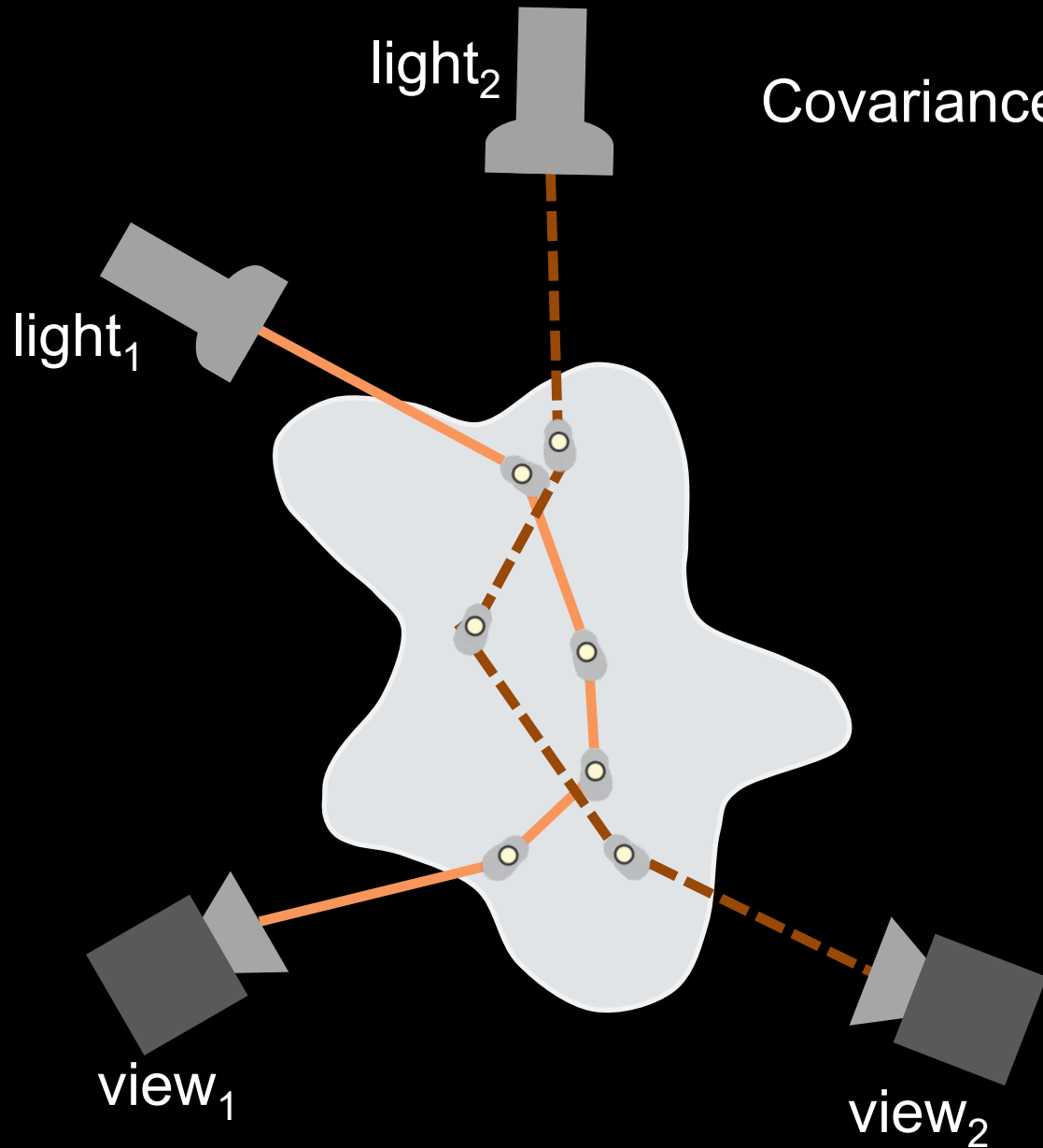
Covariance rendering



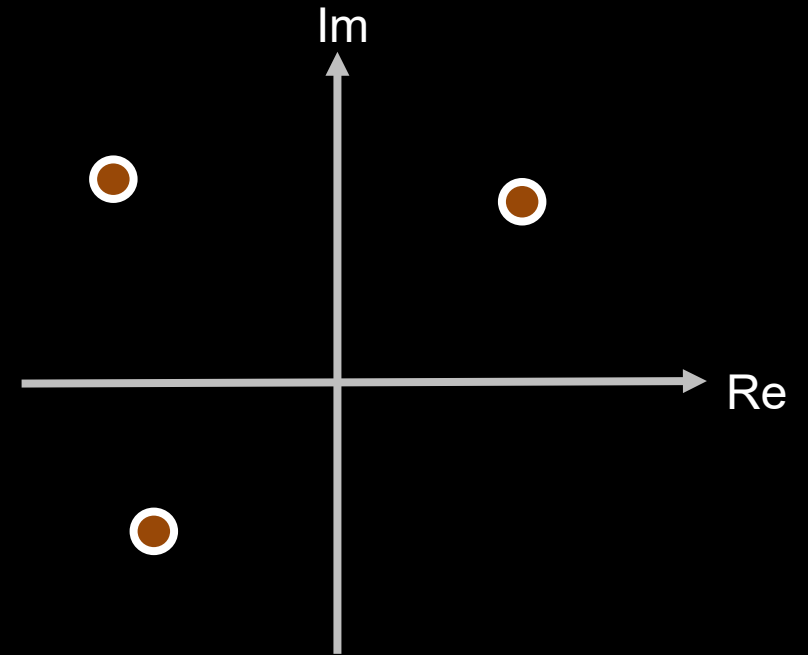
$$\text{Covariance} = \int_{\text{path}_1, \text{path}_2} u(\text{path}_1) \cdot u^*(\text{path}_2)$$



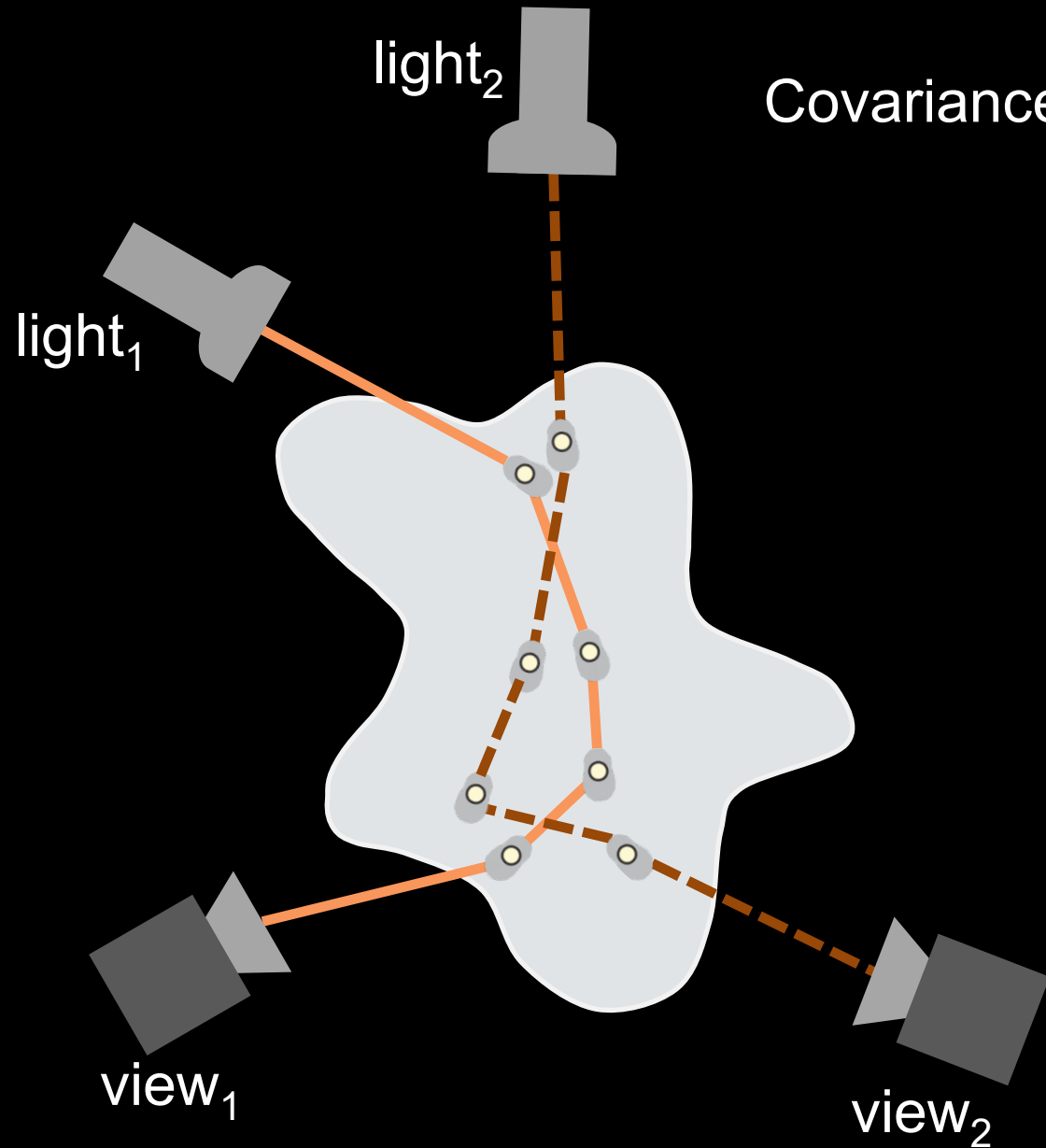
Covariance rendering



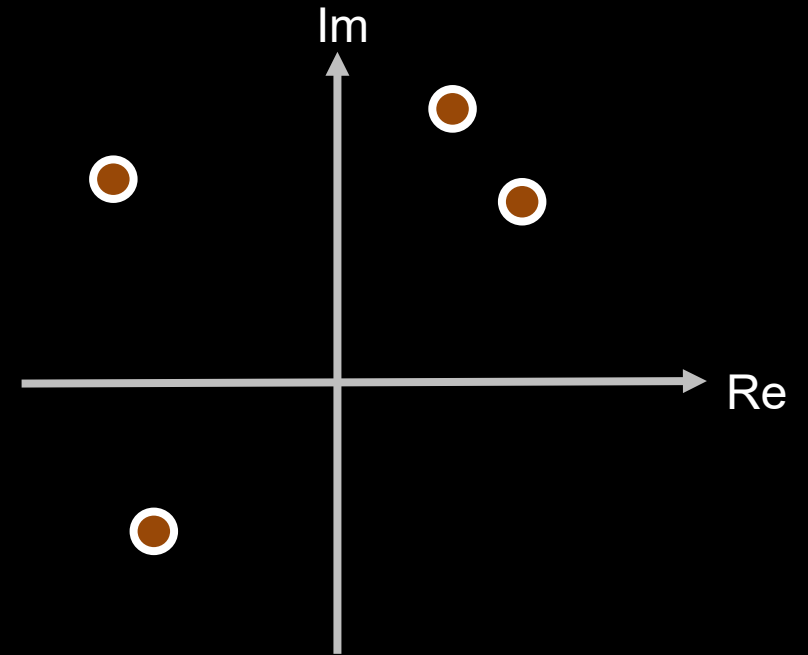
$$\text{Covariance} = \int_{\text{path}_1, \text{path}_2} u(\text{path}_1) \cdot u^*(\text{path}_2)$$



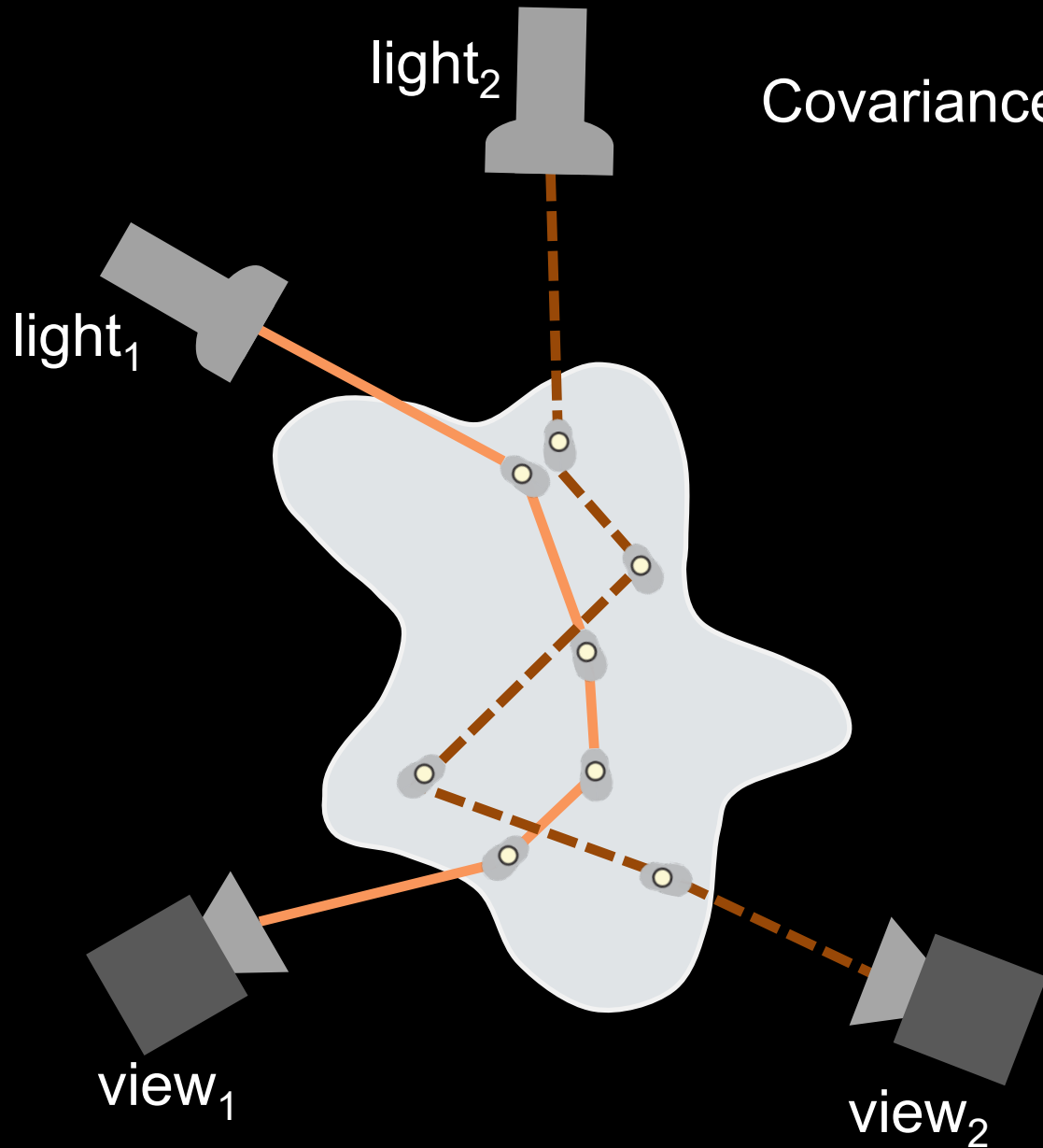
Covariance rendering



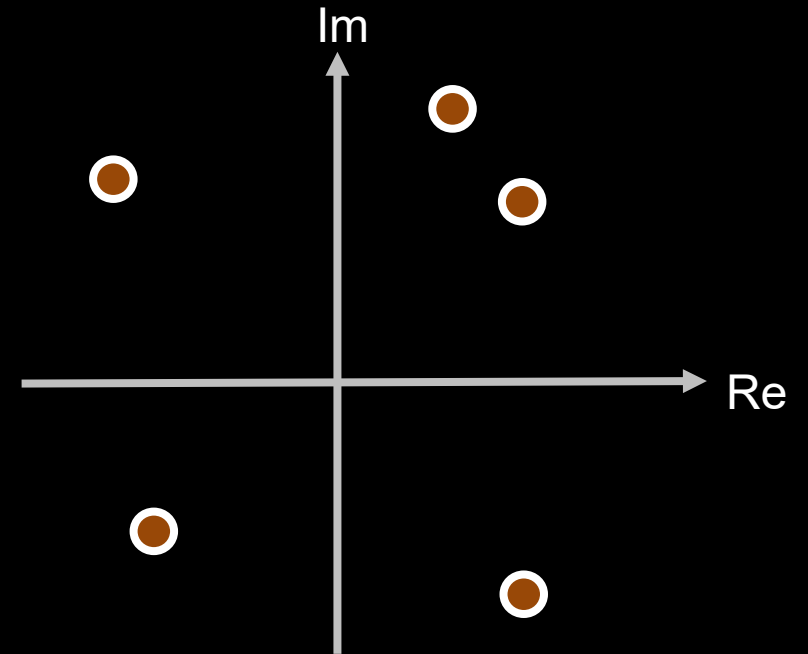
$$\text{Covariance} = \int_{\text{path}_1, \text{path}_2} u(\text{path}_1) \cdot u^*(\text{path}_2)$$



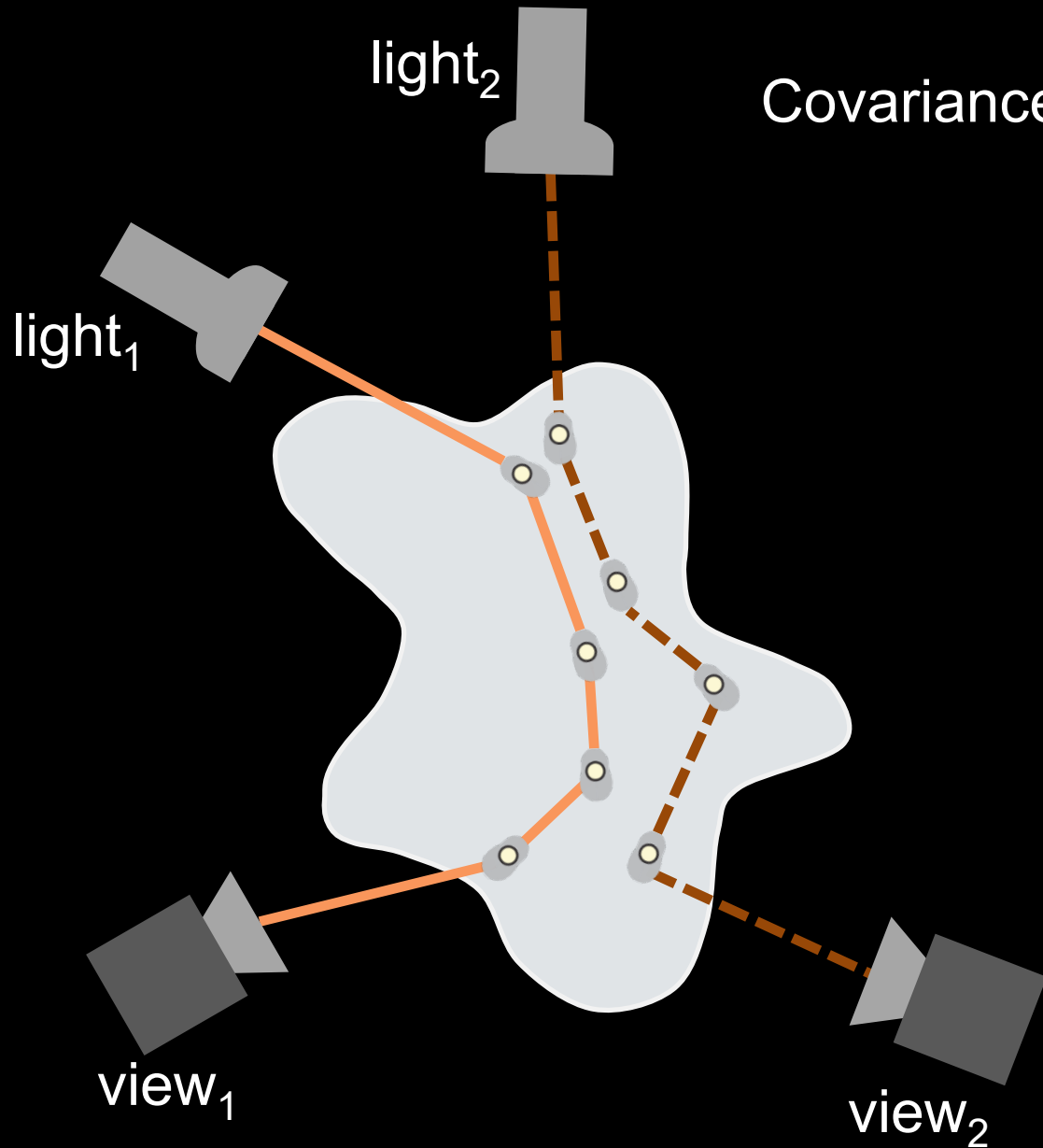
Covariance rendering



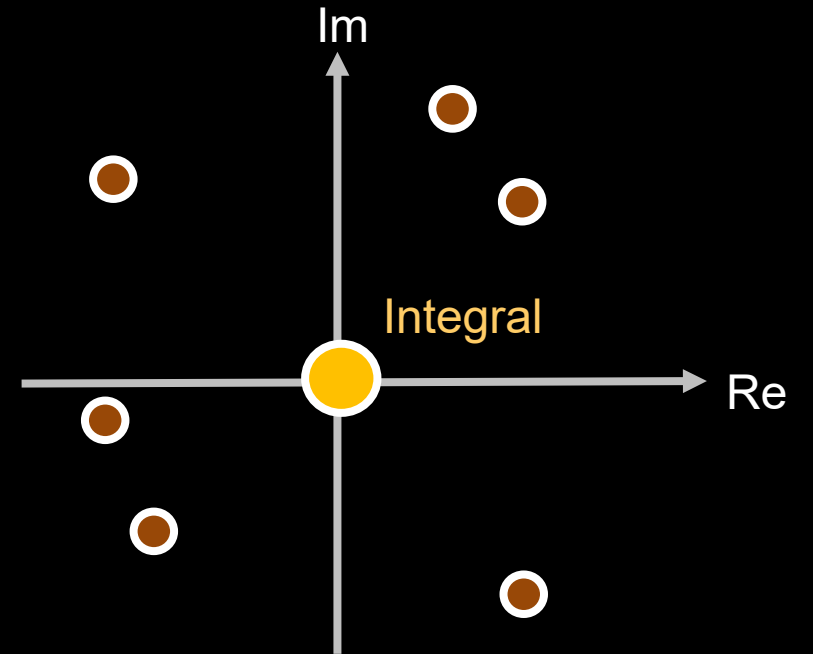
$$\text{Covariance} = \int_{\text{path}_1, \text{path}_2} u(\text{path}_1) \cdot u^*(\text{path}_2)$$



Covariance rendering

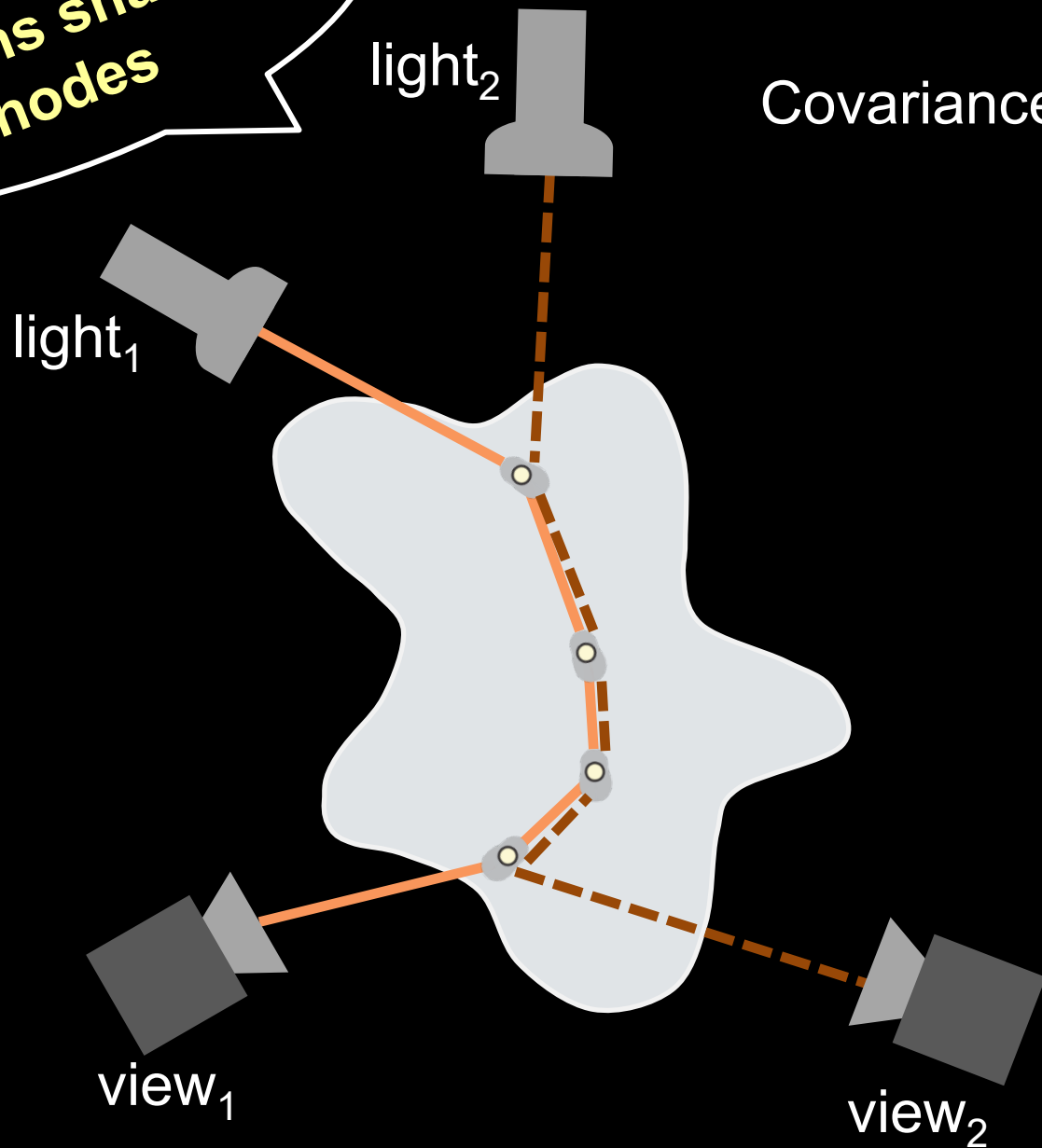


$$\text{Covariance} = \int_{\text{path}_1, \text{path}_2} u(\text{path}_1) \cdot u^*(\text{path}_2)$$

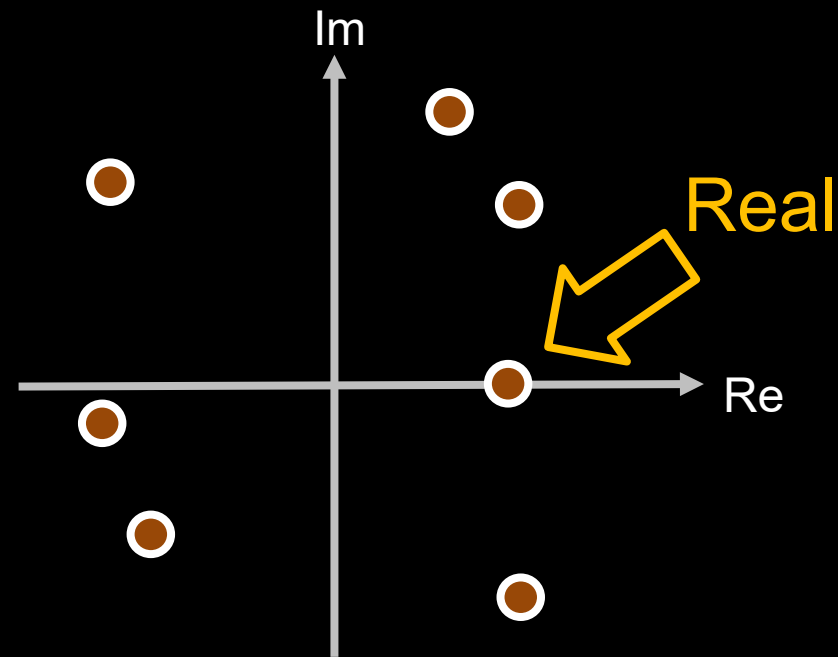


Covariance rendering

Paths share nodes

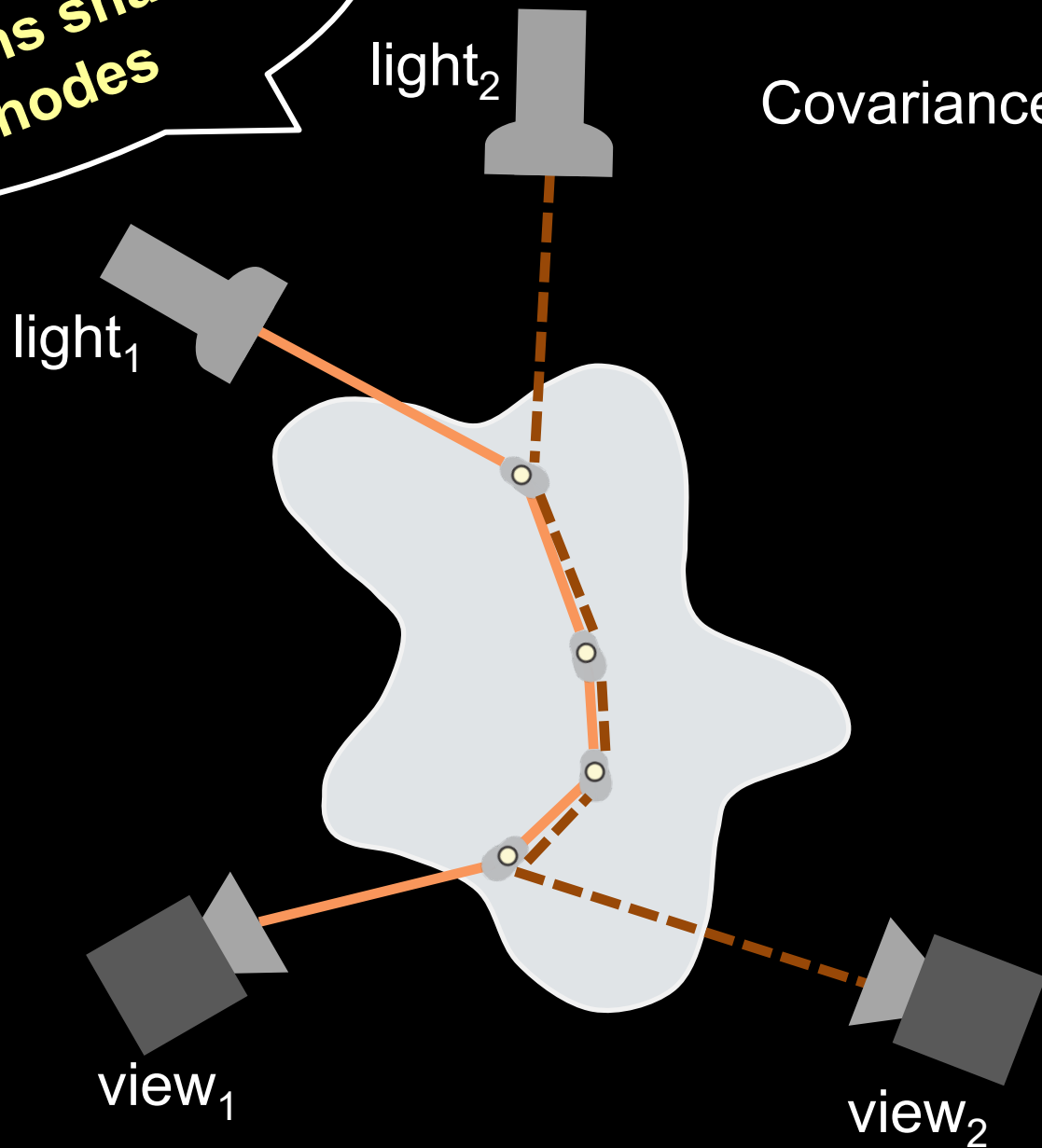


$$\text{Covariance} = \int_{\text{path}_1, \text{path}_2} u(\text{path}_1) \cdot u^*(\text{path}_2)$$

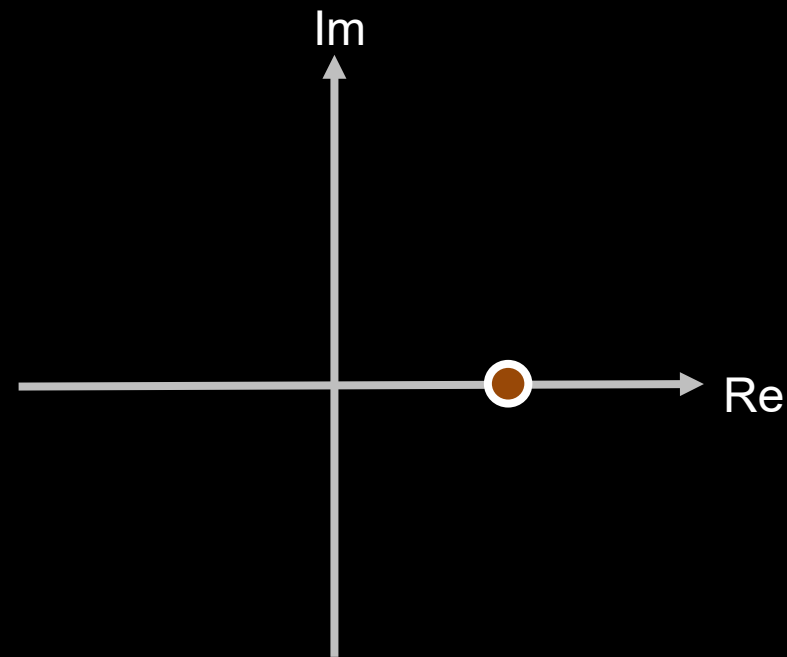


Covariance rendering

Paths share nodes

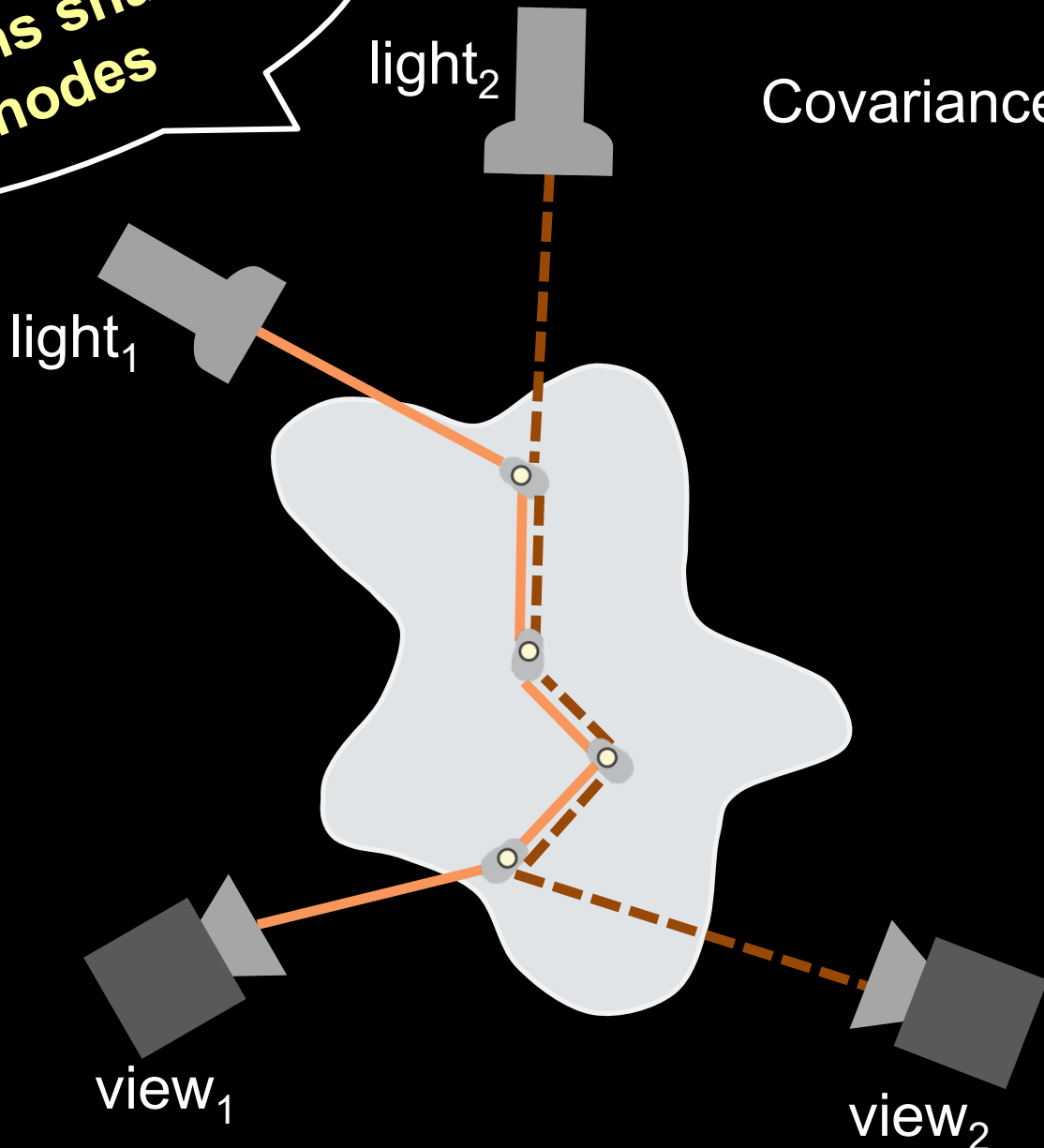


$$\text{Covariance} = \int_{\text{path}_1, \text{path}_2} u(\text{path}_1) \cdot u^*(\text{path}_2)$$

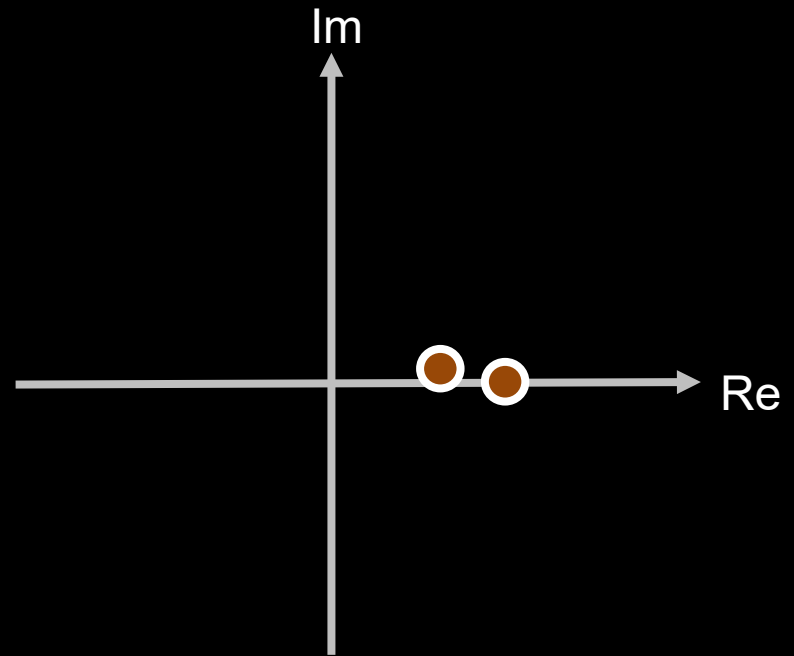


Covariance rendering

Paths share nodes

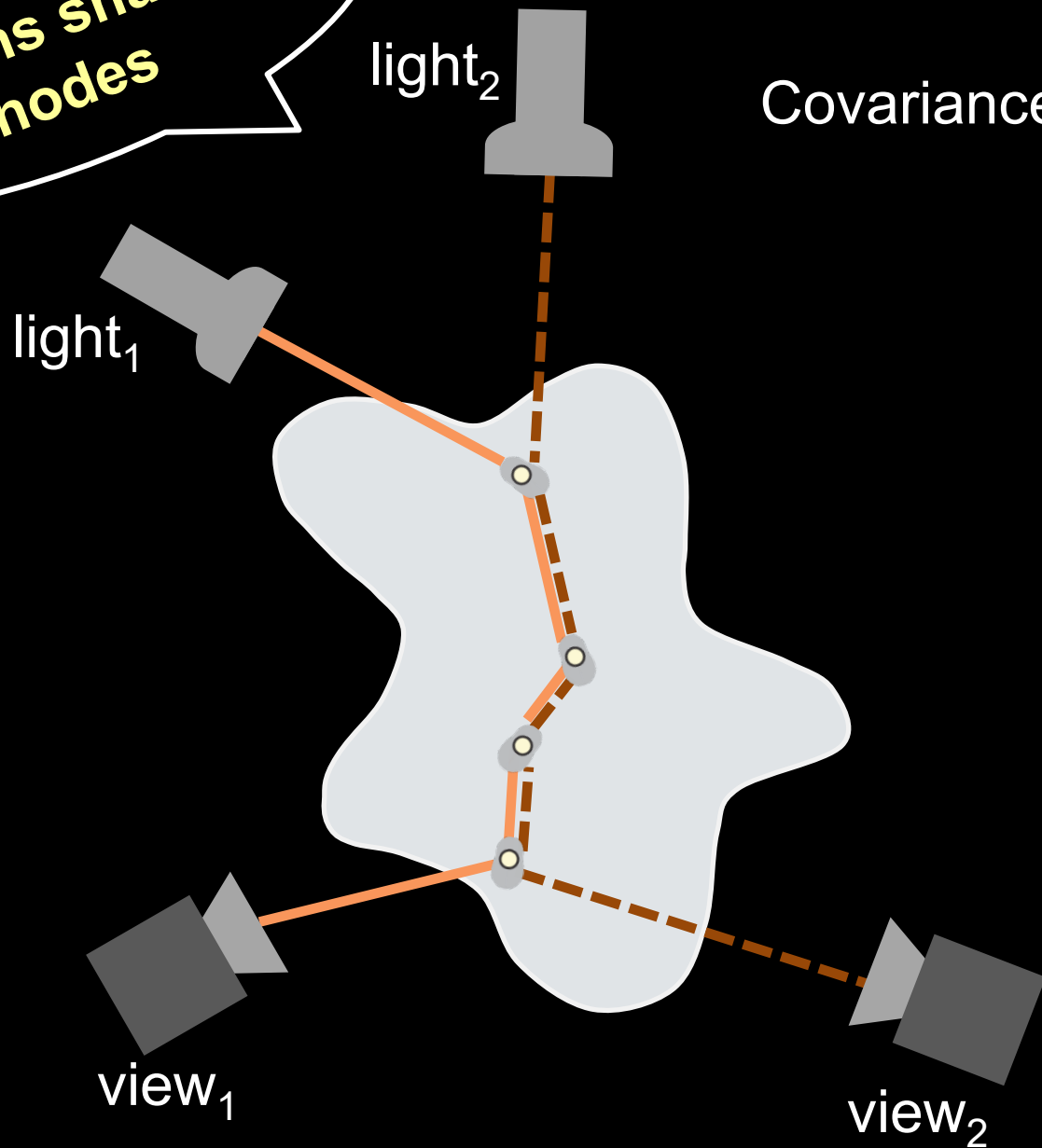


$$\text{Covariance} = \int_{\text{path}_1, \text{path}_2} u(\text{path}_1) \cdot u^*(\text{path}_2)$$

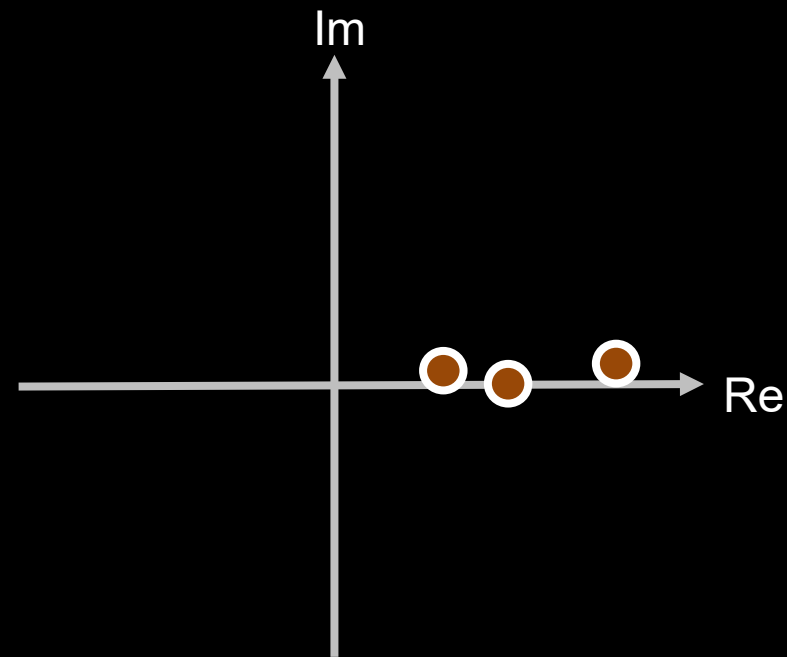


Covariance rendering

Paths share nodes

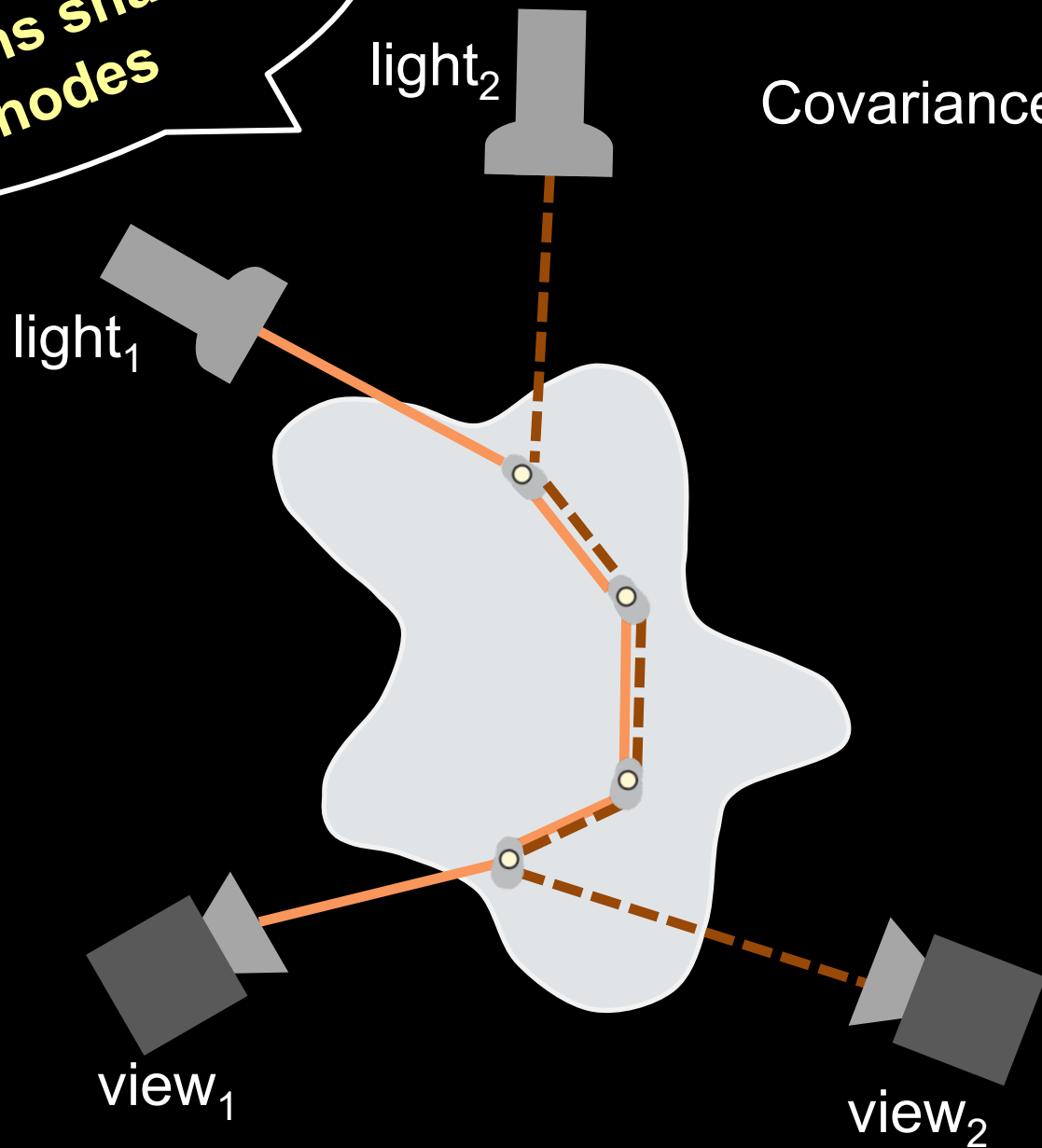


$$\text{Covariance} = \int_{\text{path}_1, \text{path}_2} u(\text{path}_1) \cdot u^*(\text{path}_2)$$

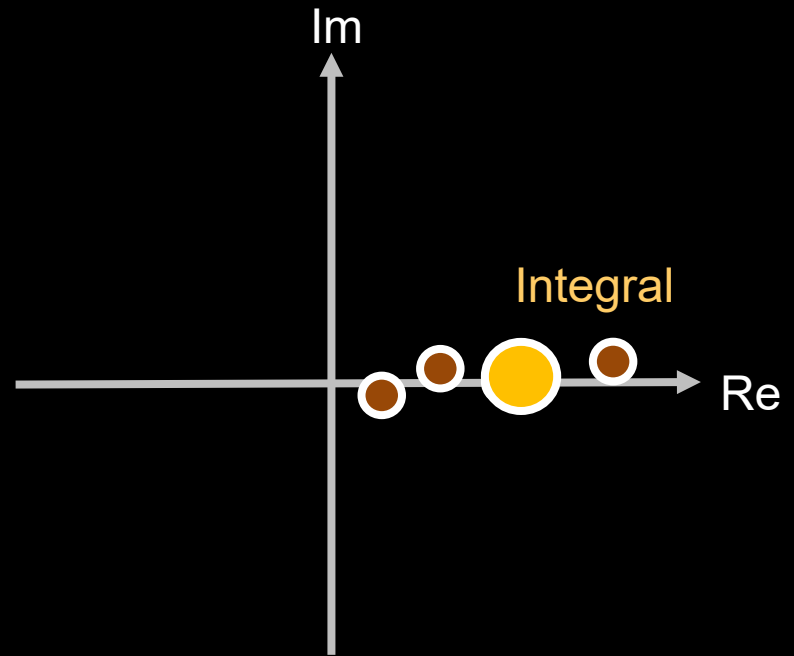


Covariance rendering

Paths share nodes



$$\text{Covariance} = \int_{\text{path}_1, \text{path}_2} u(\text{path}_1) \cdot u^*(\text{path}_2)$$



Covariance rendering

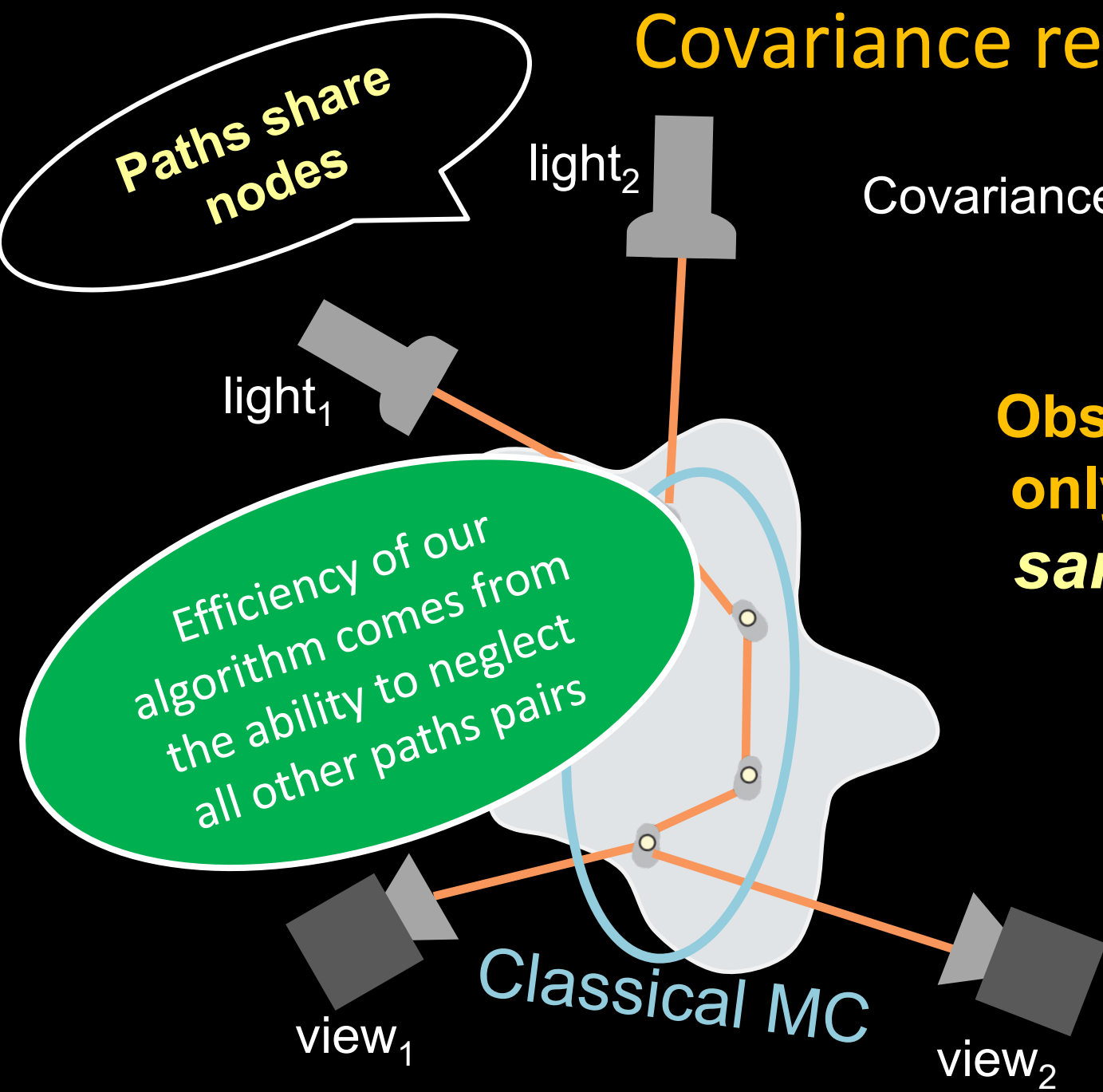
$$\text{Covariance} = \int_{\text{path}_1, \text{path}_2} u(\text{path}_1) \cdot u^*(\text{path}_2)$$

Observation: need to consider only path pairs that share the same nodes (except at the end)

Paths share nodes

Efficiency of our algorithm comes from the ability to neglect all other paths pairs

Classical MC



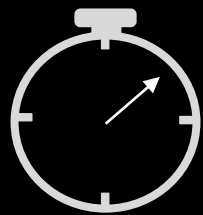
A Monte Carlo Framework for Rendering Speckle Statistics in Scattering Media

CHEN BAR, Department of Electrical Engineering, Technion, Israel
MARINA ALTERMAN, Department of Electrical Engineering, Technion, Israel
IOANNIS GKIOULEKAS, Robotics Institute, Carnegie Mellon University, USA
ANAT LEVIN, Department of Electrical Engineering, Technion, Israel

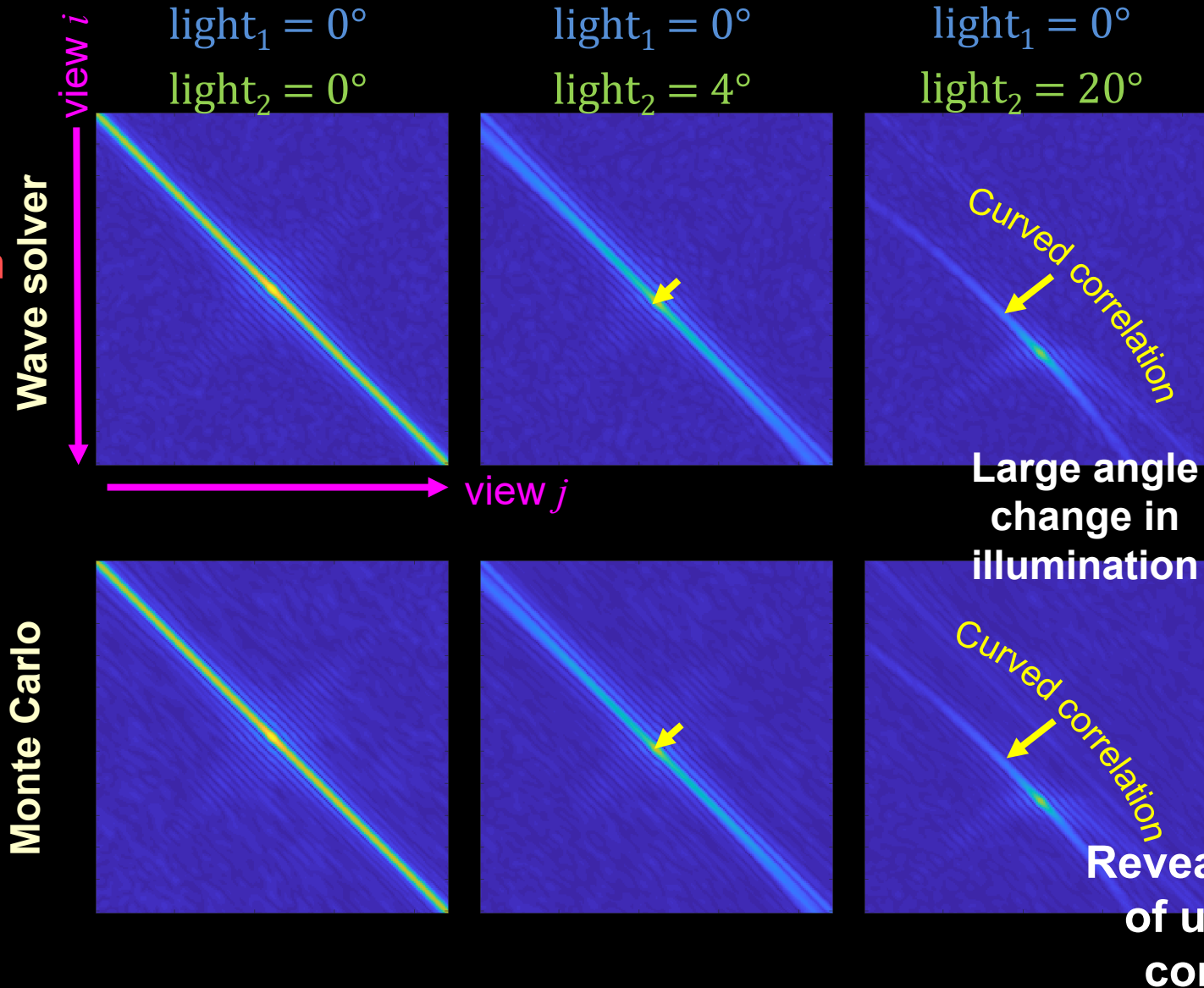
See paper for details

Validation: Wave Equation Covariances v.s. MC

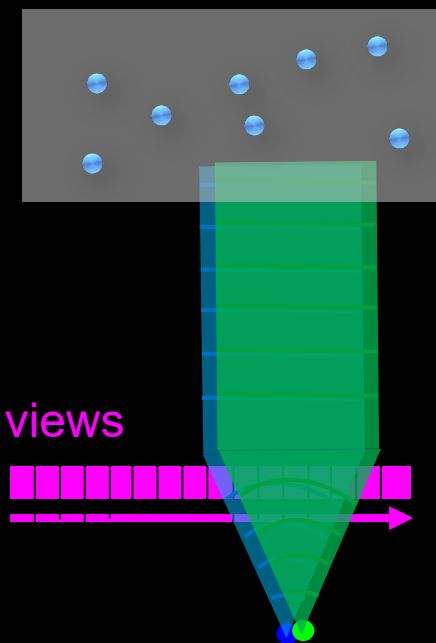
Computation takes days



Several minutes

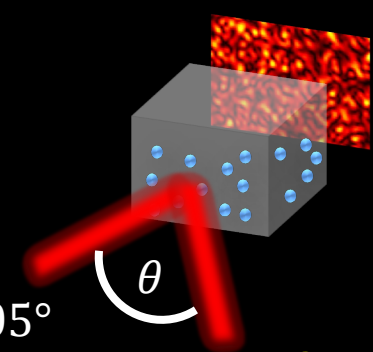


Classical ME holds for relatively small angles
Setup

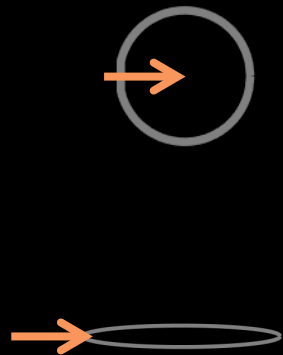


Reveal new types of unexplored correlations

Rendering Speckles



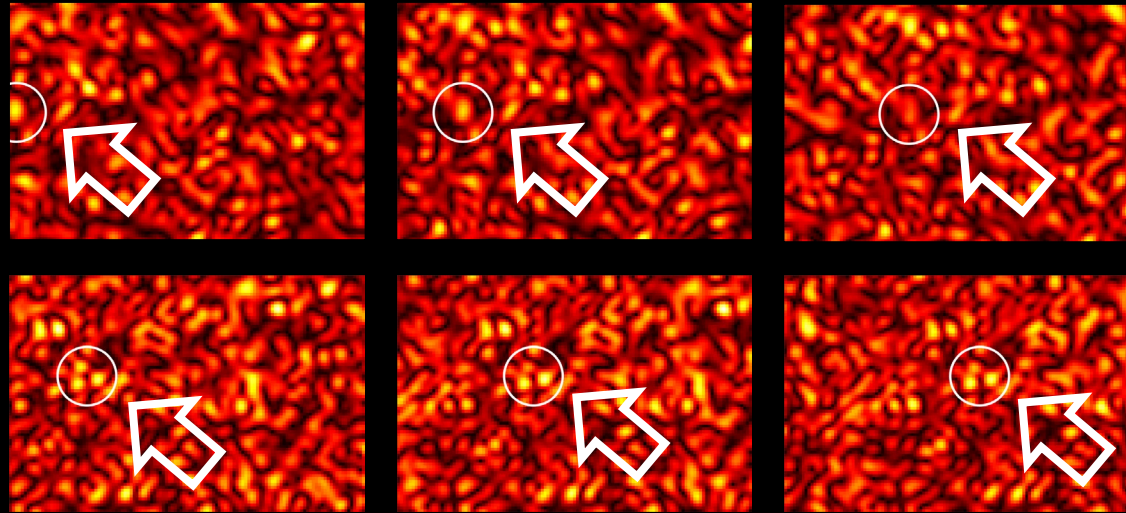
Phase Function



$\theta = 0^\circ$

$\theta = 0.0025^\circ$

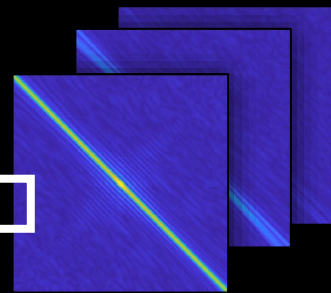
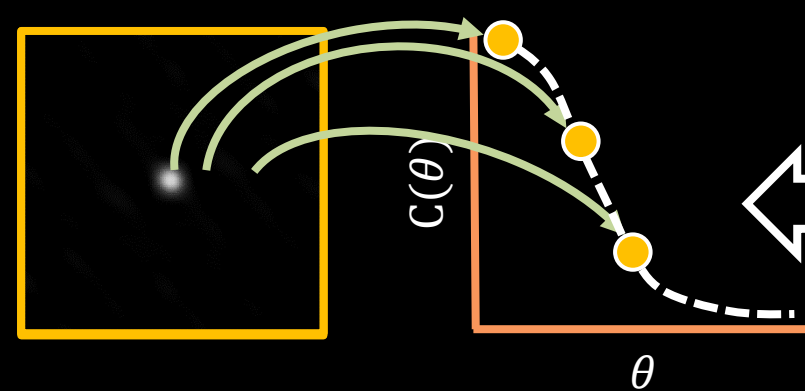
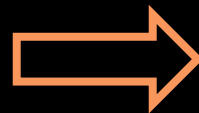
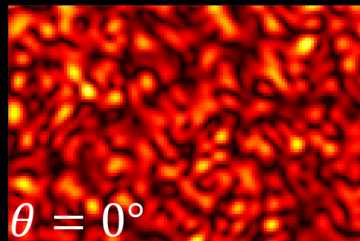
$\theta = 0.005^\circ$



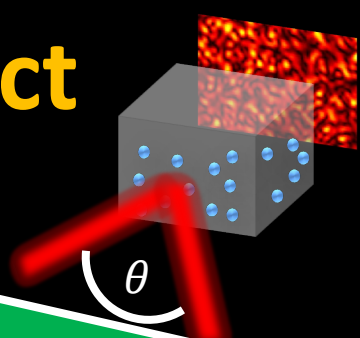
Classical ME holds for relatively small angles

Exact ME extent is different for different materials.

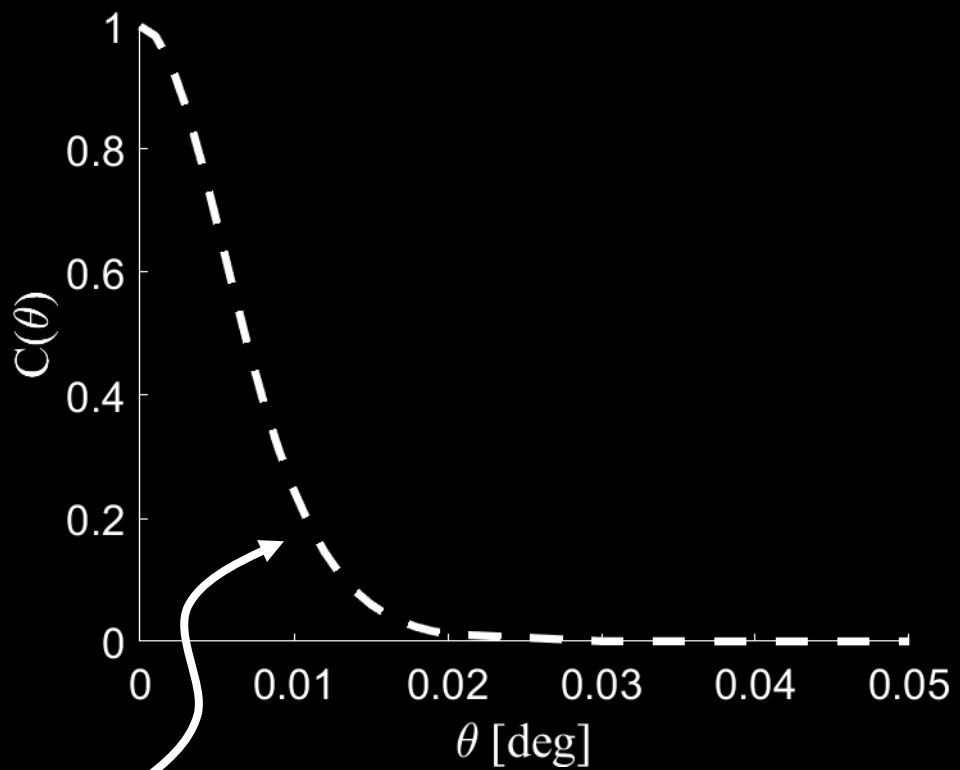
Computing ME extent as a function of θ :



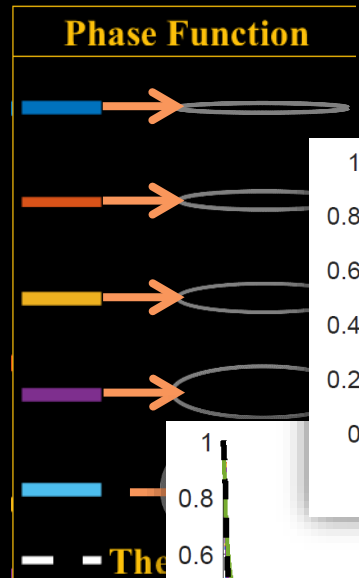
Evaluating the Memory Effect



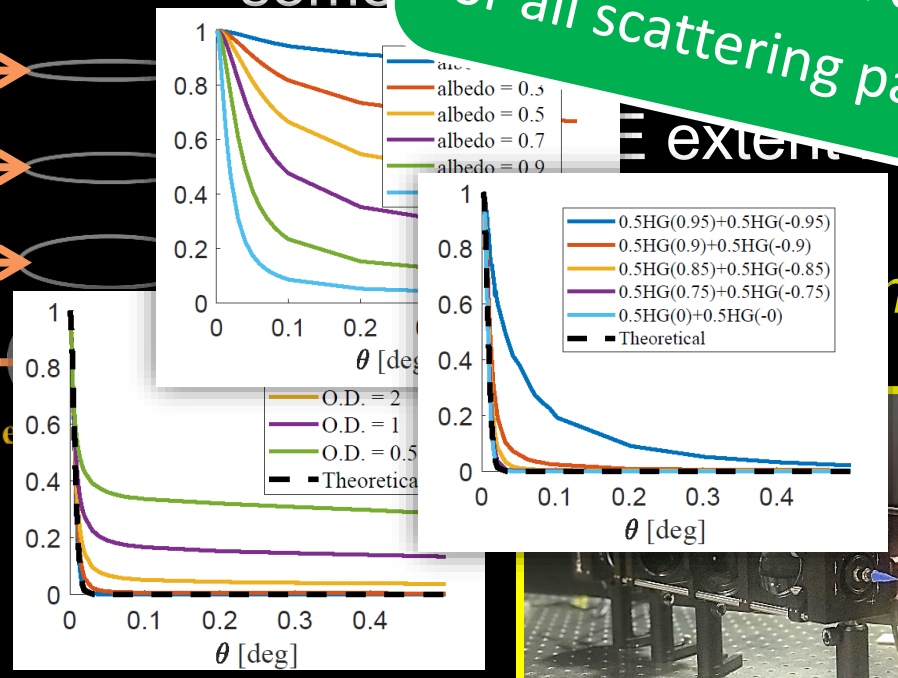
Now we can efficiently compute ME curves for all scattering parameters



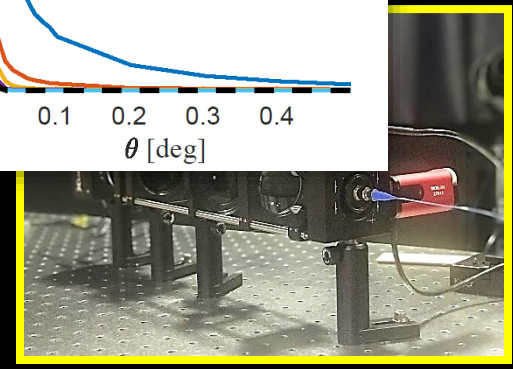
Analytical solution based on diffusion approximation



This a some

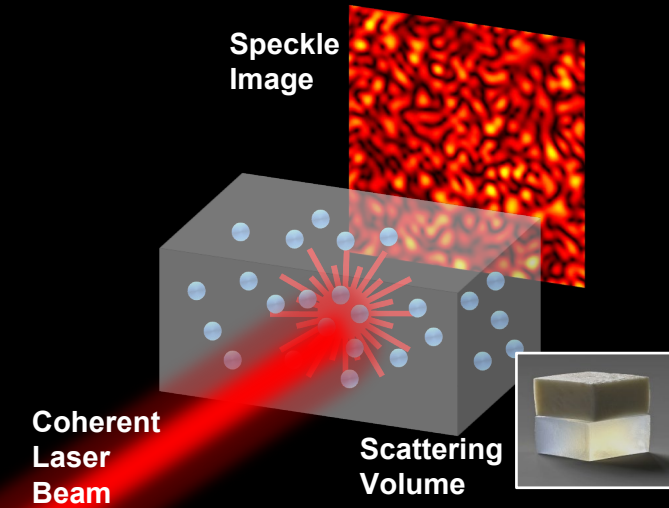


empirically in



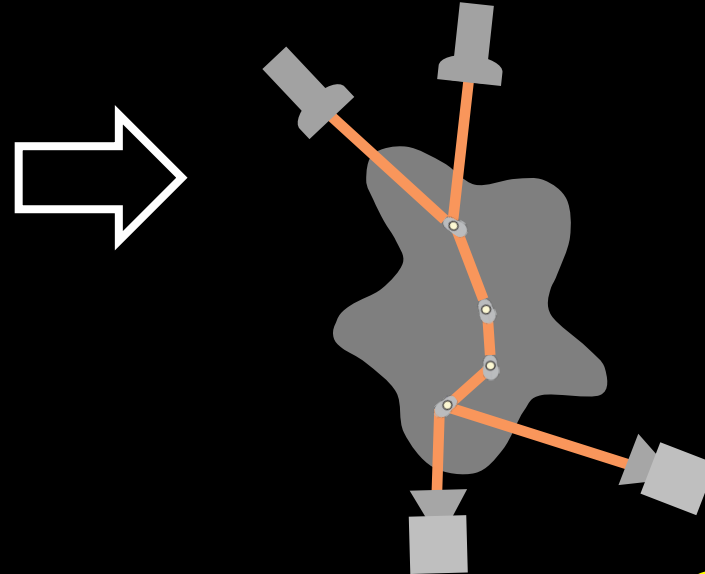
Summary

Problem:
Coherent Scattering

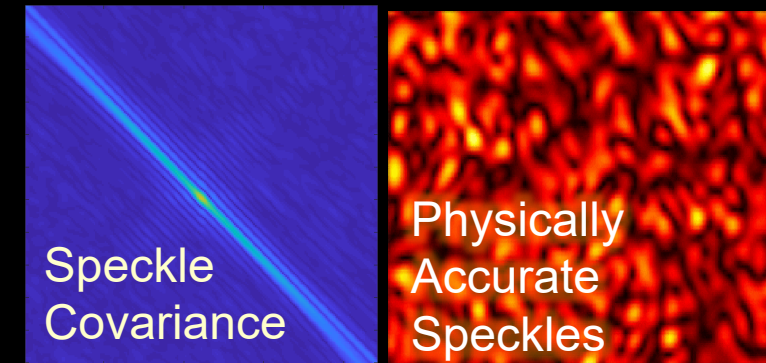


Path-integral formulation
for speckle covariance

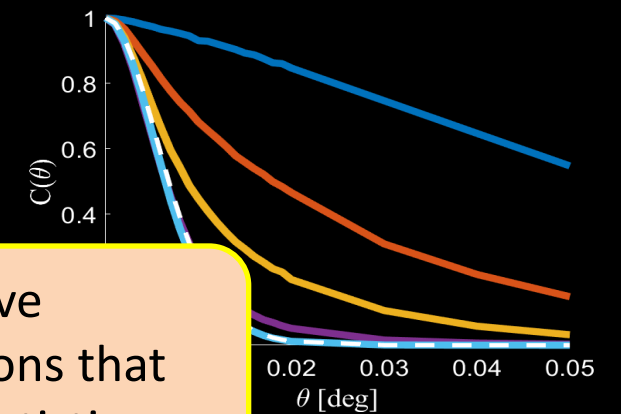
$$\text{Covariance} = \int_{\text{path}_1, \text{path}_2} u(\text{path}_1) \cdot u^*(\text{path}_2)$$



Efficient MC Rendering

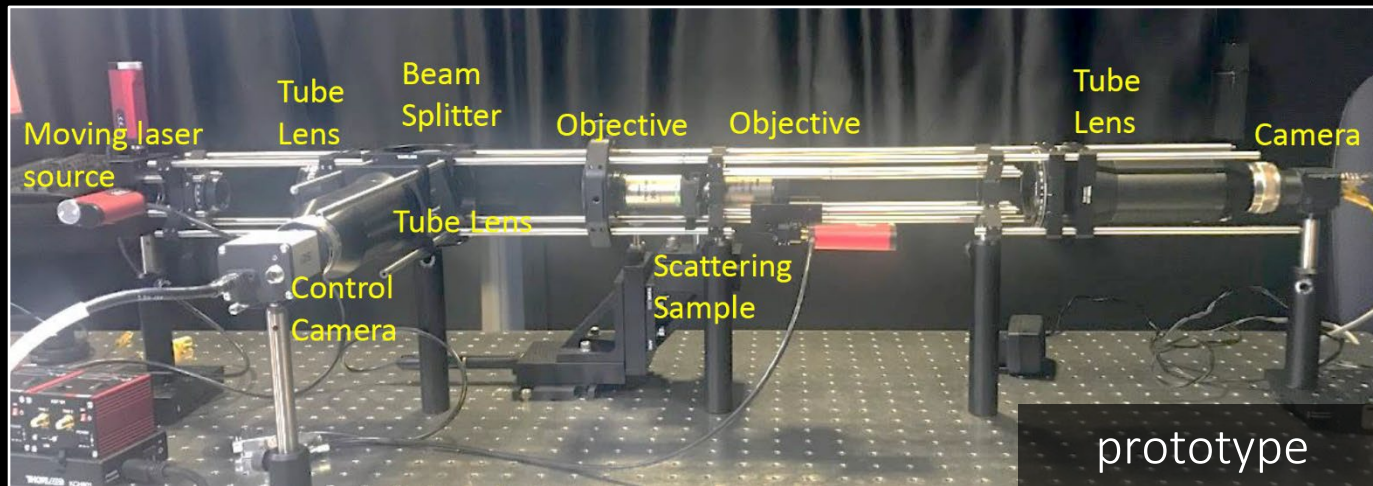
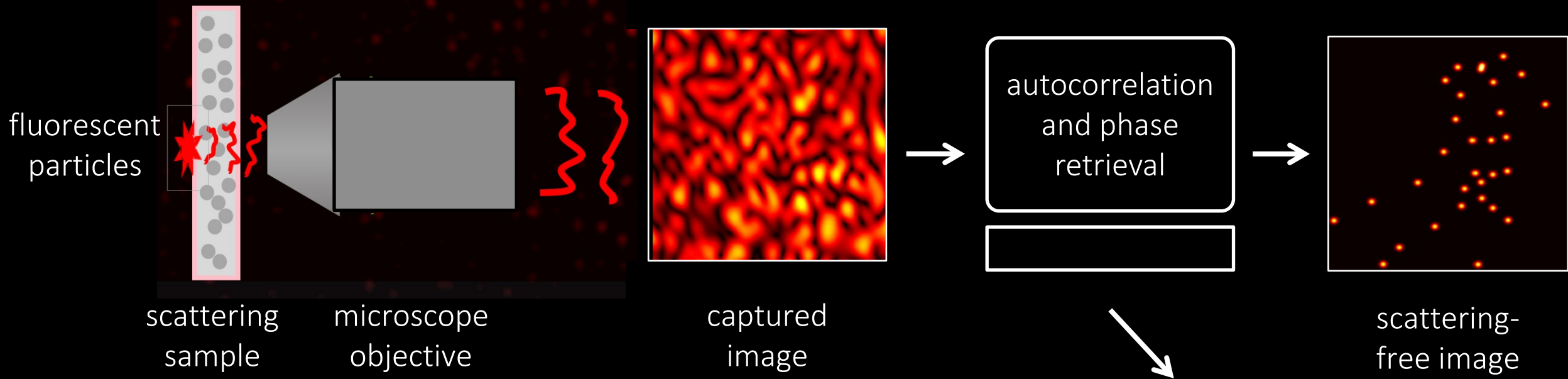


Memory Effect Evaluation



Potentially improve
imaging applications that
rely on speckle statistics

Speckle-based fluorescence microscopy



Performance strongly depends on:

- speckle statistics
- image priors
- tissue parameters

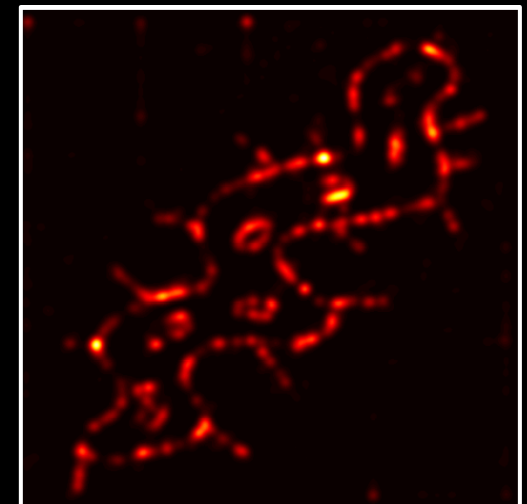
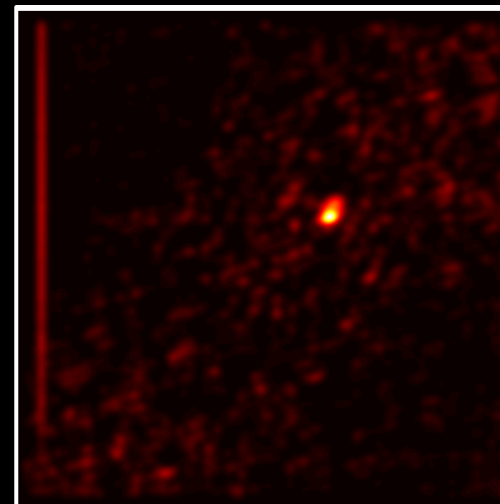
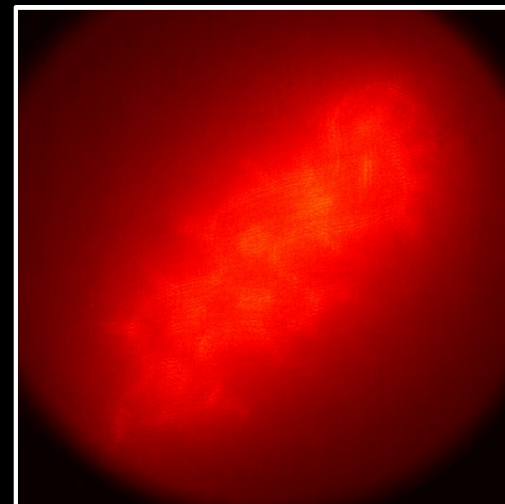
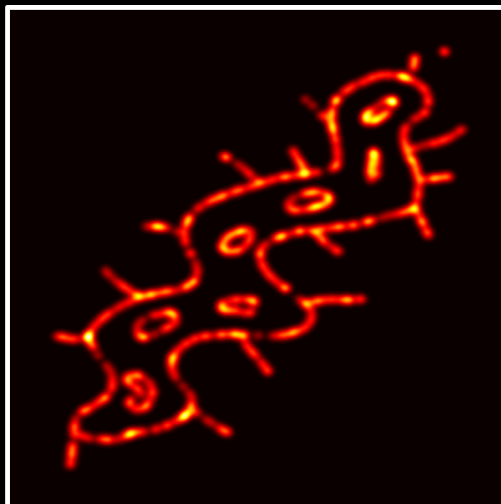
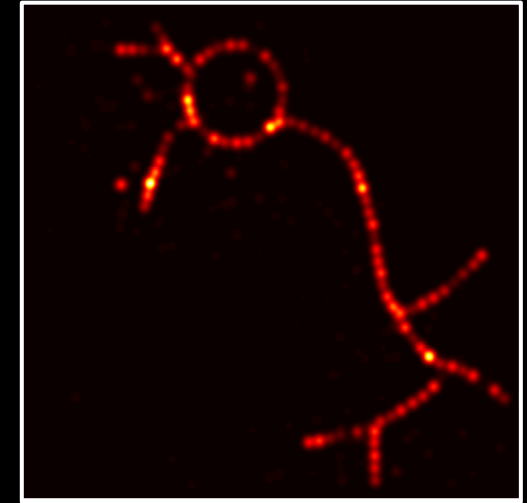
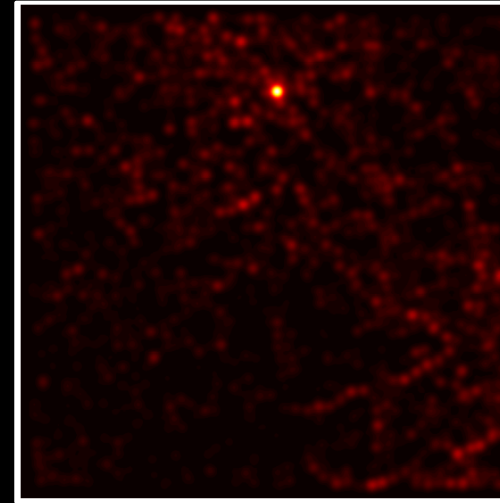
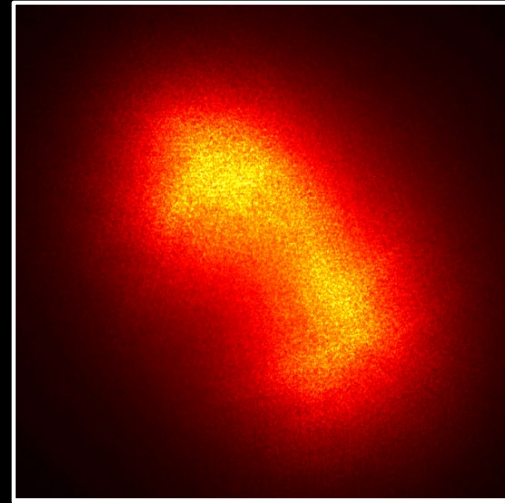
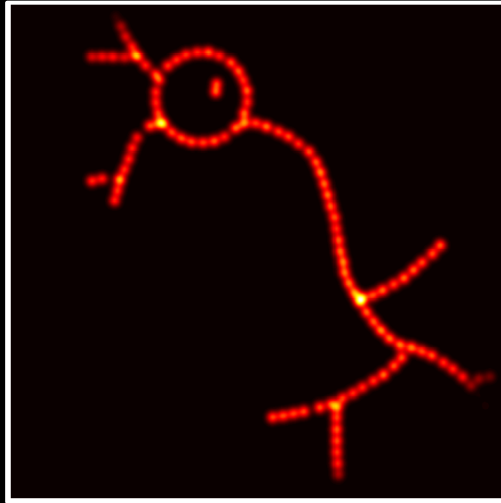
Better algorithms for fluorescence microscopy

groundtruth

input image

prior algorithm

our algorithm



Acquisition of scattering materials

Use differentiable speckle rendering to recover material parameters from speckle images

